POSITION-DEPENDENT ENERGY TRANSFER BETWEEN RUTHENIUM(II) AND OSMIUM(II) MODIFIED COILED-COIL α-HELICAL PEPTIDES AND OLIGOPROLINE RECOGNITION BY A β-HAIRPIN PEPTIDE

Dale Joseph Wilger

A dissertation submitted to the faculty of the University of North Carolina at Chapel Hill in partial fulfillment of the requirements for the degree of Doctor of Philosophy in the Department of Chemistry.

Chapel Hill
2011

Approved by:

Professor Marcey Waters

Professor Maurice Brookhart

Professor John Papanikolas

Professor Joseph Templeton

Professor Christopher Fecko

ABSTRACT

DALE JOSEPH WILGER: Position-Dependent Energy Transfer Between Ruthenium(II) and Osmium(II) Modified Coiled-coil α-Helical Peptides & Oligoproline Recognition by a β-Hairpin Peptide

Two different research projects are discussed throughout this dissertation. The first project relates to the study of position-dependent energy transfer between specially synthesized metallopeptides that contain Ru^{II} and Os^{II} bipyridyl complexes. The second project relates to the measurement of aromatic-prolyl interactions in a model peptide system.

The study of excited-state energy transfer processes is of interest due to its implications in natural and artificial photosynthesis. In this work, a series of coiled-coil α-helical metallopeptides were designed, synthesized, and characterized. The metallopeptides contain Ru^{II} and Os^{II} bipyridyl complexes that serve as excited-state energy donors and acceptors, respectively.

Rates for energy transfer between the metallopeptides are position dependent and intimately linked with the structure of the peptide scaffold itself. The results indicate that energy transfer phenomena can be fine-tuned using peptide primary sequence and secondary structure. The metallopeptide system could be used to better understand the mechanisms of Ru^{II} to Os^{II} excited-state energy transfer, and may potentially be applied to the construction of synthetic light-harvesting antenna, or as a sensitizer for dye-sensitized solar cells.

As a second project, aromatic-prolyl interactions were studied in a model peptide system composed of a β-hairpin peptide motif known as a tryptophan zipper (trpzip). Interactions between the amino acid proline and aromatic amino acids are of importance in

the context of both protein folding and protein-protein interactions. The intermolecular recognition of the polyproline type II (PPII) helix peptide secondary structure by aromatic residues is important in a large number of cellular signaling events. Also, the *cis-trans* isomerization of amide bonds containing proline is often rate-limiting during protein folding. A disulfide exchange system was designed for studying aromatic-prolyl interactions between a trpzip peptide and a series of oligoproline peptides which adopt the PPII helix conformation. Favorable aromatic-prolyl interactions with energies up to 2.3 $kcal \cdot mol^{-1}$ were measured. A β-hairpin peptide which also contains tryptophan, WKWK, does not have favorable interactions with the oligoproline peptides. The WKWK β-hairpin peptide contains a different configuration of tryptophan residues and demonstrates the importance of structure when considering aromatic-prolyl interactions in the context of complex peptide environments.

ACKNOWLEDGEMENTS

First and foremost, I would like to thank Professor Marcey Waters for welcoming me into her lab and providing an environment where I could learn about a broad range of research topics. I have thoroughly enjoyed the developments I have made, both professionally and personally. They would not have been possible if I did not have her as an advisor, as a mentor, and as a friend.

I would like to thank my committee members, Professor Maurice Brookhart, Professor John Papanikolas, Professor Joseph Templeton, Professor Christopher Fecko, and the rest of the UNC chemistry faculty for their help. Professor Papanikolas has, in particular, provided me with considerable help, and even more patience during the whole process.

I would like to thank all the members of the Waters lab, both past and present. Without their help, none of this would have been possible. I would especially like to thank Dr. Alexander Riemen and Dr. Lauren Latshaw Cline for teaching me not only about chemistry, but also about how to be a good chemist.

I would like to thank Stephanie Bettis for her help with the energy transfer studies. She has helped us realize a goal we have both pursued for several years. Without her help, it might never have been possible.

I would like to thanks all of my friends throughout the department who have helped me along the way, especially Austin, Dan, Anne-Marie, Tim, and Jen. I can only hope that our paths cross frequently in the coming years.

I would like to thank my parents for their love and support, and for teaching me right from wrong. I would like to thank my sister Elizabeth and her husband Joe for always being a steady rock for me to rely on when I have come home. Lastly, I would like to thank Colleen for making my life so much better than I ever thought it could be.

TABLE OF CONTENTS

LIST OF TABLES

LIST OF FIGURES

LIST OF ABBREVIATIONS AND SYMBOLS

Å	Angstrom
A	Amplitude of a time-resolved emission measurement
Ac	Acetyl group
ACN	Acetonitrile
AcOH	Acetic acid
Arg, R	Arginine
Asn, N	Asparagine
ATP	Adenosine triphosphate
AUC	Analytical ultracentrifugation
β	Preexponential factor for Dexter energy transfer
BET	Back electron transfer
Boc	*tert*-Butyloxycarbonyl group
bpy	Bipyridyl ligand, bipyridine ligand
BS	Beam splitter
n-BuOH	*n*-Butanol
*t*BuOH	*tert*-Butanol
c	Concentration in $mol \cdot L^{-1}$
°C	Degrees Celsius
CD	Circular dichroism spectroscopy
cm	Centimeter
C_m	Chemical denaturation midpoint
CuAAC	Cu(I)-catalyzed azide-alkyne 1,3-dipolar cycloaddition

Cys, C	Cysteine
DBU	1,8-Diazabicyclo[5.4.0]undec-7-ene
DCC	Dicyclohexylcarbodiimide
deg	degrees of arc
DIPEA	Diisopropylethylamine
DMF	N,N-Dimethylformamide
dmol	decamole
DMSO	Dimethylsulfoxide
DNA	Deoxyribonucleic acid
DSSC	Dye-sensitized solar cell
e	Elementary charge
ε	Molar extinction coefficient
EDC	1-Ethyl-3-(3'-(dimethylamino)propyl)carbodiimide hydrochloride
ES	Excited state
ESI-MS	Electrospray ionization mass spectrometry
EtOAc	Ethyl acetate
EtOH	Ethanol
EVH1	Ena/VASP homology 1 domain
Fmoc	Fluorenylmethyloxycarbonyl group
fs	Femtosecond
Φ	Quantum yield
ΔG_D	Gibbs free energy change at a specific denaturant concentration
ΔG_F	Gibbs free energy change of unfolding

ΔG_{H20}	Gibbs free energy change in water/buffer
$\Delta\Delta G_D$	Difference between ΔG_D values at two different GndHCl concentrations
Gln, Q	Glutamine
Glu, E	Glutamic acid, or glutamate
Gly, G	Glycine
GndHCl	Guanidinium hydrochloride
GS	Ground state
GYF	Glycine-tyrosine-phenylalanine domain
HATU	7-Aza-benzotriazole-N,N,N',N',-tetramethyluronium hexafluorophosphate
HBTU	O-Benzotriazole-N,N,N',N',-tetramethyluronium hexafluorophosphate
His, H	Histidine
HOBt	N-hydroxybenzotriazole
HPLC	High pressure liquid chromatography
Ile, I	Isoleucine
IPA	Isopropanol, 2-propanol
ISC	Intersystem crossing
ITC	Isothermal titration calorimetry
J	Spectral overlap integral
K	Kelvin, absolute temperature scale
κ^2	Orientation factor
k_D	Rate of energy transfer (Dexter mechanism)
k_F	Rate of energy transfer (Förster mechanism)
kcal	kilocalorie

K_d	Dissociation constant
kHz	Kilohertz
L	Liter
l	Optical path length
λ	Wavelength
LC-MS	Liquid chromatography-mass spectrometry
Leu, L	Leucine
LH2	Light-harvesting complex II
LHE	Light-harvesting efficiency
Lys, K	Lysine
M	Isotopic mass, exact mass
m	Slope of a line
μM	Micromolar
mAU	Milliabsorbance unit
MD	Molecular dynamics
MeOH	Methanol
MHz	Megahertz
mL	Milliliter
MLCT	Metal-to-ligand charge-transfer
mM	Millimolar
mol	Mole
MRE	Mean molar residue ellipticity
MS	Mass spectrometry

m/z	Mass-to-charge ratio
n	Refractive index
η	Efficiency of a process
nm	Nanometer
NMP	N-Methylpyrrolidinone
NMR	Nuclear magnetic resonance spectroscopy
NOE	Nuclear Overhauser effect
NOESY	Nuclear Overhauser effect spectroscopy
ns	Nanosecond
Orn, O	Ornithine
pdb	Protein data bank
PDI	Polydispersity index
PPII	Polyproline type II helix
PRM	Proline-rich motif
Pro, P	Proline
D-Pro, P	D-Proline
ps	Picosecond
R	Molar gas constant
R_0	Förster radius for a specific donor and acceptor
R^2	Coefficient of determination
RESP	Restrained electrostatic potential
RP-HPLC	Reversed-phase high pressure liquid chromatography
RT	Room temperature

SAF	Self-assembling fiber
Ser, S	Serine
SH3	Src-homology 3 domain
SPPS	Solid-phase peptide synthesis
SSE	Steady-state emission
T	Temperature (Kelvin scale)
τ	Lifetime of a time-resolved emission measurement
$[\theta]$	Mean molar residue ellipticity
TCEP	Tris(2-carboxyethyl)phosphine
TCSPC	Time-correlated single photon counting
TFA	Trifluoroacetic acid
Thr, T	Threonine
TIPS	Triisopropylsilane
TLC	Thin layer chromatography
TOCSY	Total correlation spectroscopy
Trp, W	Tryptophan
trpzip	Tryptophan zipper peptide
Tyr, Y	Tyrosine
UEV	Ubiquitin E2 variant domain
UV-vis	Ultraviolet-visible spectroscopy
V	Volt
Val, V	Valine
v:v	Volume-to-volume ratio

WW	Tryptophan-tryptophan domain
X_{aa}	Any nonproline amino acid

Chapter I

INTRODUCTION: POSITION-DEPENDENT ENERGY TRANSFER BETWEEN RUTHENIUM(II) AND OSMIUM(II) MODIFIED COILED-COIL α-HELICAL PEPTIDES

A. Significance

Mankind currently faces the overwhelming task of meeting the ever-increasing energy demands of our developing global community.[1] The expanding energy requirements of our developing world, coupled with worsening environmental and political issues related to energy use have animated new endeavors in the study of light absorption and energy transfer processes.[1] These studies have been inspired by the simple observation that the vast majority of the energy required to sustain all life on earth is essentially supplied by solar radiation. Natural sunlight is diffuse and intermittent. Photosynthetic life forms have adapted to this by evolving complex light-harvesting antennae systems that absorb multiple photons at different chromophore sites and couple them to localized reactive centers through a series of highly synchronized excited-state energy transfer and electron transfer steps (Figure 1.1).[2] These processes have been optimized within photosynthetic organisms in order to increase effective molar absorptivity, broaden the spectral window for light absorption, and to couple multielectron redox processes to single-photon absorption processes. The basic mechanisms by which these energy transfer and electron transfer events occur are of interest if mankind is to ever mimic the complex energy conversion systems developed within natural photosynthetic organisms.[3]

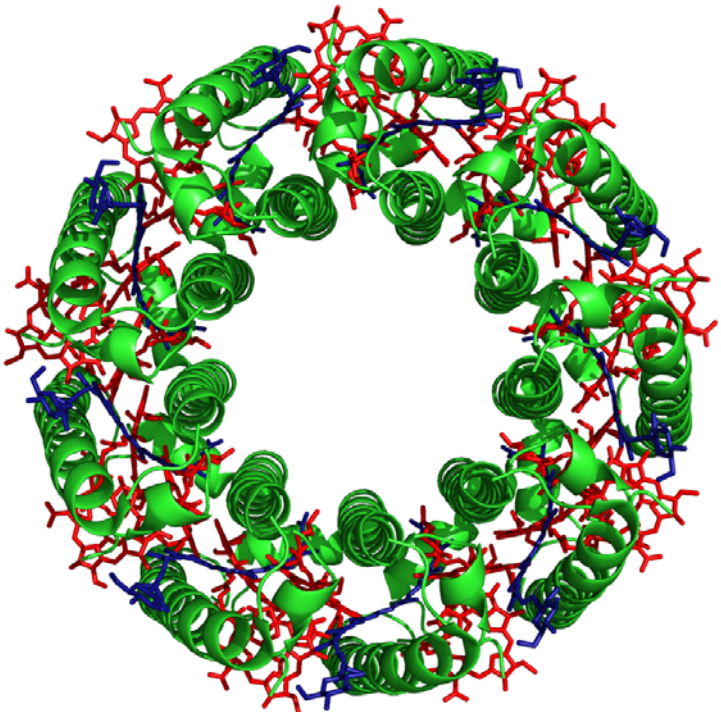

Figure 1.1 The crystal structure for the light-harvesting complex II LH2 from *Rhodobacter sphaeroides* (pdb code: 2FKW).[2a] The peptide segments of the light-harvesting complex are shown in green. The protein complex has 27 different bacteriochlorophyll molecules (red) bound tightly along with 9 different carotenoid chromophores (rhodopsin glucoside, blue) that serve as primary and secondary light absorbing units, respectively. The peptide architecture of the complex holds many of the bacteriochlorophyll molecules within less than 9 angstroms of each other. The distance between chromophore molecules has been optimized through evolution and allows for the rapid transfer of excited-state energy within the complex, and then ultimately to a photosynthetic reaction center (not shown).

B. Background

i. Covalent and noncovalent scaffolds for studying energy transfer

A large number of covalent linkages, assemblies, and scaffolds have been used in order to study energy transfer phenomenon. These scaffolds vary in complexity from simple alkyl chains,[4] to high molecular weight synthetic polymers,[5] and extremely complex oligonucleotide molecules including duplex DNA.[6] These synthetic architectures are all used to spatially preorganize excited-state energy donors and acceptors in order to facilitate, expedite, and in most cases study energy transfer.

The constant obsession for studying excited-state energy transfer between spatially preorganized partners has been motivated by a number of interwoven factors. The first consideration is practical in nature. Energy transfer is, fundamentally, always a distance-dependent behavior. Energy transfer will in many cases occur more efficiently when excited-state donors and acceptors are held in close proximity. Although this is not strictly true for all energy transfer processes, we have only to look at natural light-harvesting structures to see the concept at work. Natural light-harvesting protein complexes never rely on diffusion controlled energy transfer in order to couple light absorption and photosynthetic reactions.[2] Instead, chromophores are held in intimate contact with both spacing and orientation optimized for the vectoral transfer of excited-state energy (Figure 1.1). This elaborate energy transfer organization is certainly a design feature many researchers would like to mimic synthetically.[3]

Another primary consideration for studying preorganized energy transfer is more academic in pursuit. While energy transfer is always distance-dependent to some extent, the exact mechanism of energy transfer has a pronounced effect on the degree of the observed distance-dependence. Indeed, the study of distance-dependent energy transfer for many systems has led to the general acceptance of the current excited-state energy transfer models.

Excited-state energy transfer has historically been analyzed according to two distinct models (Figure 1.2). The dipole-dipole mechanism was originally described by Theodor Förster,[7] while the electron exchange mechanism was originally described by David Dexter.[8]

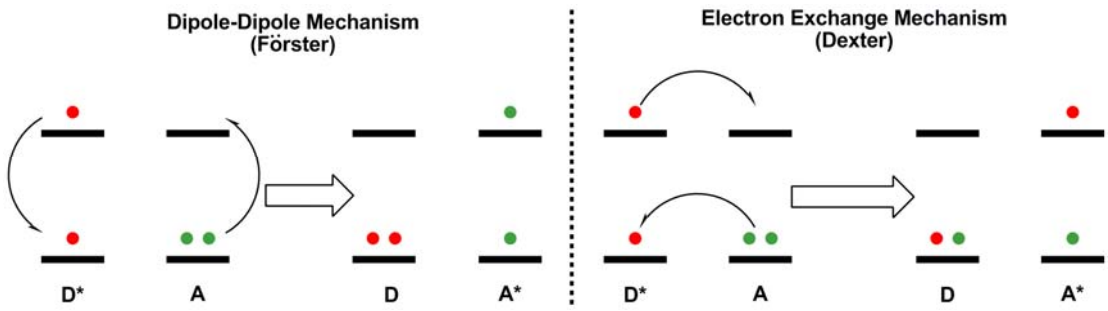

Figure 1.2 Diagram representing the dipole-dipole mechanism (Förster, left) and the electron exchange mechanism (Dexter, right) for excited-state energy transfer. The Förster mechanism relies on a through space dipole-dipole coupling and typically occurs over greater distances than the Dexter mechanism. The Dexter mechanism relies on orbital overlap between the donor and acceptor and is typically operative over extremely short distances.

The dipole-dipole mechanism of energy transfer describes a process where an excited-state electron can relax back to the ground state while simultaneously elevating an electron in another molecule to an electronically excited state through a nonradiative process. The coupled excitation/relaxation event occurs through the interaction of induced electronic dipoles on the donor and acceptor. Energy transfer through a Förster mechanism can occur over distances up to several nanometers (~10 nm), but requires an overlap of emission wavelengths for the donor molecule and absorption (excitation) wavelengths for the acceptor molecule. The extent of this overlap is measured by a spectral overlap integral (J) that determines the relative efficiency of energy transfer. The efficiency of energy transfer by the Förster mechanism also depends on the relative orientation of the donor and acceptor molecules (κ^2), the fluorescence quantum yield of the donor (Φ_D), the refractive index of the medium (n), and the distance between the donor and acceptor (r). The rate of energy transfer predicted by the Förster mechanism (k_F) will vary with the distance (r) to the inverse sixth power according to Equation 1:[9,10]

$$k_F = \frac{0.592 \cdot \kappa^2 \cdot \Phi_D \cdot J(\lambda)}{N \cdot n^4 \cdot \tau_D \cdot r^6} \qquad Equation\ 1$$

where N is the Avogadro number. The orientational factor and κ^2 is often taken to be 2/3, assuming the donor and acceptor undergo isotropic reorientation on a time scale shorter than the excited-state lifetime of the donor. The distance dependence of energy transfer by the Förster mechanism is often expressed as an efficiency quotient according to Equation 2:[9,10]

$$E = \frac{1}{1 + \left({}^{r}/_{R_0}\right)^6} \qquad Equation\ 2$$

where R_0 is the distance at which energy transfer efficiency is 50%. This distance is known as the Förster radius and is specific for a donor/acceptor pair. If the spectroscopic parameters (Equation 1) are known for a desired donor, acceptor, and medium then the Förster radius (R_0) can also be directly calculated. One consequence of Förster's predicted energy transfer mechanism is the requirement that both donor and acceptor transitions be optically allowed in order for energy transfer to manifest. For example, singlet-singlet transitions are allowed by the Förster mechanism, while triplet-triplet transitions are typically forbidden.

The electron exchange mechanism (Dexter) for energy transfer describes a process where an excited electron and hole (orbital vacancy) are simultaneously transferred from the donor molecule to the acceptor molecule. The movement of a combined electron and hole is often referred to as an exciton. The Dexter mechanism for energy transfer relies on orbital (wave function) overlap between the donor and acceptor molecules and occurs over much shorter distances compared to the Förster mechanism. The rate of energy transfer predicted by the Dexter mechanism (k_D) will vary with the distance (r) according to Equation 3:[10]

$$k_D = \frac{2\pi}{\hbar} \cdot \beta \cdot \exp\left(-\frac{-2r}{L}\right) \qquad Equation\ 3$$

where L is the average van der Waals radius for the initial and final molecular orbitals of the donor/acceptor system and β is a parameter that depends on spectral overlap between the donor emission and acceptor absorbance spectra, similar to the Förster model. Unlike Förster's predicted mechanism, the rate of energy transfer cannot be calculated directly from measured spectroscopic data, and the preexponential factor (β) must be experimentally determined. Another consequence of Dexter's predicted mechanism is that energy transfer efficiency by electron exchange will decrease exponentially with the donor/acceptor distance (r). The Dexter theory of energy transfer can also be applied to formally forbidden processes, including triplet-triplet transitions.[10] If the donor and acceptor molecules in question are covalently linked then Dexter energy transfer can also occur with a significant through-bond electronic coupling component in a process known as superexchange.[10]

Experimental studies on the distance dependence for energy transfer have long been the proving ground for the previously described mechanistic interpretations. The predicted distance dependence (r^{-6}) for the Förster mechanism of energy transfer was experimentally confirmed by Stryer and Haugland using a series of oligoprolines as molecular spacers.[11] The oligoproline bridges acted as rigid spacers that held the donor (naphthyl) and acceptor (dansyl) groups at known fixed distances (Figure 1.3a). These experiments confirmed the use of Förster energy transfer as a "spectroscopic ruler" for measuring distances on the nanometer scale.[11] Similarly, Speiser and Katriel were able to show that the distance dependence for excited-state energy transfer in a series of covalently linked benzyl-biacetyl molecules followed an inverse exponential trend as predicted by Dexter (Figure 1.3b).[12] In Speiser's studies, aryl moieties served as energy donors, while biacetyl moieties served as the

energy acceptors. Both these examples serve to emphasize the intertwined roles that the theoretical and experimental disciplines have played in the field of energy transfer study.

(a)

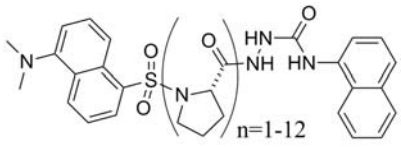

(b)

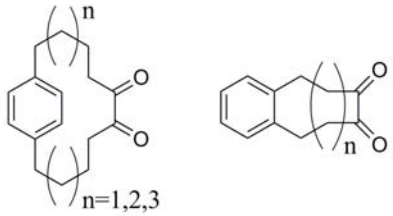

Figure 1.3. (a) The oligoproline system used by Stryer and Haugland to confirm the distance dependence (r^{-6}) for the Förster mechanism of energy transfer. The naphthyl moiety (C terminus) served as the energy donor, while the dansyl moiety (N terminus) served as the energy acceptor. (b) Two molecular systems used by Speiser and Katriel to determine the distance dependence (exponential) for the Dexter mechanism of energy transfer (n = 1, 2, 3). The benzyl moiety served as the energy donor, while the biacetyl moiety served as the energy acceptor.

ii. Photophysical properties of Ru^{II} and Os^{II} bipyridyl complexes

The polypyridyl complexes of ruthenium (Ru^{II}), and to a lesser extent osmium (Os^{II}), have been central to the study of excited-state energy transfer and solar energy conversion for many researchers due to a number of combined favorable properties including their: (a) relative chemical inertness in the ground state; (b) relatively long-lived excited state lifetimes; (b) useful redox properties in the excited sate; and (d) ease of synthesis with an often modular design.[3a,b]

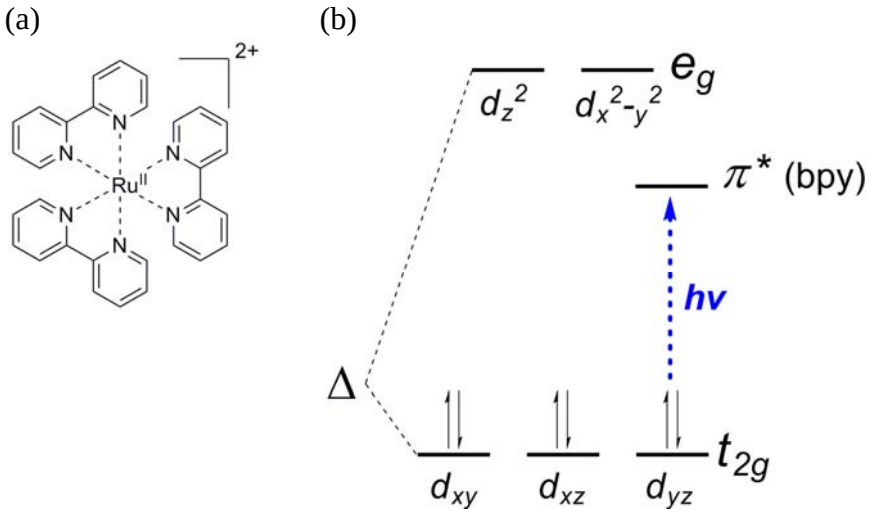

Figure 1.4. (a) The chemical structure of $Ru(bpy)_3^{2+}$, the tris(bipyridyl) ruthenium dication. (b) The ground-state electronic structure of $Ru(bpy)_3^{2+}$, including the filled t_{2g} orbitals (d_{xy}, d_{xz}, and d_{yz}) and empty e_g orbitals (dz^2 and d_x^2-$_y^2$). The electronic transition corresponding to the excitation of a t_{2g} electron to a π* orbital on the bipyridyl ligand (MLCT) is shown in blue.

The tris(bipyridyl) ruthenium cation ($Ru(bpy)_3^{2+}$) has served as the prototypical model for the study of excited-state energy transfer (Figure 1.4a).[13] Being a third row octahedral d^6 transition metal complex, with chelating ligands, $Ru(bpy)_3^{2+}$ is quite stable in the ground state. The crystal structure of $Ru(bpy)_3^{2+}$ shows a decreased Ru-N bond length (2.06 Å) when compared to the Ru-N bond length (2.10 Å) in $Ru(NH_3)_6^{3+}$.[14] Since the Ru^{II} ionic radius is expected to be larger than the Ru^{III} ionic radius, the apparent decrease in the Ru-N bond length indicates significant π-bonding between the filled Ru t_{2g} orbitals and the empty bipyridyl π* orbitals. The complex is kinetically stable towards racemization and ligand exchange, even at elevated temperatures, a property not similar to polypyridyl complexes of Fe.[15]

The excited state of interest for the $Ru(bpy)_3^{2+}$ dication arises through a metal-to-ligand charge transfer (MLCT) process whereby an electron occupying a t_{2g} orbital on Ru is transferred to a π* orbital localized on one of the bipyridyl ligands (Figure 1.4b). This MLCT

transition renders the complex a strong absorber of light in the visible region (λ_{max} = ~450 nm, ε = 13,000 in acetonitrile, ε = 14,600 in water).[13] The strong absorbance of light over a range of wavelengths in the blue region of the visible spectrum gives $Ru(bpy)_3^{2+}$ a characteristic red color. The MLCT band (λ_{max}) is slightly sensitive to solvent polarity, indicating some instantaneous shielding of the dipolar excited state by solvent molecules.[16] The initial absorption of a photon at 450 nm leads to a ^{1}MLCT state that undergoes intersystem crossing to the ^{3}MLCT state (Figure 1.5). Intersystem crossing is extremely rapid, requiring approximately 300 fs, and proceeding with a quantum yield (Φ_{ISC}) that is essentially unity.[17] Intersystem crossing occurs concomitantly with spin-allowed processes including vibrational relaxation and relaxation/reorientation of the solvent shell. Experiments using ultrafast absorption anisotropy measurements have shown that, while the $Ru(bpy)_3^{2+}$ excited-state electron is initially delocalized over all three bipyridyl ligands, localization of this electron on one of the bipyridyl ligands occurs within several hundred femtoseconds.[18]

The ^{3}MLCT state for $Ru(bpy)_3^{2+}$ may be the most extensively studied electronically excited molecule to date. The ^{3}MLCT excited state contains about 2.1 eV (~ 48 kcal·mol^{-1}) excess energy relative to the ground state, and actually exists as a manifold of triplet exited states that are mixed with higher-lying singlet excited states. An attractive feature for studying the $Ru(bpy)_3^{2+}$ (^{3}MLCT) excited state is its persistent lifetime, which is several hundred nanoseconds in water, and more than a microsecond in acetonitrile.[19] This slow decay back to the ground state has allowed for any number of energy and electron transfer phenomena to be studied. The excited-state lifetime of the molecular ion can be monitored using its phosphorescent emission (λ_{max} = ~630 nm).

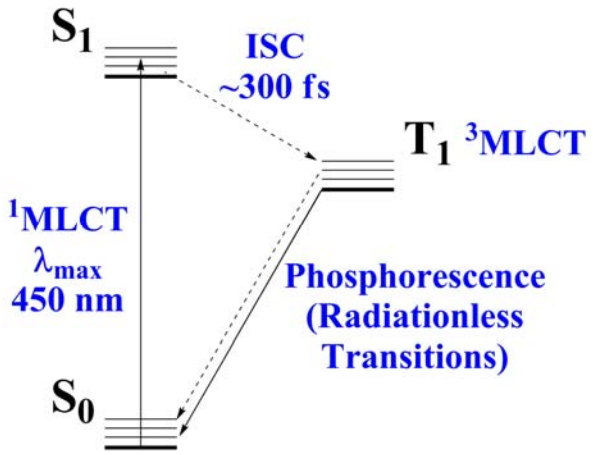

Figure 1.5 Jablonksi diagram showing all of the relevant photophysical events for $Ru(bpy)_3^{2+}$ excitation. Initial absorption of light at 450 nm produces a short lived ^{1}MLCT state. Intersystem crossing to the ^{3}MLCT state occurs within several hundred femtoseconds and has a quantum yield (Φ_{ISC}) close to unity. The ^{3}MLCT configuration can last several hundred nanoseconds and is the excited state of interest for many chemists. Relaxation from the ^{3}MLCT state occurs via a combination of phosphorescence (λ_{max} = ~630 nm) and radiationless transitions. The quantum yield for phosphorescence is typically less than 10% at room temperature, regardless of solvent.

The excess energy contained within the electronic configuration of the ^{3}MLCT state manifests as an increased willingness to undergo redox chemistry (Figure 1.6). Oxidation and reduction are disfavored for $Ru(bpy)_3^{2+}$ in the ground-state, but reducing and oxidizing potentials are both enhanced in the excited-state complex (Figure 1.6).[3b] The excited-state redox potentials for the $Ru(bpy)_3^{2+}$ molecular ion imply the thermodynamic ability to oxidize water ($E°$ (pH = 8) = -0.76 V), a property that has pushed the molecular ion into the artificial photosynthesis limelight.[3a] Also of high interest is the fact that the excited-state $Ru(bpy)_3^{2+}$ molecular ion has an energy appropriate for electron injection into wide-bandgap oxide semiconductors, including titanium dioxide (TiO_2).[20]

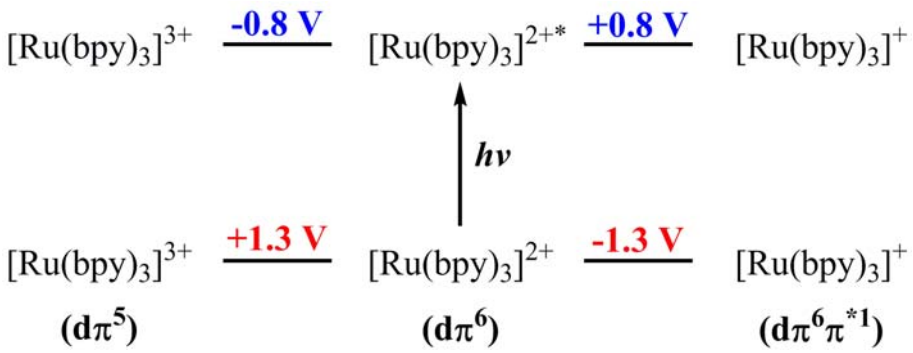

Figure 1.6. Latimer diagram showing the redox properties for the excited- and ground-state $Ru(bpy)_3^{2+}$ molecular ion. Values are reported for acetonitrile at 25 °C. The complex does not have a potent oxidizing or reducing potential in the ground state, but excitation to the ^{3}MLCT state results in favorable potentials for both oxidation and reduction.

The excited-state $Ru(bpy)_3^{2+}$ molecular ion is capable of not only electron transfer reactions, but also energy transfer phenomena if an appropriate acceptor is selected. A full account of energy transfer and electron transfer partners studied for $Ru(bpy)_3^{2+}$ would be needlessly long, but the tris(bipyridyl) osmium cation ($Os(bpy)_3^{2+}$) used throughout the current study deserves mention. The $Os(bpy)_3^{2+}$ molecular ion also absorbs light strongly in the visible region (λ_{max} = ~480 nm, ε = 12,000 in water) due to a ^{1}MLCT excitation band.[19] Unlike the ruthenium analog, $Os(bpy)_3^{2+}$ has a significant absorbance above 600 nm associated with the direct excitation to a triplet (^{3}MLCT) state. This normally optically forbidden transition is allowed for Os due to spin-orbit coupling in the heavier metal. The initial excited state dynamics of $Os(bpy)_3^{2+}$ are similar to $Ru(bpy)_3^{2+}$, with vibrational relaxation, solvent shell relaxation, and excited-state localization all occurring in a matter of femtoseconds.[21] The ^{3}MLCT state for $Os(bpy)_3^{2+}$ is, however, considerably lower in energy compared to ruthenium, and an increased Stokes shift for the complex (λ_{max} = ~730 nm) is apparent in the emission spectrum. The $Os(bpy)_3^{2+}$ molecular ion also has a much shorter excited-state lifetime (τ = 19 ns in water).[19] The ^{3}MLCT state for $Os(bpy)_3^{2+}$ is roughly 0.40

eV lower in energy compared to $Ru(bpy)_3^{2+}$ and can serve as an efficient energy transfer acceptor for the complex. Both Dexter and Förster energy transfer mechanisms are theoretically possible for Ru^{II} to Os^{II} energy transfer. Emission spectra for $Ru(bpy)_3^{2+}$ overlap with absorption spectra for $Os(bpy)_3^{2+}$ from 550-690 nm, a requirement for both mechanisms of energy transfer.[19] While the relaxation of the Ru^{II} ^{3}MLCT requires a spin flip that would normally be forbidden by Förster's predicted mechanism, spin-orbit coupling in the heavier Os atom could allow for triplet-triplet energy transfer to occur.

iii. Previous studies on energy transfer between Ru^{II} and Os^{II} bipyridyl complexes

Researchers have previously studied energy transfer between Ru^{II} and Os^{II} bipyridyl complexes attached to short covalent tethers,[4] high molecular weight polymers,[5] and complex oligonucleotides.[6] The coiled-coil peptide scaffold employed throughout this work has not been previously studied, and represents a very different chemical environment for studying energy transfer processes.

Furue and coworkers studied Ru^{II} to Os^{II} energy transfer by linking a series of bipyridyl complexes through short covalent tethers (Figure 1.7).[4] All of the heterobinuclear complexes exhibited intramolecular energy transfer based on a quenching of Ru^{II} emission at 610 nm that was accompanied by an enhancement in Os^{II} emission at 800 nm. Time-correlated single-photon counting (TCSPC) measurements indicated that Ru^{II} to Os^{II} energy transfer in these bridged complexes occurred with first-order rate constants varying from 1.2 x 10^8 to 1.2 x 10^9 s^{-1} in water (τ = 0.86 to 8.1 ns). Furue attributed energy transfer to a Förster-type mechanism based on the distance-dependence (to the inverse sixth power) observed for the quenching rates.

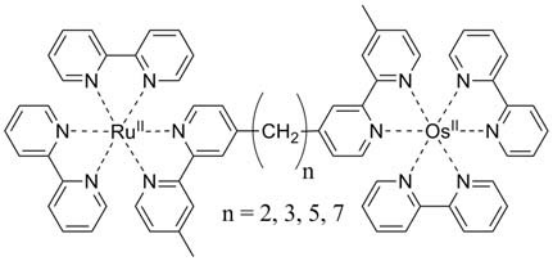

Figure 1.7 Covalently linked binuclear Ru^{II} and Os^{II} complexes used by Furue to study energy transfer. Excitation of the Ru^{II} center results in energy transfer to Os^{II}, as indicated by TCSPC experiments. The binuclear complexes exhibit first-order rate constants varying from 1.2×10^8 s^{-1} (n = 7) to 1.2×10^9 s^{-1} (n = 2) in water.

Meyer and coworkers have used a series of polystyrene-based polymers derivatized with bipyridyl complexes of Ru^{II} and Os^{II} to study energy transfer and light-harvesting phenomena (Figure 1.8).[5] The polymers typically contained 16 to 30 repeat units and were synthesized using specialized techniques. After polymerization, Ru^{II} and Os^{II} bipyridyl complexes were conjugated to the polystyrene molecules using different chemical methods. The authors showed that polystyrene molecules derivatized with ether linkages were efficient promoters of Ru^{II} to Os^{II} energy transfer with first-order rate constants greater than 2×10^8 s^{-1} ($\tau < 5$ ns) (Figure 1.8a).[23a] While Ru^{II} to Os^{II} excited-state energy transfer was fast in the ether-linked polymers, energy migration from Ru^{II} to Ru^{II} ($\Delta G = 0$) was comparably slow with measured rate constants less than 1×10^6 s^{-1}($\tau > 1$ μs). Polystyrene molecules derivatized with amide linkages had similar Ru^{II} to Os^{II} energy transfer rates, but vastly improved Ru^{II} to Ru^{II} energy migration rates (Figure 1.8b).[23c] The marked increase of the Ru^{II} to Ru^{II} energy migration rates (greater than 2×10^8 s^{-1}, similar to energy transfer rates) was attributed to the fact that in these amide-linked systems the charge transfer electron resides on the bipyridyl-amide ligand. In contrast to the ether-linked systems where the excited-state electron resides on an exterior bipyridyl ligand, the amide substituent orients the excited-state dipole towards the polymer backbone. Later generation polystyrene molecules

with mixed ligand designs were studied using ultrafast spectroscopy techniques (Figure 1.8c).[5e] The average rate of Ru^{II} to Ru^{II} energy migration in these systems was measured as 2.5 x 10^8 to 1.0 x 10^9 s^{-1} (τ = 1-4 ns), with Ru^{II} to Os^{II} energy transfer rates averaging to 2.5 x 10^9 s^{-1} (τ = 400 ps). Although this analysis indicated an efficient energy transfer to Os^{II} from a number of Ru^{II} donors, interpretation was difficult due to the statistical composition of the polymers. Specialized polymerization techniques were used to control the polydispersity (PDI = 1.08) of the samples, but some degree of nonhomogeneity for polymer length, donor/acceptor loading, and acceptor distribution were still typical. The authors use Monte Carlo simulations in order to rationalize donor/acceptor spacing and the energy transfer kinetics. A Dexter mechanism for energy transfer was discussed for these polymer systems based on the close donor/acceptor spacing predicted by molecular modeling. Any contribution from a through-bond superexchange mechanism was considered negligible due to the large number of intervening saturated bonds between donor/acceptor complexes. A Förster mechanism for energy transfer was also generally discounted due to the low degree of singlet character in the phosphorescent MLCT states for Ru^{II} (~11) and Os^{II} (~30%).

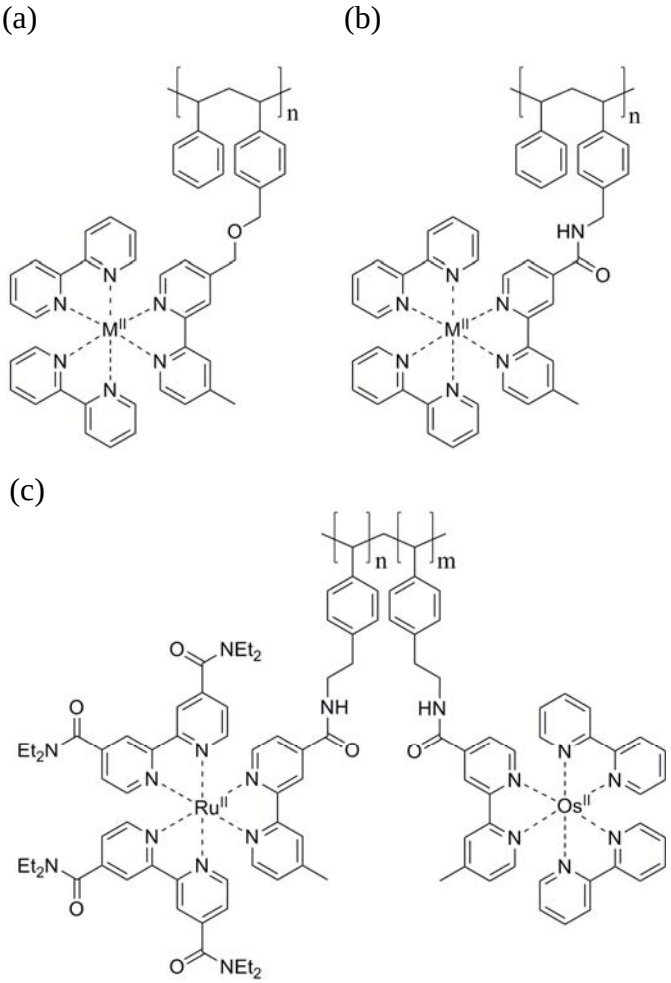

Figure 1.8. Polystyrene-based systems used to study energy transfer between Ru^{II} and Os^{II} (M^{II} = Ru^{II} and Os^{II}). (a) The ether-linked polymers are efficient promoters of Ru^{II} to Os^{II} energy transfer, but were less efficient at promoting Ru^{II} to Ru^{II} energy migration. (b) Second-generation amide-linked polymers were more efficient promoters of Ru^{II} to Ru^{II} energy migration. (c) Ru^{II} and Os^{II} derivatized polystyrenes with mixed bipyridyl ligand designs were later used to study energy migration/transfer dynamics using ultrafast time-resolved emission spectroscopy (ps-ns).

Tor and coworkers studied Ru^{II} to Os^{II} energy transfer in a series of modified oligonucleotides.[6] A series of ethynyl-linked and ethylene-linked bipyridyl complexes containing Ru^{II} and Os^{II} were developed for incorporation into DNA during standard solid-phase oligonucleotide synthesis (Figure 1.9). Tor performed a systematic study of Ru^{II} to Os^{II} energy transfer in a series of DNA duplexes in order to define the relationship between donor/acceptor distance and energy transfer efficiency. The donor/acceptor separation

distances were determined based on the helical model for B-form DNA. The ethynyl-linked bipyridyl complexes were designed to project the donor/acceptor complexes away from the DNA base stack (Figure 1.9a) since intercalation phenomena have a dramatic affect on energy transfer rates in similar systems.[22] The DNA duplexes incorporating the ethynyl-linked donor/acceptor complexes displayed a shallower distance dependence than would be expected for a Förster-type mechanism. As previously mentioned (Section B), the orientation factor for Förster energy transfer (κ^2) is typically assumed to be 2/3, although it has been shown that this approximation can lead to gross misinterpretation of energy transfer rates.[9] A series of DNA duplexes incorporating the ethylene-linked Ru^{II} donor were studied in an attempt to ameliorate any undesired orientation effects. Duplexes incorporating the more flexibly linked donor gave similar results however, and the observed distance dependence was again shallower than would be expected based on a Förster-type mechanism. The authors conclude that a Förster-type mechanism could account for a significant component of the observed energy transfer, with some contribution of "Dexter-like behavior" under certain circumstances. The simple helical model used to interpret the donor/acceptor distances in these systems may have provided a significant source of error, and the authors admit that end fraying, conformational changes, or other nondescript duplex dynamics may be the source of the anomalous distance-dependent behaviors. Tor excluded any role of the DNA duplex in mediating energy transfer beyond providing the structurally defined spatial organization. This conclusion was based on the observation that the ethynyl-linked and ethylene-linked bipyridyl complexes gave similar distance dependences. This conclusion is in contrast to the results of Barton and coworkers who demonstrated a significant role for the DNA duplex during energy transfer processes.[22]

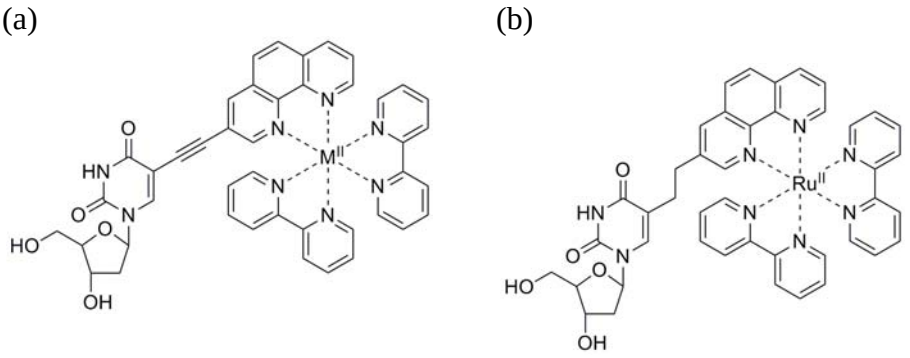

Figure 1.9 (a) Ethynyl-linked nucleosides containing Ru^{II} and Os^{II} bipyridyl complexes. The rigid alkyne bridge was designed to project the bipyridyl complexes away from the DNA base stack. (b) The ethylene-linked nucleoside containing Ru^{II} was designed to allow isotropic motion of the donor moiety prior to energy transfer.

C. Purpose of this work

We have studied Ru^{II} to Os^{II} energy transfer using a designed coiled-coil α-helical peptide scaffold. The positional dependence for energy transfer in these systems has been established and corroborated with the appropriate control experiments. The design of the coiled-coil scaffold used throughout this work is described in Chapter II. The synthetic techniques required to access these metallopeptides are described in Chapter III. The physical characterization of these metallopeptides, including binding constants required for interpretation during energy transfer studies, is described in Chapter IV. A full evaluation of the Ru^{II} to Os^{II} energy transfer behaviors for these coiled-coil metallopeptides, including the positional dependence, is described in Chapter V. A new strategy for attaching Ru^{II}-containing metallopeptides to nanocrystalline semiconductors, including TiO_2, is described in Chapter VI.

The ultimate goal for the development and study of these coiled-coil metallopeptides is to provide a new platform for the study of energy transfer. The coiled-coil peptide scaffold represents a new chemical environment for the study of Ru^{II} to Os^{II} energy transfer processes. We hope that this metallopeptide system will be used to further the understanding

of energy transfer mechanisms between Ru^{II} and Os^{II} bipyridyl complexes. The individual roles of synthetic chemists, spectroscopists, and theoreticians have never been truly discrete within the field of energy transfer study. We hope that our coiled-coil metallopeptide system will contribute to the field of energy transfer study in the same manner the research discussed throughout Chapter I already has.

References

[1](a) Nocera, D. G. *Chem. Soc. Rev.* **2009**, *38*, 13-15. (b) Hoffert, M. I.; Caldeira, K.; Jain, A. K.; Haites, E. F.; Harvey, L. D.; Potter, S. D. ; Schlesinger, M. E.; Schneider, S. H.; Watts, R. G.; Wigley, T. M.; Wuebbles, D. J. *Nature* **1998**, *395*, 881-884. (c) Bates, B. C.; Kundzewicz, Z. W.; Wu, S.; Palutikof, J. P. *Climate Change and Water. Technical Paper of the Intergovernmental Panel on Climate Change,* ed., IPCC Secretariat, Geneva, 210pp. (d) Lewis, N. S.; Nocera, D. G. *Proc. Natl. Acad. Sci. U.S.A.* **2006**, *103*, 15729-15735.

[2](a) Cherezov, V.; Clogston, J.; Papiz, M. Z.; Caffrey, M. *J. Mol. Biol.* **2006**, *357*, 1605-1618. (b) Ferreira, K. N.; Iverson, T. M.; Maghlaoui, K.; Barber, J.; Iwata, S. *Science*, **2004**, *303*, 1831-1838. (c) Jordan, P.; Fromme, P.; Witt, H. T.; Klukas, O.; Saenger, W.; Krauss, N. *Nature* **2001**, *411*, 909-917.

[3](a) Meyer, T. J. *Acc. Chem. Res.* **1989**, *22*, 163-170. (b) Alstrum-Acevedo, J. H.; Brennaman, M. K.; Meyer, T. J. *Inorg. Chem.* **2005**, *44*, 6802-6827. (c) Gust, D.; Moore, T. A.; Moore, A. L. *Acc. Chem. Res.* **2009**, *42*, 1890-1898. (d) Gust, D.; Moore, T. A. *Science* **1989**, *244*, 35-41.

[4](a) Furue, M.; Kinoshita, S.; Kushida, T. *Chem. Lett.* **1987**, 2355-2358. (b) Furue, M.; Yoshidzumi, T.; Kinoshita, S.; Kushida, T.; Nozakura, S.; Kamachi, M. *Bull. Chem. Soc. Jpn.* **1991**, *64*, 1632-1640. (c) Gholamkhass, B.; Nazaki, K.; Ohno, T. *J. Phys. Chem. B* **1997**, *101,* 9010-9021.

[5](a) Jones, Jr., W. E.; Baxter, S. M.; Strouse, G. F.; Meyer, T. J. *J. Am. Chem. Soc.* **1993**, *115*, 7363-7373. (b) Dupray, L. M.; Meyer, T. J. *Inorg. Chem.* **1996**, *35*, 6299-6307. (c) Dupray, L. M.; Devenney, M.; Striplin, D. R.; Meyer, T. J. *J. Am. Chem. Soc.* **1997**, *119*, 10243-10244. (d) Friesen, D. A.; Kajita, T.; Danielson, E.; Meyer, T. J. *Inorg. Chem.* **1998**, *37*, 2756-2762. (e) Fleming, C. N.; Maxwell, K. A.; DeSimone, J. M.; Meyer, T. J.; Papanikolas, J. M. *J. Am. Chem. Soc.* **2001**, *123*, 10336-10347.

[6](a) Hurley, D. J.; Tor, Y. *J. Am. Chem. Soc.* **1998**, *120*, 2194-2195. (b) Hurley, D. J.; Tor, Y. *J. Am. Chem. Soc.* **2002**, *124*, 3749-3762. (c) Hurley, D. J.; Tor, Y. *J. Am. Chem. Soc.* **2002**, *124*, 13231-13241.

[7]Förster, Th. *Discuss. Faraday Soc.* **1959**, *27*, 7-17.

[8]Dexter, D. L. *J. Chem. Phys.* **1953**, *21*, 836-850.

[9]Iqbal, A.; Arslan, S.; Okumus, B.; Wilson, T. J.; Giraud, G.; Norman, D. G.; Ha, T.; Lilley, D. M. J. *Proc. Natl. Acad. Sci. U.S.A.* **2008**, *105*, 11176-11181.

[10]Speiser, S. *Chem. Rev.* **1996**, *96*, 1953-1976.

[11]Stryer, L.; Haugland, R. P. *Proc. Natl. Acad. Sci. U.S.A.* **1967**, *58*, 719-726.

[12]Speiser, S.; Katriel, J. *Chem. Phys. Lett.* **1983**, *102*, 88-94.

[13]Juris, A.; Balzani, V.; Barigelletti, F.; Campagna, S.; Belser, P.; Von Zelewski, A. *Coord. Chem. Rev.* **1988**, *84*, 85-277.

[14]Rillema, D. P.; Jones, D. S.; Levy, H. A. *J. Chem. Soc., Chem. Commun.* **1979**, 849-851.

[15]Brandt, W. W.; Dwyer, F. P.; Gyarfas, E. D. *Chem. Rev.* **1954**, *54*, 959-1017.

[16]Kober, E. M.; Sullivan, B. P.; Meyer, T. J. *Inorg. Chem.* **1984**, *23*, 2098-2104.

[17](a) Demas, J. N.; Crosby, G. A. *J. Am. Chem. Soc.* **1971**, *93*, 2841-2847. (b) Damrauer, N. H.; Cerullo, G.; Yeh, A.; Boussie, T. R.; Shank, C. V.; McCusker, J. K. *Science* **1997**, *275*, 54-57.

[18]Yeh, A. T.; Shank, C. V.; McCusker, J. K. *Science* **2000**, *289*, 935-938.

[19]Creutz, C.; Chou, M.; Netzel, T. L.; Okumura, M.; Sutin, N. *J. Am. Chem. Soc.* **1980**, *102*, 1309-1319.

[20](a) Clark, W. D. K.; Sutin, N. *J. Am. Chem. Soc.* **1977**, *66*, 4276-4282. (b) Desilvestro, J.; Grätzel, M.; Kavan, L.; Moser, J. *J. Am. Chem. Soc.* **1985**, *107*, 2988-2990. (c) Vlachopoulos, N.; Liska, P.; Augustynski, J.; Grätzel, M. *J. Am. Chem. Soc.* **1988**, *110*, 1216-1220.

[21]Shaw, G. B.; Brown, C. L.; Papanikolas, J. M. *J. Phys. Chem. A.* **2002**, *106*, 1483-1495.

[22]Homlin, R. E.; Tong, R. T.; Barton, J. K. *J. Am. Chem. Soc.* **1998**, *120*, 9724-9725.

Chapter II

DESIGN OF α-HELICAL COILED-COILS FOR THE STUDY OF ENERGY TRANSFER BETWEEN RU^{II} AND OS^{II} BIPYRIDYL COMPLEXES

A. General design principles for coiled-coil peptides

The coiled-coil structural motif is comprised of multiple α-helical peptides wrapped around each other in a left-handed supercoiled arrangement.[1] Coiled-coil domains typically contain between two and seven α-helical peptide segments and are perhaps the most widely studied group of protein structural units (Figure 1.1). A significant portion of what we know about natural protein folding behavior has been established based on the exhaustive study of thermodynamic driving forces and structure-determining elements for coiled-coil association.[2] Coiled-coil assemblies now represent arguably the most complex class of *de novo* designed proteins.[3] Different coiled-coil motifs hold promise for application in affinity tagging, surface functionalization, supramolecular chemistry, and biotechnology applications including tissue engineering.[4,5]

The coiled-coil motif was originally identified by Francis Crick to be the primary structural element of α-keratin, the well known scleroprotein .[6] At the time, several researchers had identified that α-helices, the common secondary structural element discovered by Linus Pauling only one year earlier,[7] constituted an important part of α-keratin. Crick realized that certain X-ray diffraction patterns for α-keratin could only be

rationalized if the α-helical segments present in α-keratin were tilted and wrapped around each other in a tangled arrangement.[6] Crick also put forth a simple model for coiled-coil sidechain packing arrangements known as the "knobs-into-holes" rationale that is still the currently accepted model. Since that initial discovery, coiled-coil structures have been identified in any number of proteins including transcription factors that regulate gene expression,[8] chaperone proteins that promote the correct folding of other proteins,[9] and actin-binding proteins that regulate muscle contraction.[10]

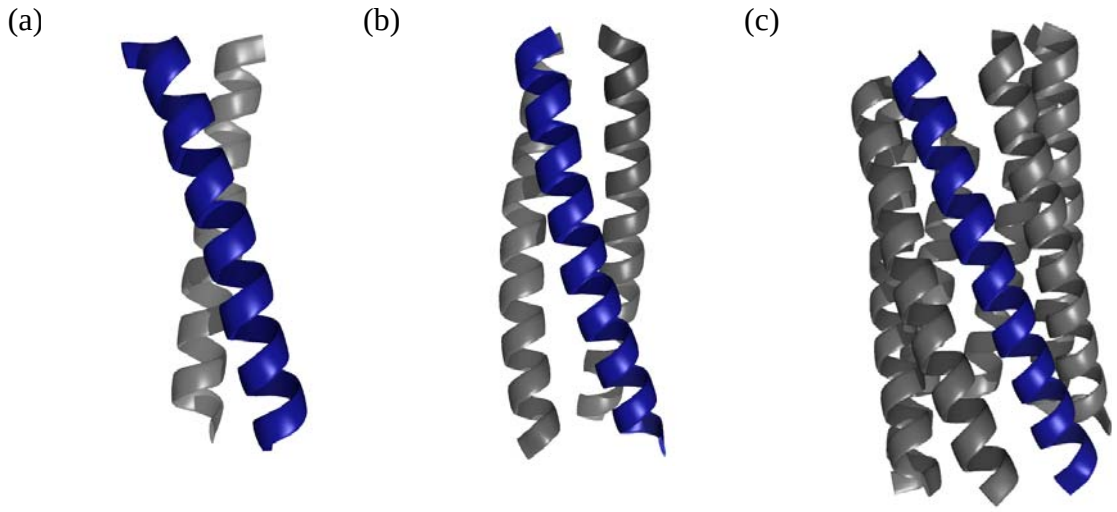

Figure 2.1. Crystal structures are shown for several coiled-coil peptides indicating the variety of oligomerization states available. (a) A dimeric coiled-coil structure (pdb code: 1A93). (b) A trimeric coiled-coil structure (pdb code: 3GJP). (c) A heptameric coiled-coil structure (pdb code: 2HY6). A single α-helical subunit in each structure is highlighted in blue for clarity.

All of the coiled-coil structures described to date, both natural and synthetically designed, contain a common seven residue repeating sequence known as a heptad unit.[1] The amino acid positions of the heptad unit are typically designated with the letters ***a, b, c, d, e, f,*** and ***g***. This common heptad repeat sequence is a consequence of the α-helical structures found within coiled-coil subunits. Since α-helices have approximately 3.6 residues per turn, an amino acid residue will repeat along the vertical axis of the helix every seven residues.

Placing hydrophobic residues at the ***a*** and ***d*** positions (first and fourth within the heptad) creates a highly nonpolar surface that provides the primary driving force for association via solvent exclusion. Ile and Leu residues are often specifically chosen for the ***a*** and ***d*** sites, respectively, when a parallel dimeric coiled-coil structure is desired.[11] β-Branched aliphatic residues at the ***a*** positions (typically Val or Ile), in combination with Leu residues at the ***d*** positions, are superior promoters for parallel dimeric structures due to geometric packing requirements.[11] The intermolecular interactions that commonly stabilize the coiled-coil structure can be schematically represented using a helical wheel diagram (Figure 1.2a).

Amino acids corresponding to the ***e*** and ***g*** positions are directly adjacent to the coiled-coil interface and are capable of making secondary interactions during folding (Figure 1.2a,c). These positions are typically designed (or evolved) with oppositely charged residues, most often Lys and Glu, in order to provide complementary charge-charge interactions.[12] These residue positions not only serve to positively reinforce a desired folding pattern, but additionally serve as negative control elements since many undesired folding arrangements may be disfavored by charge-charge repulsions.[12] The remaining ***b***, ***c***, and ***f*** positions within a coiled-coil structure do not typically provide favorable interhelix interactions (Figure 1.2a). These residues are typically hydrophilic in nature and serve to reinforce the general amphipathic nature of the coiled-coil. High helical propensity is quite common, but not absolutely required, for most amino acids in coiled-coil structures. Based on the previously described design principles, it is of no surprise that Gly, Cys, and Pro occur much less frequently the coiled-coil secondary structure when compared to protein sequences in general.[2]

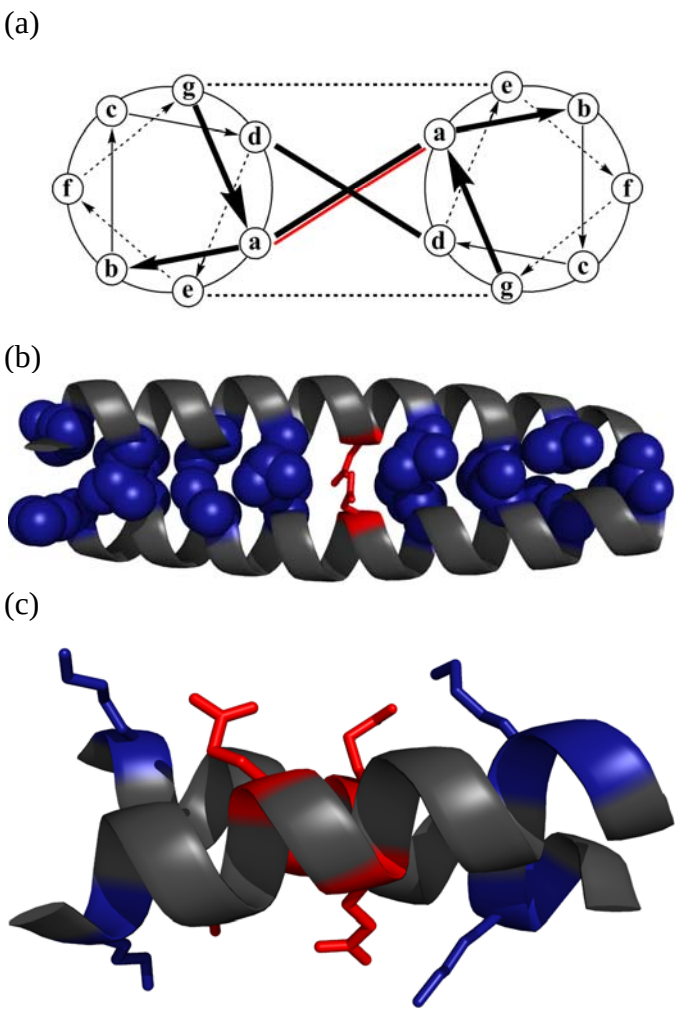

Figure 2.2. (a) A typical helical wheel diagram used to represent the stabilizing forces present in a dimeric coiled-coil. Hydrophobic contacts (between ***a*** and ***d*** positions) are shown as solid black lines. Salt bridges between charged residues (***e*** and ***g***) are shown as dashed lines. The single solid red line represents the Asn-Asn hydrogen bond present within a single ***a*** layer of the coiled-coil. (b) Crystal structure (pdb code: 2ZTA) showing the hydrophobic packing arrangement of the ***a*** and ***d*** positions (blue spheres). The hydrogen bonded Asn-Asn pair is also shown (red stick model). Amino acid sidechains are only shown for ***a*** and ***d*** position amino acids in order to improve clarity. (c) Two heptads of the crystal structure (structure was truncated and rotated 90° along the longitudinal axis of the coiled-coil) are shown in order to highlight four distinct salt bridges. All four ionic interactions are made between Lys (blue) and Glu (red).

Perhaps the most important negative design principle that has been established for coiled-coil sequences is the selective inclusion of buried polar residues within the hydrophobic interface. Like most coiled-coil design principles, the strategy is based on

observations of natural coiled-coil domains in proteins.[13] Polar residues, such as Asn, when included at two complementary ***a*** positions must satisfy their hydrogen bonding potential, and impart folding specificity through mutual alignment (Figure 1.2a,b). Although the incorporation of two asparagine residues within the hydrophobic core of a parallel coiled-coil dimer interface is slightly destabilizing, alternative arrangements required for the undesired structures including trimers, tetramers, antiparallel dimers, and misaligned dimers are far more destabilizing. [13] Oakley and Kim were able to measure an energetic cost of 2.3 kcal·mol^{-1} for the antiparallel alignment of two sequences including Asn at complementary ***a*** positions.

B. Previous work of interest using coiled-coil peptides

A coiled-coil structure has not previously been used to study the mechanism or distance dependence of energy transfer between Ru^{II} and Os^{II} bipyridyl complexes. Ogawa and coworkers studied both ground state and photoexcited state electron transfer in a series of dimeric coiled-coil peptides.[14] These designed metallopeptides were typically constructed using ruthenium pentaammine [$Ru(NH_3)_5$-] derivatized His residues as electron donors and ruthenium polypyridyl ([Ru(bpy)(Im)-], [Ru(trpy)(bpy)-], or [$Ru(bpy)_2$(phen)-]) derivatized His residues as electron acceptors. Ogawa's work demonstrated that peptide primary sequence and secondary structure can be used to direct intermolecular electron transfer between dimers.[14c] Ogawa also showed that biomimetic electron transfer could be directed across the hydrophobic interface within a single coiled-coil metallopeptide.[14b] Ogawa used similarly designed coiled-coil metallopeptides to probe the effects of α-helix dipole on intramolecular electron transfer, but was unable to determine an effect on rate due to the coiled-coil macrodipole.[14e]

Ogawa's examples of intradimer electron transfer all employed nonspecific homodimeric coiled-coil sequences. The peptides were chemically derivatized differentially, but peptide primary sequence was identical and was not designed to favor donor/acceptor assembly. As a result, these donor/acceptor mixtures contained statistical quantities of the desired donor/acceptor partners along with undesired partners (donor/donor and acceptor/acceptor) incapable of electron transfer behavior.

Ogawa investigated a *heterodimer* metallopeptide system, presumably in order to induce a more specific donor/acceptor interaction.[14c] The designed heterodimer contained Glu residues at all of the ***e*** and ***g*** positions within one peptide sequence, and Lys residues within all of the ***e*** and ***g*** positions of the complementary sequence. As previously described, this arrangement favors a partnering of the heterodimer with complementary charge-charge interactions, but disfavors homodimers where significant repulsions between like charges will result. Interestingly, electron transfer in this designed heterodimer did not occur across the coiled-coil scaffold, but instead occurred between coiled-coil heterodimers in solution. This drastic change in behavior was attributed to complementary charges surrounding the donor/acceptor complexes on the exterior surfaces of the heterodimer. None of Ogawa's coiled-coil sequences included an Asn-Asn interaction as a negative control feature.

C. Current system design

A designed heterodimeric coiled-coil structure was selected as the scaffold for studying energy transfer in the current system. The primary sequences were adopted and modified from the heterodimeric self-assembled fiber (SAF) system originally reported by Woolfson and coworkers (Figure 1.3a).[15] Woolfson's SAF peptides were designed with a primary sequence meant to provide complementary interactions that promote a staggered

heterodimer structure referred to as the “sticky-ends” design (Figure 1.3b).[15] These staggered interactions, or “sticky ends”, promote dimer-dimer association and subsequent fiber formation. The P1 and P2 peptides are both 28 residue sequences, and the P2 peptide remains unchanged from several of Woolfson’s publications.[15b-e] Both peptide sequences contain two positively charged heptad repeat units (Lys at all ***e*** and ***g*** positions) and two negatively charged heptad repeat units (Glu at every ***e*** and ***g*** position). The P1 peptide has these charged heptads rearranged from Woolfson’s sequence in order to discourage longitudinal association, and therefore fiber formation (Figure 1.3a). Natural coiled-coil peptides all share this “blunt” end assembly. Woolfson demonstrated that this simple permutation fails to oligomerize beyond the dimer state, and therefore does not form fibers.[15a] As previously described, Asn substitutions at ***a*** positions play a critical role within both systems. These substitutions prevent the two peptides from associating in an antiparallel fashion, an undesired arrangement where charge-charge interactions would remain favorable.

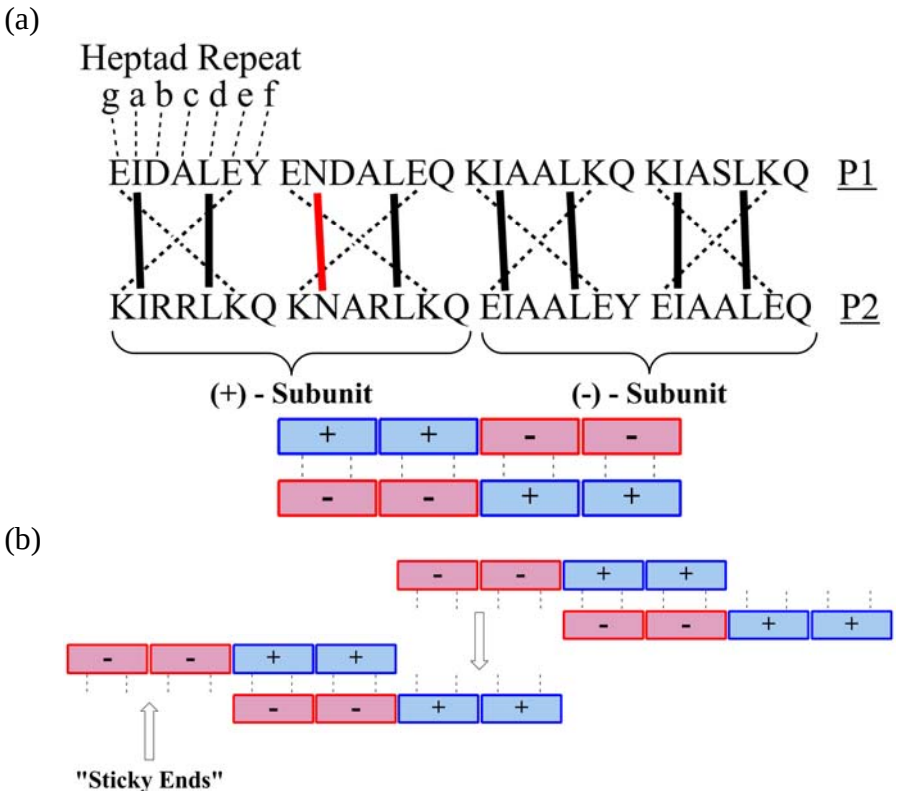

Figure 2.3 (a) The primary sequences for the P1 and P2 peptides are given using single letter amino acid codes in capitals. The letter designations for the heptad positions are labeled (lower case) for the first heptad only. Hydrophobic contacts made by Ile and Leu residues are represented as solid black lines. The hydrogen bonded Asn-Asn brace is represented as a red line. The complementary charge-charge interactions between Lys and Glu residues are represented as dashed lines. For a schematic representation of these interactions see Figure 1.2a. The "blunt" ends assembly pattern that the P1 and P2 peptide sequences produces is also represented as a simple diagram below the primary sequences. (b) The "sticky-ends" assembly produced by Woolfson's original sequence is schematically represented.

D. Conclusions for the system design

The P1 and P2 sequences were selected in order to form the most desirable coiled-coil structures suitable for the study of energy transfer. The heterodimeric design was chosen to favor conditions where donor/acceptor structures can be easily examined with minimal influence due to homodimer formation. The sequences contain both positively charged and negatively charged heptad repeat units, so no single electrostatic potential dominates the surfaces of either peptide. Because studying the mechanisms, including any observable

position dependence, was the governing intent of this research, two Asn residues are included in order to enforce the alignment of the two peptides. This strict conformational preference should make the identification of any position dependence simpler, since subtle yet undesired conformational isomers will be strongly discouraged.

Woolfson's established route towards micro-feature protein fibers served as further encouragement for the selection of this sequence. It was anticipated that if an efficient energy transfer system were developed on the molecular level, it could potentially be expanded towards functional materials for use as light harvesting antennae in solar cells and artificial photosynthetic constructs.[15e]

The coiled-coil peptide structure represents an interesting, and previously uninvestigated, scaffold for studying energy transfer between Ru^{II} and Os^{II} containing bipyridyl complexes. A multitude of positions could have potentially been modified for the study of energy transfer. The P1 peptide was ultimately modified with an Os^{II} bipyridyl complex at the 2*c*, 2*f*, and 2*g* positions in order to study energy transfer. The Os^{II}-containing metallopeptides are referred to as 2*c*-Os, 2*f*-Os, and 2*g*-Os throughout the rest of the report. The P2 peptide was similarly modified with a Ru^{II} bipyridyl complex at the 2*b*, 2*e*, and 2*f* positions in order to produce the 2*b*-Ru, 2*e*-Ru, and 2*f*-Ru metallopeptides. The development of the chemistry used to modify the coiled-coil scaffold and synthesize the metallopeptides is described in Chapter III. The choice of substitution positions and how they relate to both coiled-coil structure and the study of energy transfer is described in Chapter IV. The metallopeptides exhibit position-dependent energy transfer behavior that is related to their design and structure. The full characterization of this position-dependent energy transfer is described in detail within Chapter V.

References

[1]Mason, J. M.; Arndt, K. M. *Chem. Bio. Chem.* **2004**, *5*, 170-176.

[2]Woolfson, D. K. *Adv. Protein Chem.* **2005**, *70*, 79-112.

[3]DeGrado, W. F.; Summa, C. M.; Pavone, V.; Nastri, F.; Lombardi, A. *Annu. Rev. Biochem.* **1999**, *68*, 779-819.

[4]O'Shea, E. K.; Lumb, K. J.; Kim, P. S. *Curr. Biol.* **1993**, *3*, 658-667.

[5]Smith, A. M.; Banwell, E. F.; Edwards, W. R.; Padya, M. J.; Woolfson, D. N. *Adv. Funct. Mater.* **2006**, *16*, 1022-1030.

[6]Crick, F. H. C. *Nature* **1952**, *170*, 882-883.

[7]Pauling, L.; Corey, R. B.; Branson, H. R. *Proc. Nat. Acad. Sci., U.S.A.* **1951**, *37*, 205-211.

[8]König, P.; Richmond, T. J. *J. Mol. Biol.* **1993**, *233*, 139-154.

[9]Siegert, R.; Leroux, M. R.; Scheufler, C.; Hartl, F. U.; Moarefi, I. *Cell* **2000**, *103*, 621-632.

[10]Holtzer, A.; Holtzer, M. E. *Macromolecules* **1987**, *20*, 671-675.

[11](a) O'Shea, E. K.; Klemm, J. D.; Kim, P. S.; Alber T. *Science* **1991**, *254*, 539-544. (b) Harbury, P. B.; Zhang, T.; Kim, P. S.; Alber, T. *Science* **1993**, *262*, 1401-1407. (c) Woolfson, D. N.; Alber, T. *Protein Sci.* **1995**, *4*, 1596-1607.

[12](a) O'Shea, E. K.; Rutkowski, R.; Kim, P. S. *Cell* **1992**, *68*, 699-708. (b) Kohn, W. D.; Kay, C. M.; Hodges, R. S. *J. Mol. Biol.* **1998**, *283*, 993-1012. (c) Litowski, J. R.; Hodges, R. S. *J. Biol. Chem.* **2002**, *277*, 37272-37279. (d) Zhou, N. E.; Kay, C. M.; Hodges, R. S, *J. Mol. Biol.* **1994**, *237*, 500-512.

[13](a) Lumb, K. J.; Kim, P. S. *Biochemistry* **1995**, *34*, 8642-8648. (b) Oakley, M. G.; Kim, P. S. *Biochemistry* **1998**, *37*, 12603-12610. (c) Gonzales, L., Jr.; Woolfson, D. N.; Alber, T. *Nat. Struct. Biol.* **1996**, *3*, 1011-1018.

[14](a) Kozlov, G. V.; Ogawa, M. Y. *J. Am. Chem. Soc.* **1997**, *119*, 8377-8378. (b) Kornilova, A. Y.; Wishart, J. F.; Xiao, W.; Lasey, R. C.; Fedorova, A.; Shin, Y.-K.; Ogawa, M. Y. *J. Am. Chem. Soc.* **2000**, *122*, 7999-8006. (c) Kornilova, A. Y.; Wishart, J. F.; Ogawa, M. Y. *Biochemistry* **2001**, *40*, 12186-12192. (d) Fedorova, A.; Ogawa, M. Y. *Bioconjugate Chem.* **2002**, *13*, 150-154. (e) Fedorova, A.; Chaudhari, A.; Ogawa, M. Y. *J. Am. Chem. Soc.* **2003**, *125*, 357-362. (f) Hong, J.; Kharenko, O. A.; Ogawa, M. Y. *Inorg. Chem.* **2006**, *45*, 9974-9984.

[15](a) Pandya, M. J.; Spooner, G. M.; Sunde, M.; Thorpe, J. R.; Rodger, A.; Woolfson, D. N. *Biochemistry* **2000**, *39*, 8728-8734. (b) Ryadnov, M. G.; Woolfson, D. N. *Nat. Mater.* **2003**, *2*, 329-332. (c) Ryadnov, M. G.; Woolfson, D. N. *Angew. Chem., Int. Ed. Engl.* **2003**, *42*, 3021-3023. (d) Ryadnov, M. G.; Woolfson, D. N. *J. Am. Chem. Soc.* **2004**, *126*, 7454-7455. (e) Mahmoud, Z. N.; Gunnoo, S. B.; Thomson, A. R.; Fletcher, J. M.; Woolfson, D. N. *Biomat.* **2011**, *32*, 3712-3720.

Chapter III

SYNTHESIS OF METALLOPEPTIDES

A. Synthesis of $[Ru(bpy)_3]^{2+}$- and $[Os(bpy)_3]^{2+}$-containing metallopeptides

i. Background for $[Ru(bpy)_3]^{2+}$- and $[Os(bpy)_3]^{2+}$-containing amino acids

A number of redox-active amino acids containing Ru^{II} and Os^{II} bipyridyl complexes have previously been reported.[1] Meyer and coworkers developed a method for the acylation of lysine at the ε-N using bipyridyl-4-carboxylic acid complexes of Ru^{II} and Os^{II} (Figure 3.1a).[1a] The $[Ru(bpy)_3]^{2+}$-modified lysine complex could be incorporated into polyalanine α-helices and other simple peptides for the study of photoinduced electron transfer. Geisser and coworkers extended this method to prepare shorter chemical analogs with fewer methylene spacers (Figure 3.1b).[1b] Kise and Bowler developed a method for synthesizing a $[Ru(bpy)_3]^{2+}$-containing amino acid with a single methylene group linking the bipyridyl complex to the amino acid α-carbon (Figure 3.1c).[1c,d] Their method relied on a cinchonidinium bromide catalyst under phase-transfer conditions. The $[Ru(bpy)_3]^{2+}$-containing amino acid developed by Kise and Bowler could also be incorporated into α-helices, although specialized coupling conditions were required. Meyer and coworkers also prepared several $[Ru(bpy)_3]^{2+}$-containing proline derivatives for incorporation in polyproline helices, another common type of protein secondary structure.[1e] All of the amino acid derivatives discussed are convenient because they can be incorporated into metallopeptides

in a site-specific manner using routine solid-phase peptide synthesis (SPPS) protocols. Common drawbacks for these amino acid derivatives include the need for longer coupling times, more exotic coupling reagents, and often diminished yields relative to standard amino acids. All of these redox-active amino acids suffer from the fundamental drawback that they can only be used in the context of linear synthetic approaches.

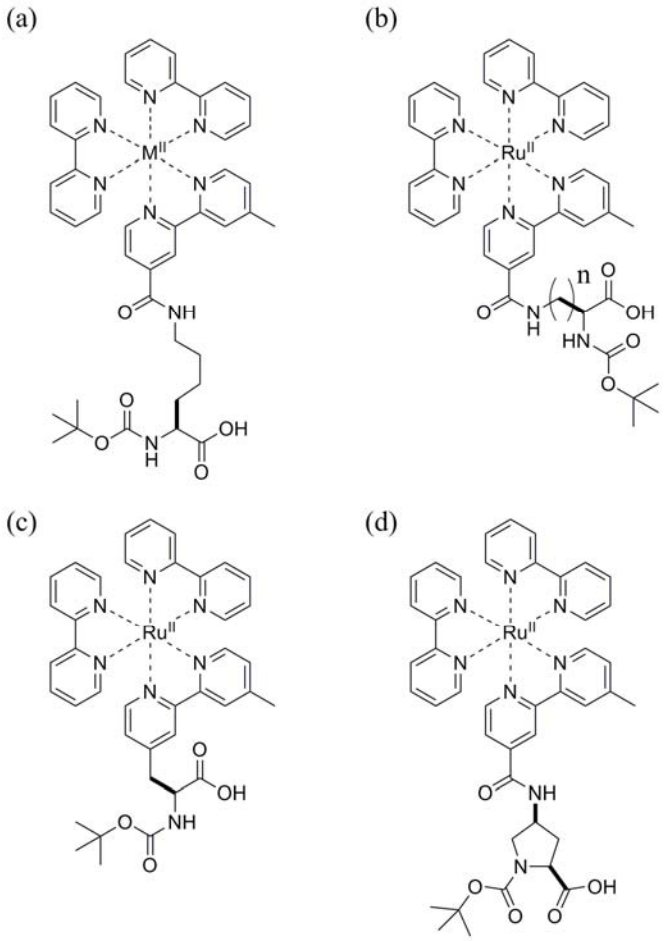

Figure 3.1. Previously reported redox-active amino acids. (a) Meyer and coworkers developed procedures for preparing $[Ru(bpy)_3]^{2+}$- and $[Os(bpy)_3]^{2+}$-containing lysine derivatives (M^{II} = Ru^{II} or Os^{II}). (b) Geisser and coworkers prepared similar (Ru^{II} only) amino acids with shorter linkers (n = 1, 2, and 3). (c) Kise and Bowler developed a $[Ru(bpy)_3]^{2+}$-containing amino acid with a single methylene group as the linker to the amino acid backbone. (d) Meyer and coworkers also developed a $[Ru(bpy)_3]^{2+}$-containing proline derivative.

Meyer's method of employing ε-N derivatized lysine amino acids was anticipated to be the most amenable for incorporating Ru^{II} and Os^{II} bipyridyl complexes in coiled-coil peptide structures. As discussed in Chapter II, a $[Ru(bpy)_3]^{2+}$-containing proline would almost certainly be destabilizing towards a coiled-coil peptide structure due to the inherently low helix propensity of the amino acid proline. The shorter amino acids (Figure 3.1b,c) were also initially disregarded due to the potentially destabilizing effect they may have on the coiled-coil peptide structure. To the best of our knowledge, all reported $[Ru(bpy)_3]^{2+}$-containing amino acids are Boc-protected at the α-N for use with Boc/benzyl synthetic strategies.

ii. Synthesis of $[Ru(bpy)_3]^{2+}$- and $[Os(bpy)_3]^{2+}$-containing Fmoc-lysine derivatives

Ru^{II}- and Os^{II}-containing Fmoc-protected amino acids were developed for use with Fmoc-based synthetic strategies. Fmoc-based SPPS does not require the use of anhydrous hydrofluoric acid, or the specialized equipment associated with it, in order to cleave peptide products from the solid support,.[2] Fmoc-based chemistry is generally considered safer compared to Boc-based SPPS chemistry for these reasons.

The developed synthetic strategy started with the commercially available ligand, 4,4'-dimethyl-2,2'-dipyridine (**1**) (Figure 3.2). Selective oxidation of **1** to the monoaldehyde (**2**) using selenium dioxide, has been reported by Bergstrom and by Peek.[3a,b] Oxidation to the carboxylic acid (**3**) can be affected using silver oxide.[3b] The succinimidyl ester can be produced using standard coupling conditions (**4**).[3c] Diisopropylcarbodiimide was typically the coupling reagent of choice, although DCC or EDC could both be used as well. The succinimidyl ester could subsequently be reacted with α-N-Fmoc-L-lysine in order to produce the desired bipyridyl ligand (**5**). Reaction of **5** with either $Ru(bpy)_2Cl_2$ or

$Os(bpy)_2Cl_2$ by heating at reflux in H_2O/EtOH (1:1, v:v) yielded the desired Ru^{II}- and Os^{II}-containing Fmoc-protected amino acids **6a** and **6b**, respectively.[4] The amino acids were typically isolated as the hexafluorophosphate salts in good yield.

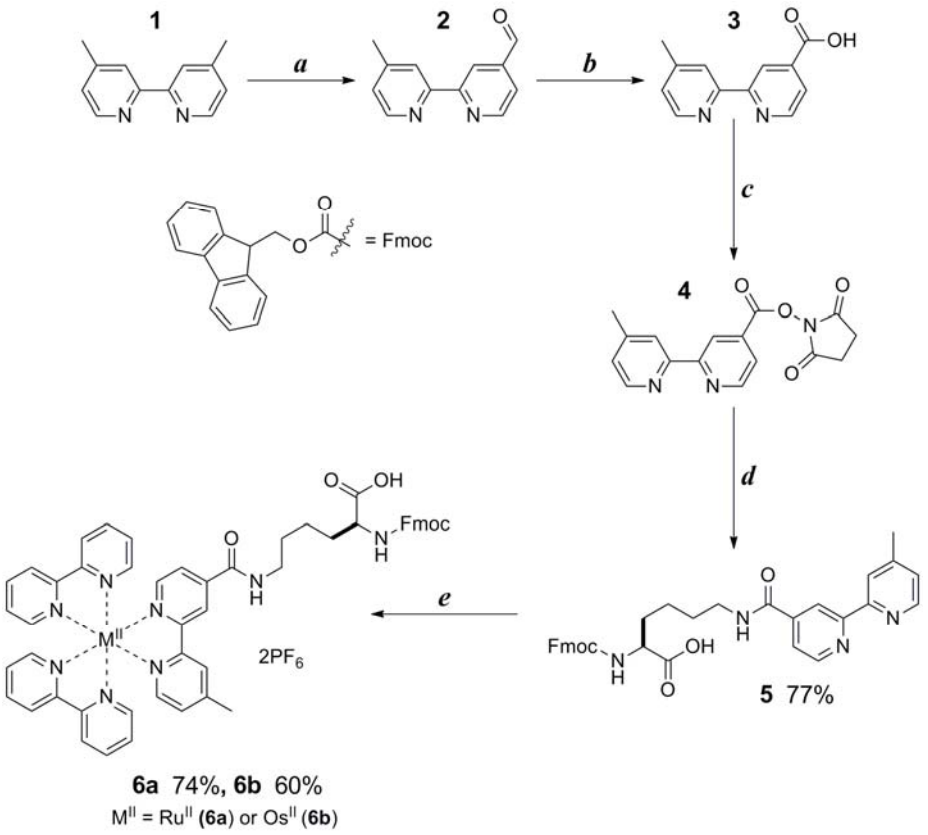

Figure 3.2 Synthesis of Fmoc-protected amino acids containing both Ru^{II} and Os^{II} bipyridyl complexes (**6a**, **6b**). Conditions: (a) SeO_2 (1.01 equiv), 1,4-dioxane, 100 °C, 24 hours. (b) $AgNO_3$ (1.1 equiv), NaOH, H_2O/EtOH, RT, 15 hours. (c) N-Hydroxysuccinimide (1.0 equiv), DIC (1.2 equiv), DMF, 8 hours. (d) α-N-Fmoc-L-Lysine (1.1 equiv), N-methylmorpholine (2.5 equiv), DMF, RT, 6 hours (77%). (e) $Ru(bpy)_2Cl_2$ or $Os(bpy)^2Cl^2$, H_2O/EtOH, 90 °C, HPF_6 (**6a** 70%, **6b** 60%).

The amino acids **6a** and **6b** could be incorporated into metallopeptides during standard SPPS using procedures typical for Fmoc-protected amino acids. Yields for metallopeptides synthesized in this manner were somewhat lower compared to peptides containing only the canonical amino acids. Multiple attempts were made to couple the redox-active Fmoc-protected amino acids using HATU at 50 °C. Although this procedure had been

useful for other researchers trying to couple large $[Ru(bpy)_3]^{2+}$-containing amino acids, in the authors hands it produced no noticeable improvement in peptide yield.[1c] Fmoc-deprotection reactions are typically performed under highly basic conditions in the presence of nucleophilic scavenger for dibenzofulvene.[2] Piperidine can serve as both base and scavenger in these reactions. After the coupling of **6b**, washing the SPPS resin did not lead to any coloring of the wash solvent after several wash aliquots. However, it was observed that solutions used for the deprotection reactions became slightly colored in a manner characteristic to Os^{II} bipyridyl complexes. This observation was apparent whether deprotection reactions were performed using 20% piperidine or 2% piperidine/2% DBU. Despite the high level of kinetic stability reported for Ru^{II} and Os^{II} bipyridyl compounds (Chapter I),[5] it is not unreasonable to conclude that inefficiencies observed when trying to incorporate **6a** or **6b** during SPPS resulted from an intolerance to the deprotection reaction conditions, and not from incomplete coupling reactions. This conclusion is supported by reports from other researchers who employed similar coupling condition for the incorporation of sterically hindered $[Ru(bpy)_3]^{2+}$-containing amino acids, but did not require Fmoc-deprotection during synthesis.[1c]

The metallopeptides 2*f*-Os* and 2*f*-Ru* were synthesized by incorporating **6b** and **6a**, at the 2f positions within P1 and P2, respectively. The asterisk label is used to differentiate these metallopeptides from those described below which contain different linkers to the peptide scaffold. Although the 2*f*-Os* and 2*f*-Ru* peptides did form stable coiled-coil structures, this approach towards synthesizing metallopeptides was abandoned for the more convergent synthetic strategy described below.

iii. Development of the CuAAC reaction for synthesizing metallopeptides

A convergent synthetic strategy allows peptide, chemical linker, and bipyridyl complex to be easily varied for systematic optimization and study. The criteria for a convergent synthetic strategy were considered as follows: (1) is the synthetic process high yielding?; (2) is the process orthogonal to the chemistry normally used to synthesize peptides (e.g. SPPS conditions)?; (3) can the byproducts of the process be removed from the product easily?; and (4) can the reactants and materials needed throughout the process be easily synthesized or obtained commercially?

There were a number of conjugation reactions that could have met the criteria for a more convergent synthesis of $[Ru(bpy)_3]^{2+}$- and $[Os(bpy)_3]^{2+}$-containing metallopeptides. The Staudinger reaction, nucleophilic addition to a Michael acceptor, and palladium catalyzed coupling reactions were all considered possible routes for the attachment of $[Ru(bpy)_3]^{2+}$ and $[Os(bpy)_3]^{2+}$ complexes convergent with traditional SPPS.[6] The Cu(I)-catalyzed azide-alkyne 1,3-dipolar cycloaddition (the CuAAC, or "click" reaction) provides general and robust conditions for bioconjugation.[7] The CuAAC reaction typically yields one exclusive regioisomer (1,4-triazole) in an extremely high yield with no resultant stereocenters. Both the alkyne and azide functional groups are tolerant to all of the chemical conditions used during routine SPPS, as is the triazole product. It was known from the outset that introducing azide functionality into amino acids was quite general,[8] and that several alkyne-functionalized Ru^{II} and Os^{II} bipyridyl complexes had previously been reported.[9] It was also anticipated that Cu(I) and other reagents used for the CuAAC could be easily removed using purification techniques typical for peptide isolation.

α-Fmoc-ε-azido-L-lysine (**8**) was chosen as the azido amino acid for the CuAAC reaction based on the desire to maintain a flexible four methylene linker (Figure 3.3).[10] The azido amino acid (**8**) could be easily synthesized by the Cu(II)-catalyzed diazotransfer reaction with the ε-amino acid (**7**). Imidazole-1-sulfonyl azide (**9**) was typically employed as the diazotransfer reagent,[11] although triflyl azide could also be used to affect the same transformation. The diazotransfer reagent (**9**) provided the advantage that it could be stored for months without losing potency, while triflyl azide must be prepared and used within a short a period of time. Both reagent have the potential for highly exothermic reactions and must be treated as detonation hazards.[12]

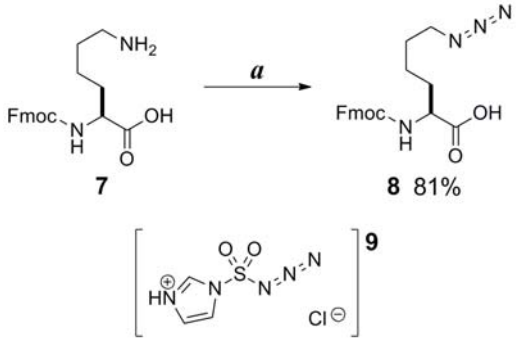

Figure 3.3 Synthesis of α-Fmoc-ε-azido-L-lysine (**8**) by diazotransfer from sulfonyl-imidazole-azide (**9**). Conditions: (a) sulfonyl-1-imidazole azide (**9**) (1.2 equiv), potassium carbonate (2.0 equiv), copper(II) sulfate pentahydrate (0.01 equiv), MeOH, RT, 18 hours (81%).

The alkyne functionalized ligand (**10**) could be easily synthesized from the previously described monocarboxylic acid (**3**) using standard coupling conditions. Reaction of **10** with either $Ru(bpy)_2Cl_2$ or $Os(bpy)_2Cl_2$ by heating at reflux in H_2O/EtOH yielded the desired alkyne functionalized bipyridyl complexes **11a** and **11b**, respectively (Figure 3.4). Bipyridyl complexes of Ru^{II} and Os^{II} containing the propargyl amide group (**10**) have spectroscopic properties very similar to those of the parent compounds, $[Ru(bpy)_3]^{2+}$ and $[Os(bpy)_3]^{2+}$.[9f]

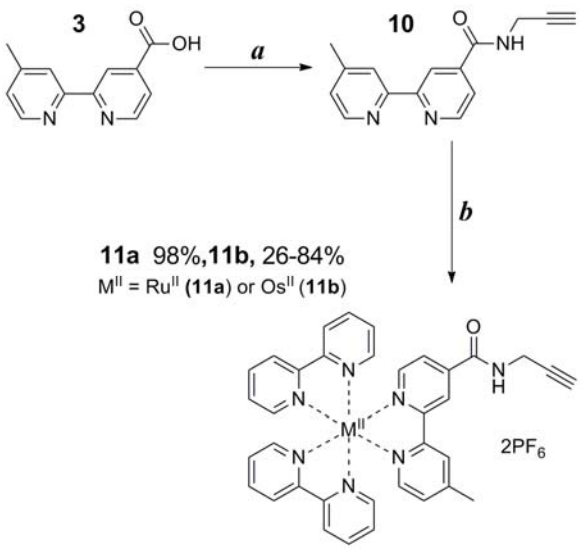

Figure 3.4 Synthesis of the alkyne-containing bipyridyl complexes **11a** and **11b** using the propargyl amide ligand **10**. Conditions: (a) N-Hydroxysuccinimide (1 equiv), EDC (1.1 equiv), ACN, 4 hours, propargyl amine (1.1 equiv), 12 hours. (b) $Ru(bpy)_2Cl_2$ or $Os(bpy)^2Cl^2$, H_2O/EtOH, 90 °C, HPF_6 (**11a** 98%, **11b** 84%).

Metallopeptides could be easily prepared by first synthesizing azidopeptides with α-Fmoc-ε-azido-L-lysine incorporated at the desired point of (**11a**/**11b**) attachment during SPPS (Figure 3.5). The azido group is completely orthogonal to both the extremely basic (piperidine, DBU, DIPEA) and extremely acidic conditions (TFA) used during SPPS. Azidopeptides could be cleaved from the solid-phase support using standard procedures. Purification was performed using RP-HPLC. Yields for azidopeptides were comparable to yields for peptides containing only the standard amino acids.

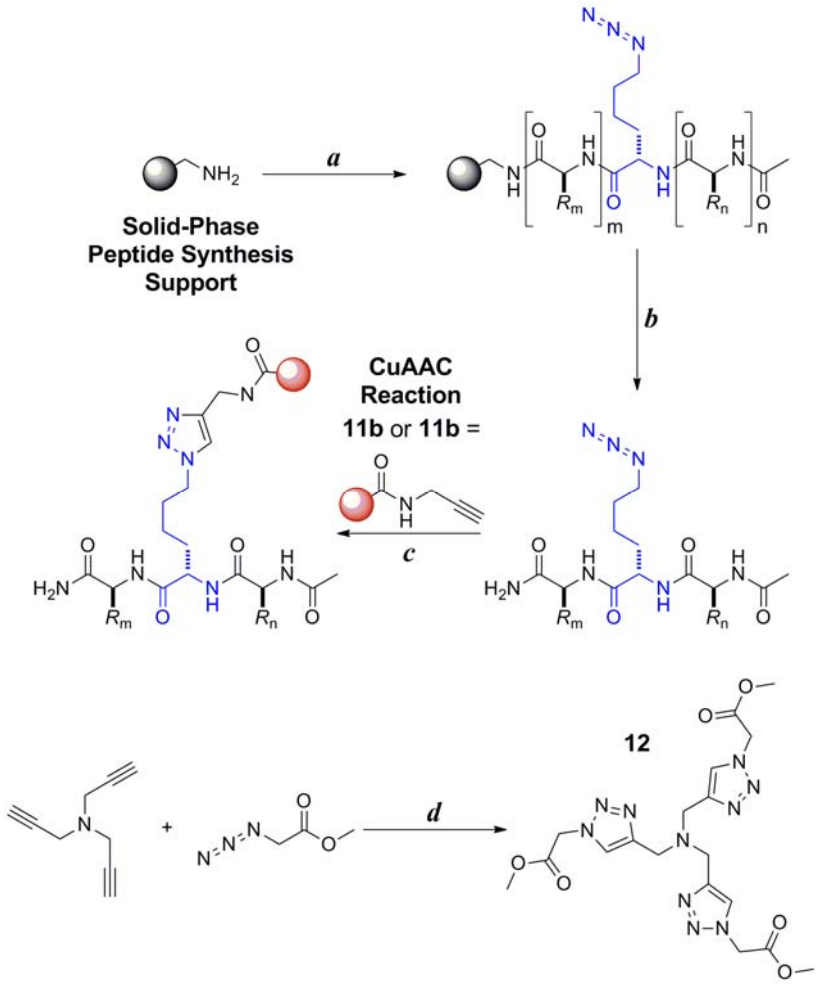

Figure 3.5 Convergent synthesis of metallopeptides starting with the synthesis of azidopeptides using α-Fmoc-ε-azido-L-lysine (**8**). Conditions: (a) Standard SPPS with *m* residues; Coupling steps: Fmoc-amino acid (5 equiv), HBTU (4 equiv), HOBt (4 equiv), DIPEA (5 equiv), DMF/NMP, 2 x 1 hour; Deprotection steps: 20% piperidine, DMF, 2 x 15 minutes; α-Fmoc-ε-azido-L-lysine (**8**) (1.5-2 equiv), HBTU (2 equiv), HOBt (2 equiv), DIPEA (4 equiv), DMF, 1 x 3 hours; Standard SPPS with *n* residues. (b) Cleavage from the SPPS support: TFA:TIPS:water (95:2.5:2.5), 3 hours; purification: RP-HPLC. (c) CuAAC reaction: **11a** or **11b** (2 equiv), $[Cu(CH_3CN)_4]PF_6$ (2 equiv), tris(triazolyl)methylamine ligand (**12**) (1 equiv), buffer (10 mM phosphate buffer, pH 8.5)/DMF (1:1; v:v), 24-48 hours; purification: size exclusion chromatography, RP-HPLC. (d) The tris(triazolyl)methylamine ligand (**12**) could be prepared from tripropargylamine by reaction with methyl azidoacetate (4 equiv), DIPEA (3 equiv), $[Cu(CH_3CN)_4]PF_6$ (0.3 equiv), 24 hours, 83%.

Conjugation of **11a** and **11b** to the azidopeptides required optimization of the CuAAC reaction (Figure 3.5). The CuAAC reaction can proceed under acidic or neutral conditions, but is typically promoted by the addition of an exogenous base, or by the use of alkaline

buffered media.[7] Reaction pH was critical in the developed metallopeptide system. The CuAAC reaction proceeded much more quickly when a basic (pH 8.5) phosphate buffer was used compared to neutral (pH 7) buffered solutions. The parent peptide sequences and the azidopeptides had solubility properties that varied considerably with pH. Under acidic conditions the peptides were readily soluble in water, methanol, and acetonitrile to a lesser extent. Purification by RP-HPLC under acidic conditions was not met with difficulty. However, attempts to determine the azidopeptide concentration using the molar absorptivity of tyrosine in 5M guanidinium hydrochloride (pH 7) failed to give reliable results, presumably due to insolubility of the azidopeptides in the highly concentrated stock solutions. Alternatively, CuAAC reactions could be performed simply by massing out azidopeptide solids, or by solution transfer to a tared vial using methanol as the transfer solvent. Azidopeptides were considerably less soluble in the basic aqueous media required for the CuAAC reaction. Cosolvents such as DMF were typically employed in order to solubilize the azidopeptides. The cosolvents DMSO and *t*BuOH could also be used to solubilize the azidopeptides in water. Interestingly, while methanol and acetonitrile were good solvents for the azidopeptides under acidic conditions, these solvents were extremely inept under the basic reaction conditions.

Any number of copper(I)-catalysts have been shown competent in the CuAAC reaction.[7c] The *in situ* reduction of copper(II) sulfate to copper(I) using sodium ascorbate has perhaps been the most widely employed catalysts system. Tetrakis(acetonitrile)copper(I) hexafluorophosphate was typically employed as the precatalyst in the metallopeptide syntheses, and therefore did not require any *in situ* reduction process, although the copper(II)/ascorbate system has been employed by other researchers within the laboratory for

similar CuAAC reactions. It was commonly observed that reaction mixtures containing a *tris*-(triazolylmethyl)amine ligand (**12**) demonstrated shorter reaction times, and increased yields compared to reaction mixtures lacking the ligand.[13] The reaction will proceed without the ligand (**12**) if higher equivalents of the copper(I)-catalysts are used (~ 10 equiv of copper(I)), but byproducts of peptide oxidation were observed under these conditions. Tetravalent ligands such as the *tris*-(triazolylmethyl)amines have been proposed to protect the copper(I)-catalyst metal center from oxidation and therefore maintain higher concentrations of active catalyst during reaction.[13] Indeed, cyclic voltammetry studies showed that *tris*-(triazolylmethyl)amine ligands can increases the Cu(I)/Cu(II) redox couple by close to 0.3 V.[13] Other researchers have proposed the effect of these ligands is not on the copper *oxidation* state, but on the copper *aggregation* state.[7c] In the absence of accelerating ligands the CuAAC reaction, under certain circumstances, demonstrates kinetics that are second order in Cu(I) and sometimes higher than first order in alkyne.[14] Many copper(I) compounds exist as assortments of aggregates in solution. For example, CuI in acetonitrile exists as number of aggregated species, ranging from Cu_2I_2 to Cu_7I_7 .[7c] Complexes of copper(I) and *tris*-(triazolylmethyl)amine ligands crystallize as bimetallic dimers where each copper center shares one triazole ring with the other.[15] The concept that bimetallic (or higher order) copper(I) aggregates are the true catalytic species in the CuAAC reaction would help to explain many of the observations made regarding the reaction. The optimized CuAAC conditions for metallopeptide synthesis employed one equivalent of the *tris*-(triazolylmethyl)amine ligand, while two equivalents of the copper(I) catalyst and alkyne were used (**11a** or **11b**). This was done to prevent the accidental addition of excess *tris*-(triazolylmethyl)amine ligand, since this has been shown to inhibit other CuAAC reactions,[16]

and also because one equivalent of the ligand was sufficient to promote the desired reaction. The CuAAC reactions between the azidopeptides and **11a** or **11b** were often complete in several hours, although reaction times of at least one day were typically employed. After the conjugation reactions were complete, the reaction mixtures were diluted tenfold with water, frozen, and lyophilized. The desired metallopeptides could be purified using a combination of size-exclusion chromatography and RP-HPLC as described in the experimental section.

iv. Conclusions

Several methods for synthesizing $[Ru(bpy)_3]^{2+}$- and $[Os(bpy)_3]^{2+}$-containing metallopeptides have been presented throughout this chapter. Methods for the synthesis of $Ru(bpy)_3]^{2+}$- and $[Os(bpy)_3]^{2+}$-containing amino acids have been presented, along with techniques for their incorporation during SPPS. Also presented in this chapter is a convergent method for metallopeptide synthesis where alkyne functionalized Ru^{II} (**11a**) and Os^{II} (**11b**) complexes could be conjugated to azidopeptides by way of a CuAAC reaction. The use of a *tris*-(triazolylmethyl)amine ligand (**12**) to accelerate the conjugation reaction was also described. As mentioned in Chapter II, the 2*b*, 2*e*, and 2*f* positions within the P2 peptide sequence were selected for the incorporation of α-Fmoc-ε-azido-L-lysine and modification with **11a** in order to produce metallopeptides that could serve as excited-state energy donors. These donor metallopeptides are from here on out referred to as the 2*b*-Ru, 2*e*-Ru, and 2*f*-Ru metallopeptides. The P2 designation corresponding to the original parent sequence that was modified is implied, but not explicitly listed. The 2*c*, 2*f*, and 2*g* positions within the P1 peptide sequence were similarly modified with **11b** in order to produce metallopeptides that could serve as excited-state energy acceptors. These acceptor metallopeptides are from here on out referred to as the 2*c*-Os, 2*f*-Os, and 2*g*-Os metallopeptides. The synthetic procedures

required to synthesize the parent peptides (P1 and P2), azidopeptides, metallopeptides, and all needed precursors described throughout Chapter III are presented within the following experimental section.

The spectroscopic properties of the synthetic metallopeptides were similar to those of $Ru(bpy)_3^{2+}$ and $Os(bpy)_3^{2+}$ (Figure 3.6a). Absorbance bands due to the π-π^*, ^{1}MLCT, and ^{3}MLCT transitions of the bipyridyl complexes dominate the spectra. The metallopeptide steady-state emission spectra also resemble those of the parent complexes (Figure 3.6b). The emission maxima for the Ru^{II}- and Os^{II}-containing metallopeptides, approximately 660 and 800nm, respectively, are both hypsochromically shifted relative to $Ru(bpy)_3^{2+}$ and $Os(bpy)_3^{2+}$. The photophysical properties of mixtures of the metallopeptides indicate a position-dependent energy transfer between the donor (Ru^{II}) and acceptor (Os^{II}) metallopeptides. The study of this energy transfer is reported later in Chapter V. The physical characterization of the coiled-coil metallopeptides is described beforehand in Chapter IV.

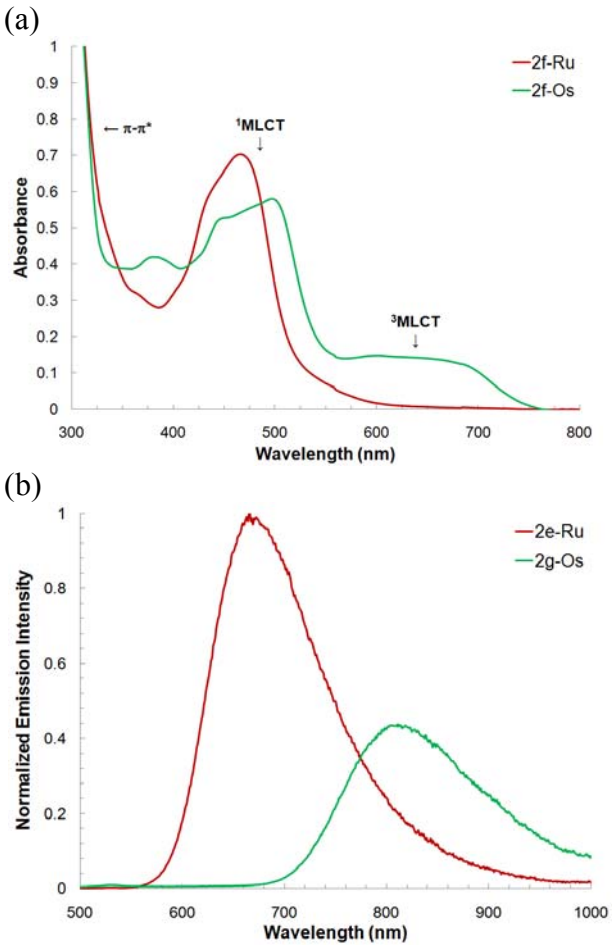

Figure 3.6 (a) Absorbance spectra for the 2*f*-Ru metallopeptide show π-π* and ^{1}MLCT transitions characteristic to Ru^{II} bipyridyl complexes. Absorbance spectra for the 2*f*-Os metallopeptide show π-π*, ^{1}MLCT, and also ^{3}MLCT transitions characteristic only to Os^{II} bipyridyl complexes. Absorbance spectra were recorded at 25°C in 10 mM PO_4^{3-}, pH 7, buffer. (b) Normalized steady-state emission spectra for the 2*e*-Ru and 2*g*-Os metallopeptides with emission maxima at approximately 660 and 800 nm. Emission spectra were recorded at 25°C in 10 mM PO_4^{3-}, pH 7, buffer that was deoxygenated with Ar for 30 minutes.

B. Experimental section

i. Materials and general methods

Solvents were purchased from Fisher Scientific and were used as received unless noted otherwise. *cis*-Dichlorobis(2,2'-bipyridine)ruthenium(II) dihydrate was purchased from Strem Chemicals. All α-N-Fmoc-amino acids, including α-N-Fmoc-lysine, were purchased from Novabiochem. Tetrakis(acetonitrile)copper(I) hexafluorophosphate, 2,2'-bipyridine,

and 4,4'-dimethyl-2,2'-bipyridine were purchased from Aldrich. The compounds 4'-methyl-2,2'-bipyridine-4-carboxaldehyde, 4'-methyl-2,2'-bipyridine-4-carboxylic acid, and succinimidyl-4-carboxy-4'-methyl-2,2'-bipyridine were synthesized according to reported procedures.[3] *cis*-Dichlorobis(2,2'-bipyridine)osmium(II) was synthesized using the procedure reported by Meyer.[4] Deuterated solvents were purchased from Cambridge Isotope Laboratories. ^{1}H and ^{13}C NMR spectra were recorded at 400 and 100 MHz, respectively, on Bruker spectrometers. Chemical shifts were given in ppm relative to solvent peaks corresponding to residual protons for the deuterated solvents. These values were taken as δ 7.26, 1.93, 2.49, 5.32 and 4.67 for $CDCl_3$, CD_3CN, $(CD_3)_2SO$, CD_2Cl_2, and D_2O, respectively. Coupling constants are given in hertz. The details for peptide synthesis and purification are provided below. High-resolution and low-resolution mass spectra were obtained using a Bruker Biotof instrument.

ii. Synthesis of $[Ru(bpy)_3]^{2+}$- and $[Os(bpy)_3]^{2+}$-containing Fmoc-lysine derivatives

*4'-Methyl-2,2'-bipyridine-4-carboxylic acid (**3**).* The bipyridyl monocarboxylic acid was prepared according to the literature procedure by Peek and Erickson.[3b]

*Succinimidyl-4-carboxy-4'-Methyl-2,2'-bipyridine (**4**).* The succinimidyl ester was prepared according to the literature procedure by Telser and Netzel.[3c]

*α-Fmoc-ε-(4'-methyl-2,2'-bipyridine-4-carboxamido-)-L-Lysine (**5**).* A suspension of succinimidyl-4-carboxy-4'-methyl-2,2'-bipyridine (.767 g, 2.5 mmol), N-methylmorpholine (0.75 mL, 6.8 mmol, 2.7 equiv), and α-N-Fmoc-lysine (1.00 g, 2.7 mmol, 1.1 equiv) was stirred in 25 mL of anhydrous DMF for 8 hours. The solvent was removed in vacuo and the remaining solid residue was suspended in 0.1 M ammonium chloride and extracted into ethyl acetate (4 x 100 mL). The organic fractions were freed of solvent and recrystallized from

hexanes/diethyl ether (1:1, v:v) to give the product as a white solid (1.07 g, 1.9 mmol, 77 %). ^{1}H NMR (400 MHz, $(CD_3)_2SO$): δ 8.96 (s, 1H), δ 8.76 (s, 1H), δ 8.57 (s, 1H), δ 8.25 (s, 1H), δ 7.99-7.85 (m, 3H), δ 7.81 (s, 1H), δ 7.80-7.60 (m, 3H), δ 7.40-7.35 (m, 2H), δ 7.32 (m, 3H), δ 5.76 (s, 1H), δ 4.25 (m, 3H), δ 3.78 (m, 1H), δ 2.74 (m, 2H), 2.43 (s, 3H), δ 1.70-1.30 (m, 6H); ^{13}C NMR (150 MHz, $CDCl_3/CD_3OD$) δ 174.8, 166.0, 156.1, 155.6, 154.5, 150.2, 150.0, 148.1, 143.8, 143.7, 143.1, 141.2, 127.6, 127.0, 125.5, 125.0, 123.0, 122.2, 119.9, 118.0, 77.21 + 77.0 + 76.8 ($CDCl_3$), 66.8, 53.6, 53.4, 50.4 (CD_3OD), 47.1, 38.9, 31.2, 29.6, 27.6, 26.4, 25.5, 21.6, 21.3. High-resolution ESI-MS: *m/z* calculated for $C_{33}H_{33}N_4O_5$ ($M + H^+$), 565.2478; found 565.2478.

Bis-(2,2'bipyridine)(α-Fmoc-ε-(4'-Methyl-2,2'-bipyridine-4-carboxamido-)-L-lysine)ruthenium(II) bis(hexafluorophosphate) (**6a**). A small round bottom, equipped with a condenser, was charged with *cis*-dichlorobis(2,2'-bipyridine)ruthenium(II) dihydrate (0.793 g, 1.52 mmol), and α-Fmoc-ε-(4'-methyl-2,2'-bipyridine-4-carboxamido-)-L-Lysine (**5**) (1.03 g, 1.82 mmol, 1.2 equiv), and then heated at reflux in 70% aqueous ethanol for 24 h. The mixture was allowed to cool to room temperature, filtered, and then acidified with several drops of 60% aqueous HPF_6. The mixture was placed in a freezer or 1 hour while a turbid orange precipitate formed. The solid orange product was collected on a medium frit. The collected product was dissolved in a minimum amount of ACN, and then added drop wise to a round bottom cooled in an ice bath and containing 150 mL IPA. The orange precipitate reformed, and was collected on a medium frit to afford the title product (1.42 g, 1.12 mmol, 74%). TLC (*n*-BuOH/EtOAc/AcOH/water, 1:1:1:1); R_f: 0.48. ^{1}H NMR (400 MHz, CD_3CN): δ 8.91 (m, 1H), δ 8.55 (s, 1H), δ 8.48-8.40 (m, 5H), δ 8.06-8.03 (m, 5H), δ 7.91-7.74 (m, 3H), δ 7.74-7.64 (m, 5H), δ 7.64-7.51 (m, 3H), δ 7.39-7.33 (m, 6H), δ 7.26-7.22 (m, 2H), δ

6.17 (m, 1H), δ 4.23 (m, 2H), δ 4.15 (m, 1H), δ 4.08 (m, 1H), δ 3.40 (m, 2H), 2.31 (m, 3H), 1.62 (m, 2H), 1.45 (m, 2H), 1.26 (m, 2H); UV-vis (CH_3CN) λ_{max} (ε): 235 (28,000), 255 (31,000), 288 (70,000), 456 (14,000); High-resolution ESI-MS: *m/z* calculated for $C_{53}H_{48}N_8O_5Ru$ (M^{2+}), 489.1396; found 489.1333.

Bis-(2,2'bipyridine)(α-Fmoc-ε-(4'-Methyl-2,2'-bipyridine-4-carboxamido-)-L-lysine)osmium(II) bis(hexafluorophosphate) (**6b**). A small round bottom, equipped with a condenser, was charged with *cis*-dichlorobis(2,2'-bipyridine)osmium(II) (0.026 g, 0.046 mmol), and α-Fmoc-ε-(4'-methyl-2,2'-bipyridine-4-carboxamido-)-L-Lysine (**5**) (0.045 g, 0.080 mmol, 1.73 equiv), and then heated at reflux in 50% aqueous ethanol for 24 h. The mixture was allowed to cool to room temperature, filtered, and then acidified by several drops of 60% aqueous HPF_6. The green mixture was extracted with EtOAc (50 mL). The EtOAc fraction was dried with anhydrous magnesium sulfate and freed of solvent. The solid product was reconstituted in a minimum volume of ACN and added drop wise to a stirring solution of 10 mM NH_4PF_6 that was cooled in an ice bath. The green precipitate was collected on a medium frit to afford the title product (0.037 g, 0.027 mmol, 60%). TLC (*n*-BuOH/EtOAc/AcOH/water, 1:1:1:1); R_f: 0.48. ^{1}H NMR (400 MHz, CD_3CN): δ 8.76 (s, 1H), δ 8.51-8.44 (m, 5H), δ 7.91-7.83 (m, 6H), δ 7.77 (d, J = 6.4, 1H), 7.67-7.62 (m, 6H), 7.58 (s, 1H), 7.48 (d, J = 6.4, 1H), 7.41-7.38 (m, 2H), 7.34-7.29 (m, 6H), 7.22-7.29 (m, 1H), 6.10 (d, J = 8.4, 1H), 4.32 (d, J = 6.8, 1H), 4.22 (m, 1H), 4.14 (m, 1H), 3.57 (m, 1H), 3.45 (m, 2H), 3.31 (m, 1H), 2.63 (s, 1.5H), 2.54 (s, 1.5 H), 1.6 (m, 3H), 1.47 (m, 3H). UV-vis (CH_3CN) λ_{max} (ε): 255 (29,000), 291 (60,000), 440, (10,000), 483 (10,000); High-resolution ESI-MS: *m/z* calculated for $C_{53}H_{48}N_8O_5Os$ (M^{2+}), 533.6642; found 534.1480.

iii. Synthesis of α-Fmoc-ε-azido-L-lysine

α-Fmoc-ε-azido-L-lysine (**8**). A 100 mL round bottom was charged with α-N-Fmoc-L-lysine (4.547 g, 12.3 mmol), imidazole-1-sulfonyl azide (**9**) (3.104 g, 14.81 mmol, 1.20 equiv), and potassium carbonate (3.411 g, 24.68 mmol, 2.0 equiv). The mixture was stirred in MeOH (60 mL) while copper(II) sulfate pentahydrate (30.8 mgs, 123.4 μmol, 1 mol %) was added. A precautionary blast shield was employed while the mixture stirred under N_2 for 18 h. The reaction mixture was concentrated under vacuum, diluted with H_2O (400 mL), and acidified via the addition of 6M aqueous HCl. The precipitate that formed was extracted with EtOAc (3 x 400 mL). The combined organic fractions were washed with H_2O (1 L), dried over anhydrous Na_2SO_4, and concentrated under vacuum. The product **8** was obtained as a white solid after chromatography on silica gel using 5% (v/v) MeOH in CH_2Cl_2 (3.96 g, 10.0 mmol, 82%). ^{1}H NMR (400 MHz, CD_3OD): δ 7.69 (d, *J* = 7.6, 2H), δ 7.60 (t, *J* = 8.0, 2H), δ 7.31 (t, *J* = 7.2, 2H), δ 7.24 (t, *J* = 7.2, 2H), δ 4.30 (d, *J* = 6.8, 2H), δ 4.19 (m, 1H), δ 4.13 (t, *J* = 6.8, 1H), δ 3.17 (m, 2H), δ 1.90-1.35 (m, 6H); ^{13}C NMR (100 MHz, CD_3OD) δ 174.4, 157.3, 143.8, 141.2, 127.4, 126.8, 124.8, 119.5, 66.6, 55.1, 53.8, 50.9, 30.9, 28.0, 22.8. High-resolution ESI-MS: *m/z* calculated for $C_{53}H_{48}N_8O_5Os$ (M^{2+}), 533.6642; found 534.1480.

*Imidazole-1-sulfonyl azide hydrochloride (**9**).* Imidazole-1-sulfonyl azide hydrochloride was synthesized according to the procedure by Goddard-Borger and Stick.[11] **Warning:** Potentially explosive intermediates formed during reaction.[12] Synthetic operations were conducted behind a blast shield whenever possible. A 100 mL round bottom charged with sodium azide (5.47 g, 84.1 mmol) and ACN (85 mL) was cooled in an ice bath and stirred magnetically while sulfuryl chloride (6.81 mL, 1 equiv) was added drop wise. The addition was performed behind a blast shield where the reaction remained while it was stirred

overnight (18 h) and slowly returned to room temperature. The mixture was again cooled in an ice bath with stirring while imidazole (11.45 g, 168.4 mmol, 2 equiv) was added in small portions over the course of 20 minutes. Behind a blast shield, the mixture was allowed to slowly warm to room temperature while stirring for 4.5 hours. The mixture was transferred to a 500 mL separatory funnel and diluted with EtOAc (170 mL). The organic solution was washed using water (2 x 170 mL) and then saturated sodium bicarbonate (2 x 170 mL). After drying with anhydrous sodium sulfate, the organic portion was filtered through a cotton plug. An acidic solution was prepared by adding acetyl chloride (22 mL) to anhydrous EtOH (75 mL). The addition was performed slowly (over 20 minutes) under a nitrogen atmosphere while the alcoholic solution was cooled in an ice bath. The filtered EtOAc solution was cooled in an ice bath while a portion of the acidic EtOH solution (40 mL) was added slowly. A white precipitate formed and the mixture was placed in a freezer (1 h) before the solid was collected. Drying the solid under vacuum overnight provided the title compound (10.4 g, 49.7 mmol, 59%). ^{1}H NMR (400 MHz, D_20): δ 9.31 (s, 1H), δ 7.89 (s, 1H), δ 7.49 (s, 1H).

iv. Synthesis of Ru^{II} and Os^{II} bipyridyl alkyne complexes and the tris-(triazolylmethyl)amine ligand

*4'-Methyl-2,2'-bipyridine-4-propargylamide (**10**).* The bipyridyl propargyl amide was prepared according to the procedure by Khan and Grinstaff.[9d] The monocarboxylic acid **3** (189 mg, 0.881 mmol) was suspended in acetonitrile (ACN) (5 mL) along with N-hydroxysuccinimide (101 mg, 0.881 mmol). EDC (185.9 mg, 0.9697 mmol, 1.10 equiv) was added. The mixture was sonicated and became more translucent while stirring for 4 h. The addition of propargyl amine completely homogenized the reaction which was allowed to stir overnight. The reaction was concentrated under vacuum. The oily residue was suspended in

20 mL of 1 M aqueous Na_2CO_3, and extracted with 3 x 20 mL of ethyl acetate. The combined organic portions were washed with saturated aqueous $NaHCO_3$, dried over anhydrous Na_2SO_4, filtered, and freed of solvents under vacuum. The product **10** was obtained as a white solid after chromatography on silica gel using 10% (v/v) MeOH in CH_2Cl_2 (178 mg, 80%). ^{1}H NMR (400 MHz, $CDCl_3$): δ 8.79 (d, *J* = 4.8, 1H), δ 8.63 (s, 1H), δ 8.53 (d, *J* = 4.8, 1H), δ 8.26 (s, 1H), δ 7.77 (dd, *J* = 4.8, 1.4, 1H), δ 7.17 (d, *J* = 4.8, 1H), δ 6.85 (br s, 1H), δ 4.29 (m, 2H), δ 2.45 (s, 3H), δ 2.30 (t, 1H); ^{13}C NMR (100 MHz, $CDCl_3$) δ 165.3, 157.1, 155.0, 150.1, 149.0, 148.4, 141.9, 125.2, 122.2, 121.7, 117.4, 72.3, 29.87, 21.2. High-resolution ESI-MS: *m/z* calculated for $C_{15}H_{13}N_3O$ ($M + H^+$), 252.1137; found 252.1137.

Bis-(2,2'bipyridine)(4'-Methyl-2,2'-bipyridine-4-propargylamide)-ruthenium(II) bis(hexafluorophosphate) ***(11a).*** The propargyl amide derivatized Ru^{II} complex was prepared according to the procedure by Khan and Grinstaff.[9d] A small round bottom, equipped with a condenser, was charged with *cis*-dichlorobis(2,2'-bipyridine)ruthenium(II) dihydrate (101.0 mg, 0.1941 mmol), and bipyridyl ligand **2** (55.5 mg, 0.2209 mmol, 1.14 equiv). The reagents were heated at reflux in 70% aqueous ethanol for 7 h, and then concentrated in vacuo. The residue was dissolved in water (25 mL), and then washed with EtOAc (50 mL). The aqueous portion was treated with several drops of concentrated aqueous NH_4PF_6. The microcrystalline product that formed was extracted into CH_2Cl_2 (50 mL), and washed with 10 mM aqueous NH_4PF_6. Concentration afforded the product as dark red solid (180.8 mg, 98%). ^{1}H NMR (400 MHz, CD_3CN): δ 8.79 (s, 1H), δ 8.54-8.52 (m, 5H), δ 8.10-8.06 (m, 4H), δ 7.90 (d, *J* = 5.6 Hz, 1H), δ 7.75 (m, 5H), δ 7.66 (dd, *J* = 6.0, 1.6 Hz, 1H), δ 7.60 (d, *J* = 5.6 Hz, 1H), δ 7.44-7.41 (m, 4H), δ 7.31 (d, *J* = 5.6 Hz, 1H), δ 4.19 (m, 2H), δ 2.57 (s, 3H), δ 2.54 (m, 1H);

UV-vis (CH_3CN) λ_{max} (ε): 246 (26,000), 288 (60,000), 455 (13,400); High-resolution ESI-MS: *m/z* calculated for $C_{35}H_{29}N_7ORu$ (M^{2+}), 332.5738; found 332.5716.

Bis-(2,2'bipyridine)(4'-Methyl-2,2'-bipyridine-4-propargylamide)-osmium(II) bis(hexafluorophosphate) ***(11b).*** The propargyl amide derivatized Os^{II} complex was prepared according to the procedure by Khan and Grinstaff.[9d] A small round bottom, equipped with a condenser, was charged with *cis*-dichlorobis(2,2'-bipyridine)osmium(II) (39.7 mg, 0.069 mmol), and bipyridyl ligand **10** (19.1 mg, 0.076 mmol, 1.1 equiv). The reagents were heated at reflux in 50% aqueous EtOH for 24 h, and then concentrated under vacuum. The residue was suspended in H_2O (100 mL), and filtered to remove unreacted *cis*-dichlorobis(2,2'-bipyridine)osmium(II). The aqueous filtrate was washed with DCM (2 x 100 mL). A portion of saturated NH_4PF_6 was added to the aqueous solution and a green precipitate formed. The precipitate was extracted into EtOAc and then concentrated to a solid under vacuum. The solid was partially dissolved in DCM, filtered, and then concentrated to provide the product as a dark green solid (18.4 mg, 26%). ^{1}H NMR (400 MHz, CD_2Cl_2): δ 8.80 (d, *J* = 1.2 Hz, 1H), δ 8.48 (s, 1H), δ 8.43-8.40 (m, 4H), δ 7.90-7.84 (m, 4H), δ 7.78 (t, *J* = 5.6 Hz, 1H), δ 7.70-7.65 (m, 4H), δ 7.63-7.59 (m, 4H), δ 7.41-7.34 (m, 4H), δ 7.44-7.41 (m, 4H), δ 7.21 (dd, *J* = 5.8, 1.0 Hz, 1H), δ 4.20 (dd, *J* = 5.6, 2.4 Hz, 2H), δ 2.69 (s, 3H), δ 2.28 (t, *J* = 2.4 Hz , 1H); UV-vis (CH_3CN) λ_{max} (ε): 247 (22,000), 291 (50,000), 485 (10,000), 593 (3,000); High-resolution ESI-MS: *m/z* calculated for $C_{35}H_{29}N_7OOs$ (M^{2+}), 337.6024; found 337.5952.

tris-(triazolylmethyl)amine ligand ***(12).*** A solution of tripropargylamine (233.0 mg, 1.777 mmol), methyl azidoacetate (805.4 mg, 6.998 mmol, 3.94 equiv), and tetrakis(acetonitrile)copper(I) hexafluorophosphate (21.9 mg, 58.8 μmol), and DIPEA (1 mL, 5.741 mmol, ~3 equiv to alkyne) in ACN (4 mL) was stirred under N_2 for 24 h. The reaction

warmed considerably when DIPEA was added and was cooled in an ice bath. The reaction was concentrated in vacuo, and the residue was suspended in saturated aqueous $NaHCO_3$ (50 mL), extracted with CH_2Cl_2 (3 x 50 mL), dried over anhydrous Na_2SO_4, filtered, and concentrated. The product (**5**) was obtained as an off white solid after chromatography on silica gel using 5% (v/v) MeOH in CH_2Cl_2. Yield, 701 mg (83%). ^{1}H NMR (400 MHz, $CDCl_3$): δ 7.84 (s, 1H), δ 5.18 (s, 2H), δ 3.79 (s, 2H), δ 3.78 (s, 3H); ^{13}C NMR (100 MHz, $CDCl_3$) δ 166.8, 144.6, 125.2, 52.9, 50.7, 47.4. High-resolution ESI-MS: *m/z* calculated for $C_{18}H_{24}N_{10}O_6$ ($M + Cs^+$), 609.0935; found 609.0920.

*Bis-(2,2'bipyridine)(4'-Methyl-2,2'-bipyridine-4-methyl-aceto-1,2,3-triazolo-methylacetamide)-osmium(II) bis(trifluoroacetate) (**13**).* A solution of **11b** (6.95 mgs, 8 μmol), methyl azidoacetate (1.42 mg, 10 μmol, 1.7 equiv) and DIPEA (3 μL) in ACN (1.5 mL) was stirred in a round bottom and cooled in an ice bath before tetrakis (acetonitrile)copper(I) hexafluorophosphate (0.56 mgs, 1.5 μmol, 20 mol %) was added. The solution was allowed to warm to room temperature slowly and stirred for 2 days under inert atmosphere. The Os^{II} complex was purified by RP-HPLC using methods identical to those described below for the metallopeptides. ESI-MS: *m/z* calculated for $C_{38}H_{34}N_{10}O_3Os$ (M^{2+}), 435.12; found 435.1. The complex is discussed briefly in Chapter V during the description of a control experiment.

v. Synthesis of peptides and metallopeptides

SPPS of the peptide parent sequences P1 and P2. Peptides were typically synthesized by standard automated SPPS using a Thuramed tetras synthesizer. Fmoc-protected amino acids were used along with a CLEAR-Amide resin from Peptides International, Inc. Amino acid residues were activated with HBTU, HOBt, and DIPEA in DMF. Amino acids were

deprotected twice with 2% DBU and 2% piperidine in DMF for 15 minutes each step. Commercially available amino acids were coupled using double coupling cycles of 30-60 minutes each. Couplings for the unnatural amino acids **6a**, **6b**, and **8** have specific procedures described below. The N-terminus of each peptide was acetylated using 5% acetic anhydride and 6% lutidine in DMF for 30 minutes. Cleavage of the peptides from the resin was performed in 95.0% TFA, 2.5% water, and 2.5% TIPS. TFA was evaporated with a stream of nitrogen and diethyl ether was added to precipitate the cleavage products. The peptides were extracted with water or collected as solids by centrifugation and lyophilized to dryness. Peptides were purified by RP-HPLC using an Atlantis Prep OBD dC-18 semi-preparative column, with a gradient of 0-100% solvent B over 40 minutes, where solvent A was 95:5 water:ACN, 0.1% TFA, and solvent B was 95:5 ACN:water, 0.1% TFA. Purified samples were lyophilized and the peptide sequence was confirmed by ESI-MS. M was calculated as 3212.73 (exact) for **P1** ($C_{142}H_{237}N_{37}O_{47}$). MS *m/z* observed: 1608.4 ($[M + 2H^+]^{2+}$), 1072.6 ($[M + 3H^+]^{3+}$), 804.7 ($[M + 4H^+]^{4+}$); M was calculated as 3363.95 (exact) for **P2** ($C_{149}H_{258}N_{46}O_{42}$). MS *m/z* observed: 1123.0 ($[M + 3H^+]^{3+}$), 842.5 ($[M + 4H^+]^{4+}$), 674.0 ($[M + 5H^+]^{5+}$).

*Synthesis of the metallopeptides **2f-Os*** (P1) and **2f-Ru*** (P2).* Metallopeptides were typically synthesized according to the primarily automated procedures described above. At times the metallopeptides were synthesized by hand. The $[Ru(bpy)_3]^{2+}$- and $[Os(bpy)_3]^{2+}$-containing Fmoc-protected amino acids **6a** and **6b** were typically coupled by hand using one of two sets of conditions: (a) 2 equiv of HBTU, 2 equiv of HOBt, 3 equiv of DIPEA, 3-5 h. (b) 2 equiv of HATU, 3 equiv of DIPEA, 50 °C, 24 hours. Amino acid deprotection reactions were performed using two sets of conditions: (a) 2% DBU, 2% piperidine, DMF, 15 minutes.

(b) 20% piperidine, DMF, 15 minutes. Traditional Kaiser tests using ninhydrin were useful for estimating the extent coupling and deprotection for metallopeptides containing **6a**, but were often more ambiguous for metallopeptides containing **6b** due to the high molar absorptivity of the $[Os(bpy)_3]^{2+}$-containing amino acid. M was calculated as 3912.93 (exact) for **2*f*-Os*-P1** ($C_{175}H_{265}N_{43}O_{47}Os$). MS *m/z* observed: 1304.7 ($[M^{2+} + H^+]^{3+}$), 978.9 ($[M^{2+} + 2H^+]^{4+}$), 783.2 ($[M^{2+} + 3H^+]^{5+}$); M was calculated as 3974.09 (exact) for **2*f*-Ru*-P2** ($C_{182}H_{286}N_{52}O_{42}Ru$). MS *m/z* observed: 1325.3 ($[M^{2+} + H^+]^{3+}$), 994.2 ($[M^{2+} + 2H^+]^{4+}$), 795.8 ($[M^{2+} + 3H^+]^{5+}$).

Synthesis of azidopeptides using α-Fmoc-ε-azido-L-lysine. Peptides containing azidolysine residues at desired positions were synthesized using an automated synthesizer as described above. α-Fmoc-ε-azido-L-lysine **8** was injected manually and a single 3 hour coupling reaction was performed. The azidopeptides were cleaved from the resin, and purified in an identical fashion. Azidopeptide identities were confirmed by ESI-MS. M was calculated as 3238.76 (exact) for **2*f*-N$_3$-P1** ($C_{143}H_{239}N_{39}O_{46}$). MS *m/z* observed: 1620.9 ($[M + 2H^+]^{2+}$), 1081.0 ($[M + 3H^+]^{3+}$), 811.0 ($[M + 4H^+]^{4+}$); M was calculated as 3295.78 (exact) for **2*c*-N$_3$-P1** ($C_{145}H_{242}N_{40}O_{47}$). MS *m/z* observed: 1649.3 ($[M + 2H^+]^{2+}$), 1099.9 ($[M + 3H^+]^{3+}$), 825.2 ($[M + 4H^+]^{4+}$); M was calculated as 3237.77 (exact) for **2*g*-N$_3$-P1** ($C_{143}H_{240}N_{40}O_{45}$). MS *m/z* observed: 1620.3 ($[M + 2H^+]^{2+}$), 1080.6 ($[M + 3H^+]^{3+}$), 810.7 ($[M + 4H^+]^{4+}$); M was calculated as 3389.97 (exact) for **2*f*-N$_3$-P2** ($C_{150}H_{260}N_{48}O_{41}$). MS *m/z* observed: 1131.0 ($[M + 3H^+]^{3+}$), 848.5 ($[M + 4H^+]^{4+}$), 679.1 ($[M + 5H^+]^{5+}$); M was calculated as 3447.00 (exact) for **2*b*-N$_3$-P2** ($C_{152}H_{263}N_{49}O_{42}$). MS *m/z* observed: 1150.3 ($[M + 3H^+]^{3+}$), 863.0 ($[M + 4H^+]^{4+}$), 690.6 ($[M + 5H^+]^{5+}$); M was calculated as 3389.94 (exact) for **2*e*-N$_3$-P2** ($C_{149}H_{256}N_{48}O_{42}$). MS *m/z* observed: 1131.0 ($[M + 3H^+]^{3+}$), 848.5 ($[M + 4H^+]^{4+}$), 679.0 ($[M + 5H^+]^{5+}$).

Synthesis of metallopeptides using the CuAAC reaction. In a typical procedure 8-15 mgs (~2-4 μmol) of azidopeptide would be partially dissolved in 1-3 mL 50% (v/v) DMF in 10 mM PO_4^{3-}, pH 8.5, buffer that was deoxygenated with N_2 for 30 minutes. The peptide was reacted with (2 equiv) either the Ru^{II} complex **11a** or the Os^{II} complex **11b** in the presence of tetrakis(acetonitrile)copper(I) hexafluorophosphate (2 equiv), and tris-(triazolylmethyl)amine ligand (**12**, 1 equiv). The mixtures were allowed to stir overnight for at least 12 h, typically longer, and then diluted with water (10 mL). The aqueous solution was frozen and lyophilized. The fully lyophilized residue was dissolved in water and filtered through a 0.22 μm PVDF syringe filter. The final metallopeptide was obtained after purification by reversed-phase HPLC using the conditions listed above. The molecular weight was confirmed by LC-MS. M^{2+} was calculated as 3993.96 (exact) for **2*f*-Os** ($C_{178}H_{268}N_{46}O_{47}Os$). MS *m/z* observed: 1997.0 ($[M^{2+}]^{2+}$), 1331.8 ($[M^{2+} + H^+]^{3+}$), 999.0 ($[M^{2+} + 2H^+]^{4+}$), 799.4 ($[M^{2+} + 3H^+]^{5+}$), 666.4 ($[M^{2+} + 4H^+]^{6+}$); M^{2+} was calculated as 4050.98 (exact) for **2*c*-Os** ($C_{180}H_{271}N_{47}O_{48}Os$). MS *m/z* observed: 2025.8 ($[M^{2+}]^{2+}$), 1350.7 ($[M^{2+} + H^+]^{3+}$), 1013.2 ($[M^{2+} + 2H^+]^{4+}$), 810.8 ($[M^{2+} + 3H^+]^{5+}$), 679.5 ($[M^{2+} + 4H^+]^{6+}$); M^{2+} was calculated as 3992.98 (exact) for **2*g*-Os** ($C_{178}H_{269}N_{47}O_{46}Os$). MS *m/z* observed: 1996.5 ($[M^{2+}]$), 1131.3 ($[M^{2+} + H^+]^{3+}$), 998.7 ($[M^{2+} + 2H^+]^{4+}$), 799.2 ($[M^{2+} + 3H^+]^{5+}$), 666.2 ($[M^{2+} + 4H^+]^{4+}$); M^{2+} was calculated as 4055.12 (exact) for **2*f*-Ru** ($C_{185}H_{289}N_{55}O_{42}Ru$). MS *m/z* observed: 1352.0 ($[M^{2+} + H^+]^{3+}$), 1014.1 ($[M^{2+} + 2H^+]^{4+}$), 811.6 ($[M^{2+} + 3H^+]^{5+}$), 676.5 ($[M^{2+} + 4H^+]^{6+}$), 580.0 ($[M^{2+} + 5H^+]^{7+}$); M^{2+} was calculated as 4112.14 (exact) for **2*b*-Ru** ($C_{187}H_{292}N_{56}O_{43}Ru$); MS *m/z* observed: 1371.7 ($[M^{2+} + H^+]^{3+}$), 1029.0 ($[M^{2+} + 2H^+]^{4+}$), 823.6 ($[M^{2+} + 3H^+]^{5+}$); M^{2+} was calculated as 4055.09 (exact) for **2*e*-Ru** ($C_{184}H_{285}N_{55}O_{43}Ru$). MS *m/z* observed: 1352.6 ($[M^{2+} + H^+]^{3+}$), 1014.5 ($[M^{2+} + 2H^+]^{+4}$).

vi. ^{1}H and ^{13}C NMR spectra.

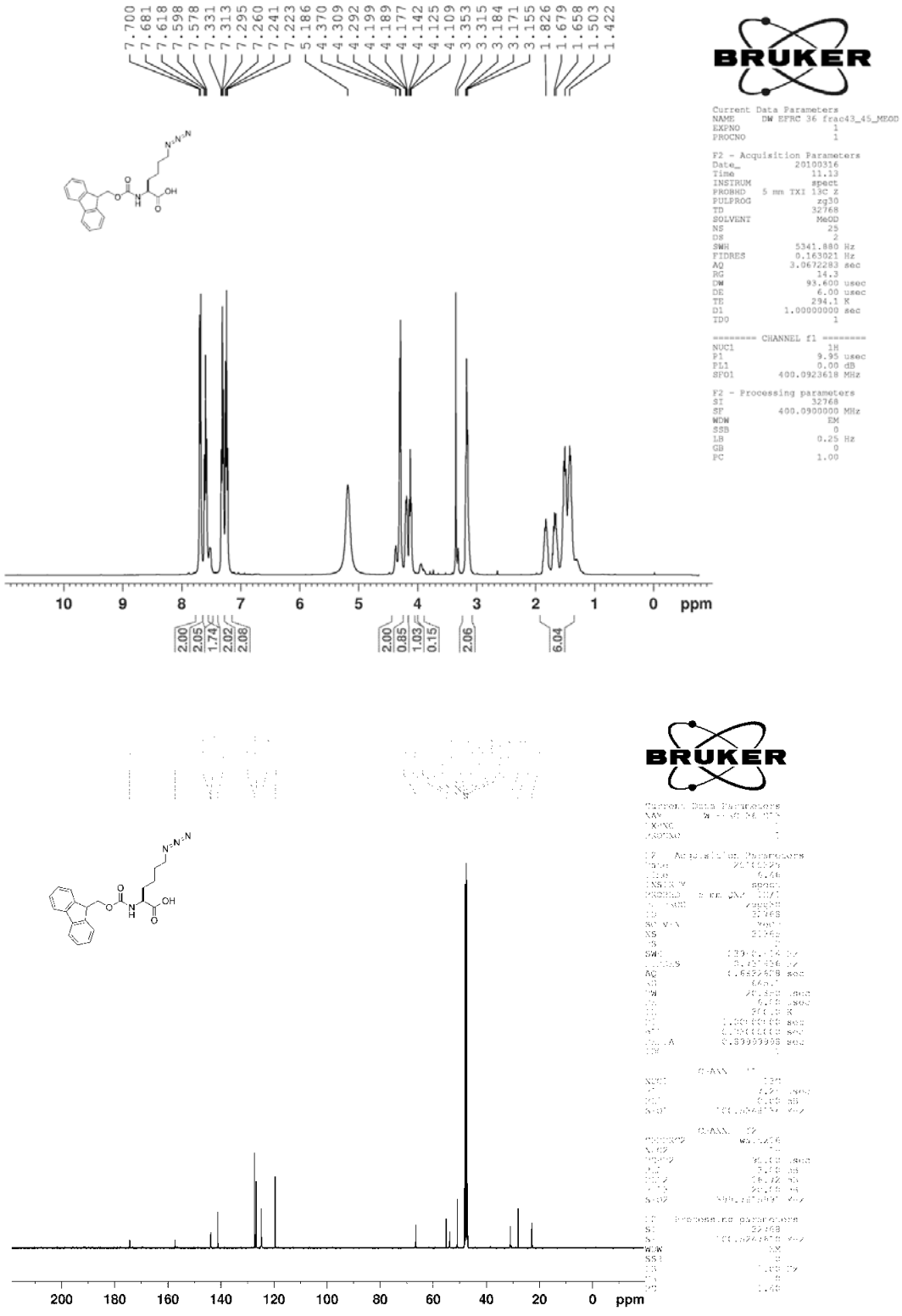

Figure 3.7. α-Fmoc-ε-azido-L-lysine (**8**). ^{1}H: CD_3OD, 400 MHz; ^{13}C CD_3OD, 100 MHz.

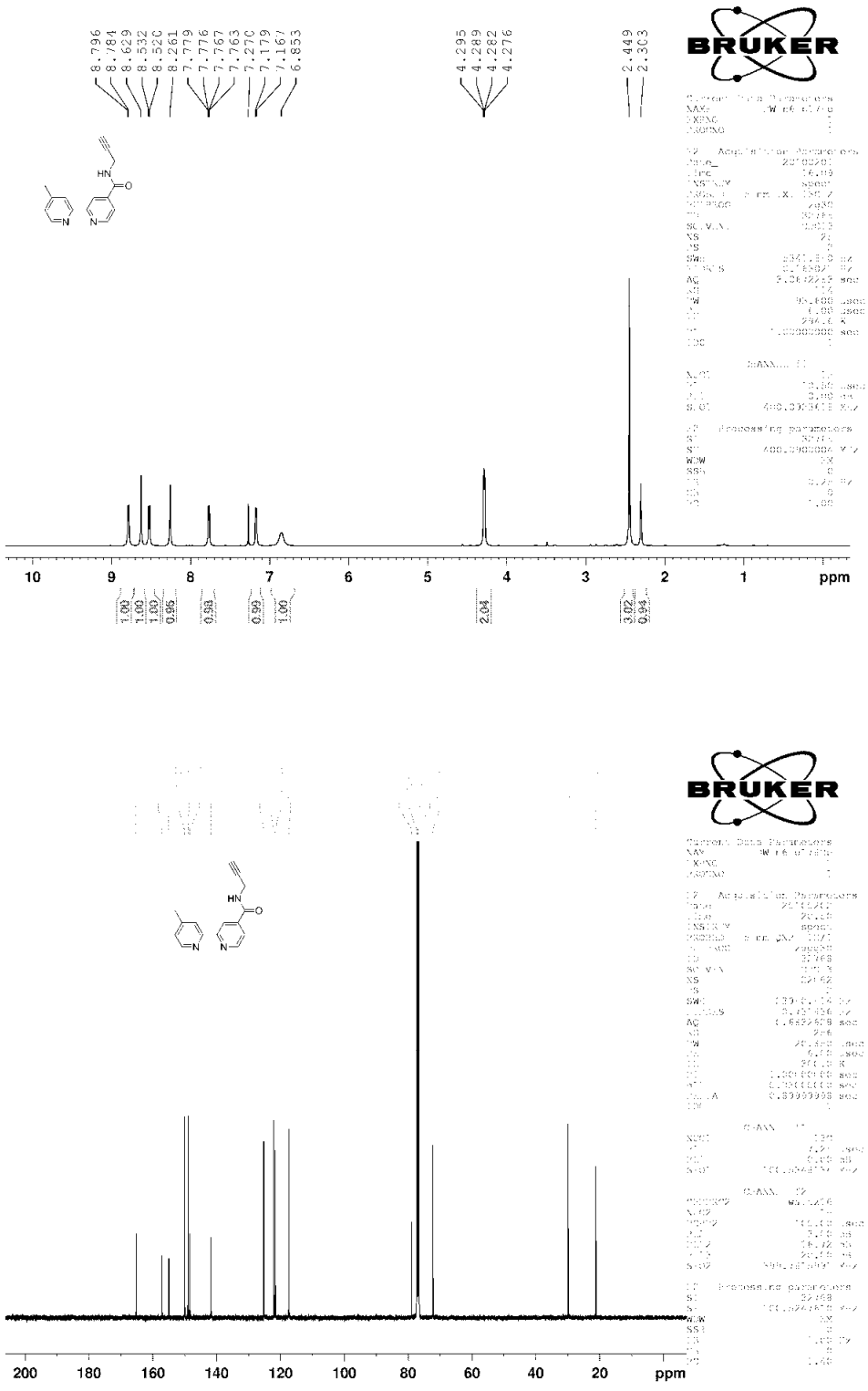

Figure 3.8 4'-Methyl-2,2'-bipyridine-4-propargylamide (**10**). ^{1}H $CDCl_3$, 400 MHz ^{13}C $CDCl_3$, 100 MHz.

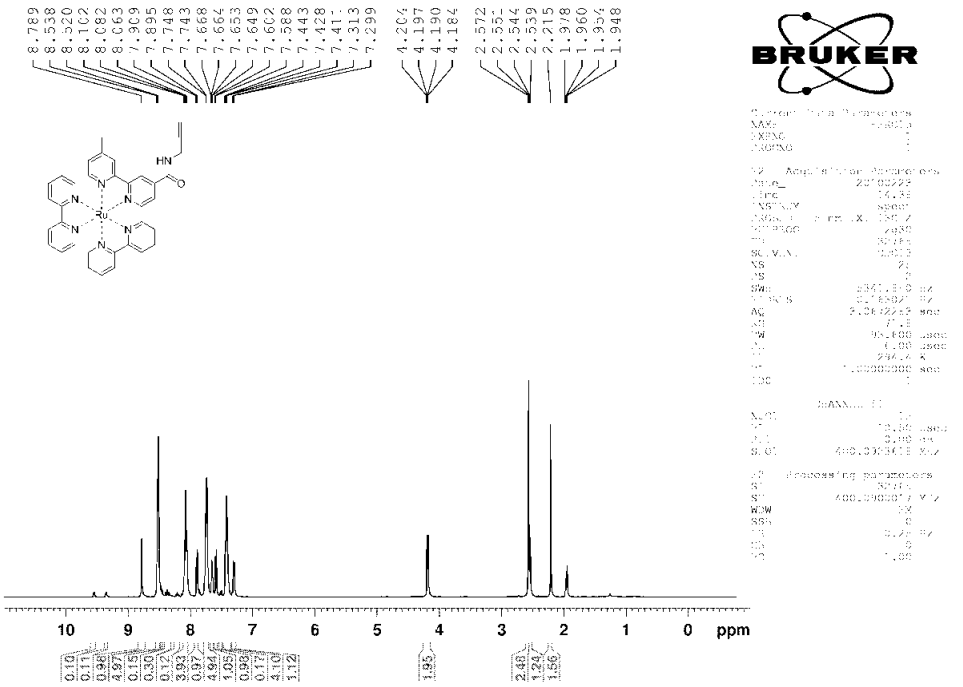

Figure 3.9 Bis-(2,2'bipyridine)(4'-Methyl-2,2'-bipyridine-4-propargylamide)-ruthenium(II) bis(hexafluorophosphate) (**11a**). ^{1}H CD_3CN, 400 MHz.

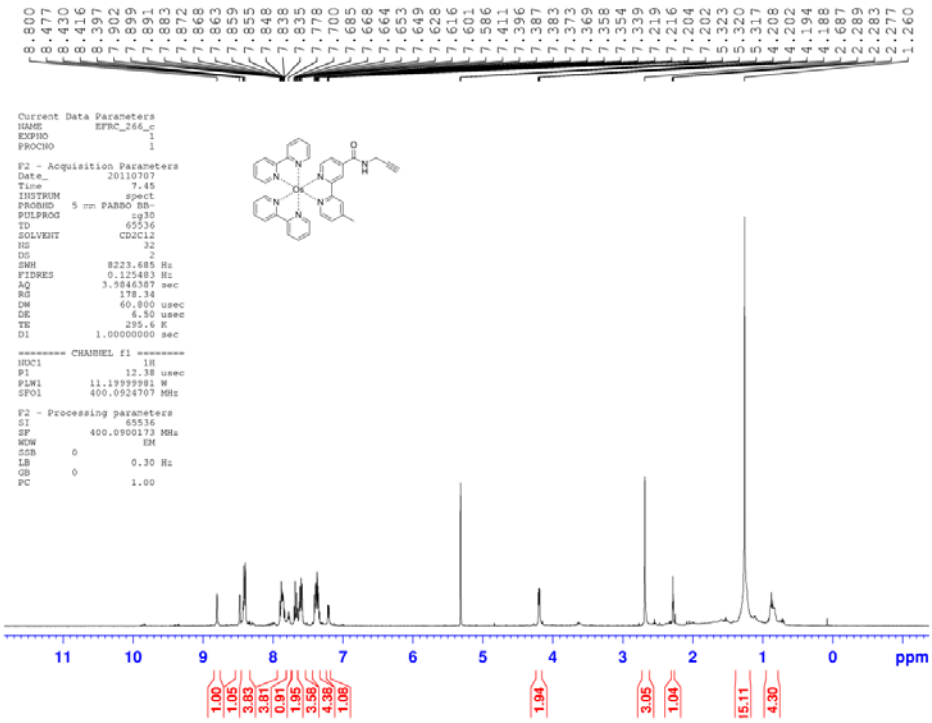

Figure 3.10 Bis-(2,2'bipyridine)(4'-Methyl-2,2'-bipyridine-4-propargylamide)-osmium(II) bis(hexafluorophosphate) (**11b**). ^{1}H CD_2Cl_2, 400 MHz.

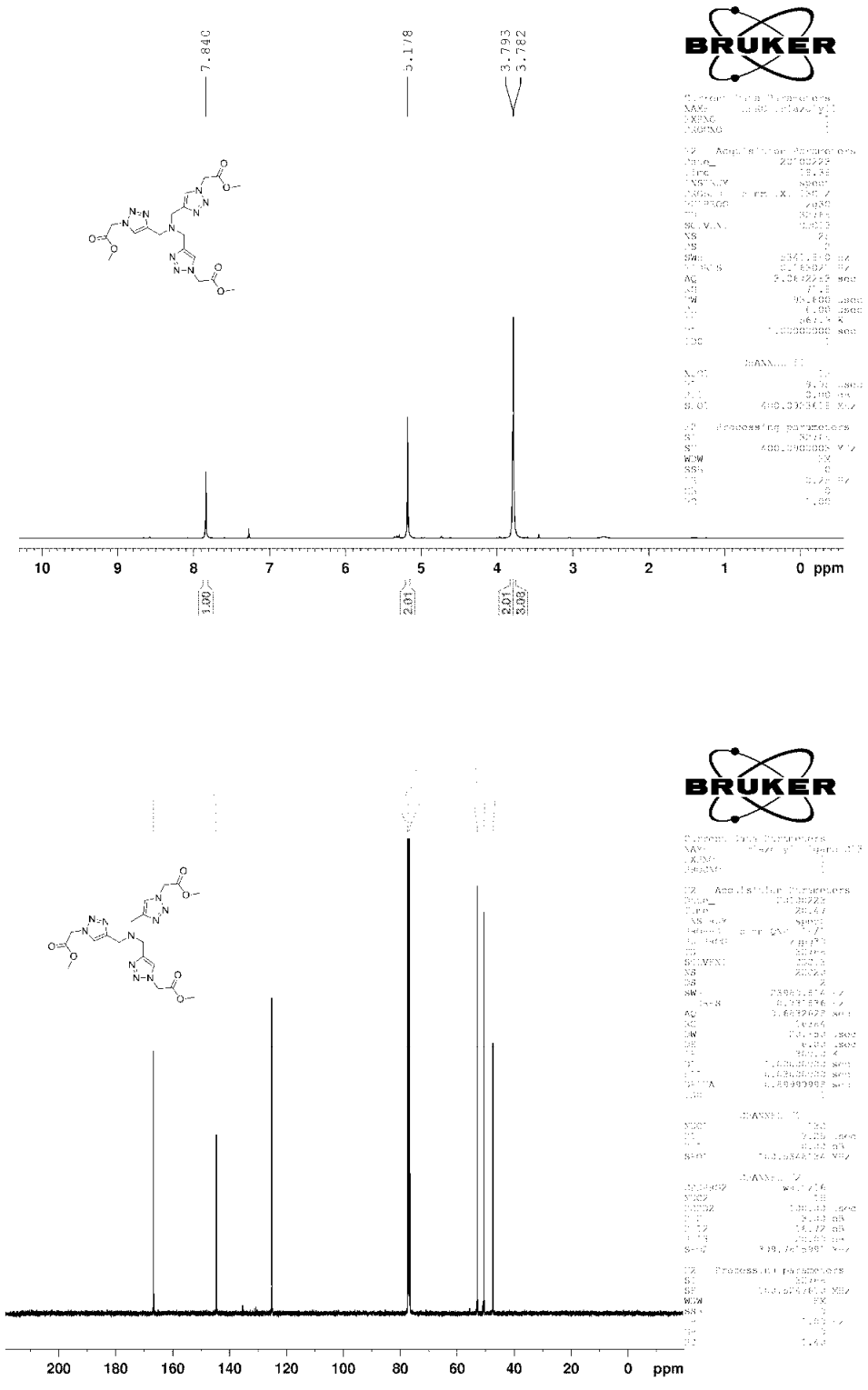

Figure 3.11 tris-(triazolylmethyl)amine ligand (**12**).^{1}H $CDCl_3$, 400 MHz. ^{13}C $CDCl_3$, 100 MHz.

References

[1](a) McCafferty, D. G.; Bishop, B. M.; Wall, C. G.; Hughes, S. G.; Mecklenberg, S. L.; Meyer, T. J.; Erickson, B. W. *Tetrahedron* **1995**, *51*, 1093-1106. (b) Geisser, B.; Ponce, A.; Alsfasser, R. *Inorg. Chem.* **1999**, *38*, 2030-2037. (c) Kise, Jr., K. J.; Bowler, B. E. *Inorg. Chem.* **2002**, *41*, 379-386. (d) Kise, Jr., K. J.; Bowler, B. E. *Inorg. Chem.* **2003**, *42*, 3891-3897. (e) McCafferty, D. G.; Friesen, D. A.; Danielson, E.; Wall, C. G.; Saderholm, M. J.; Erickson, B. W.; Meyer, T. J. *Proc. Natl. Acad. Sci. U.S.A.* **1996**, *93*, 8200-8204.

[2]Isidro-Llobet, A.; Alvarez, M.; Albericio, F. *Chem. Rev.* **2009**, *109*, 2455-2504.

[3](a) Wang, G.; Bergstrom, D. E. *Synlett* **1992**, *5*, 422-424. (b) Peek, B. M.; Ross, G. T.; Edwards, S. W.; Meyer, G. J.; Meyer, T. J.; Erickson, B. W. *Int. J. Peptide. Protein Res.* **1990**, *38*, 114-123. (c) Telser, J.; Cruickshank, K. A.; Schanze, K. S.; Netzel, T. L. *J. Am. Chem. Soc.* **1989**, *111*, 7221-7226.

[4]Johnson, S. R.; Westmoreland, T. D.; Caspar, J. V.; Barqawi, K. R.; Meyer, T. J. *Inorg. Chem.* **1988**, *27*, 3195-3200.

[5]Brandt, W. W.; Dwyer, F. P.; Gyarfas, E. D. *Chem. Rev.* **1954**, *54*, 959-1017.

[6]de Graaf, A. J.; Kooijman, M.; Hennink, W. E.; Mastrobattista, E. *Bioconjugate Chem.* **2009**, *20*, 1281-1295.

[7](a) Rostovtsev, V. V.; Green, L. G.; Fokin, V. V.; Sharpless, B. K. *Angew. Chem., Int. Ed.* **2002**, *41*, 2596-2599. (b) Tornøe, C. W.; Christensen, C.; Meldal, M. *J. Org. Chem.* **2002**, *67*, 3057-3064. (c) Meldal, M.; Tornøe, C. W. *Chem. Rev.* **2008**, *108*, 2952-3015.

[8](a) Franke, R.; Doll, C.; Eichler, J. *Tetrahedron Lett.* **2005**, *46*, 4479-4482. (b) Zaloom, J.; Roberts, D. C. *J. Org. Chem.* **1981**, *46*, 5173-5176. (c) Balducci, E.; Bellucci, L.; Petricci, E.; Taddei, M.; Tafi, A. *J. Org. Chem.* **2009**, *74*, 1314-1321.

[9](a) Hurley, D. J.; Tor, Y. *J. Am. Chem. Soc.* **1998**, *120*, 2194-2195. (b) Hurley, D. J.; Tor, Y. *J. Am. Chem. Soc.* **2002**, *124*, 3749-3762. (c) Hurley, D. J.; Tor, Y. *J. Am. Chem. Soc.* **2002**, *124*, 13231-13241. (d) Khan, S. I.; Beilstein, A. E.; Grinstaff, M. W. *Inorg. Chem.* **1999**, *38*, 418-419. (e) Khan, S. I.; Grinstaff, M. W. *J. Am. Chem. Soc.* **1999**, *121*, 4704-4705. (f) Khan, S. I.; Beilstein, A. E.; Smith, G. D.; Sykora, M.; Grinstaff, M. W. *Inorg. Chem* **1999**, *38*, 2411-2415. (g) Khan, S. I.; Beilstein, A. E.; Tierney, M. T.; Sykora, M.; Grinstaff, M. W. *Inorg. Chem.* **1999**, *38*, 5999-6002. (h) Tierney, M. T.; Sykora, M.; Khan, S. I.; Grinstaff, M. W. *J. Phys. Chem. B.* **2000**, *104*, 7574-7576.

[10]Isaad, A. L. C.; Barbetti, F.; Rovero, P.; D'Ursi, A. M.; Chelli, M.; Chorev, M.; Papini, A. M. *Eur. J. Org. Chem.* **2008**, *31*, 5308-5314.

[11]Goddard-Borger, E. D.; Stick, R. V. *Org. Lett.* **2007**, *9*, 3797-3800.

[12]Goddard-Borger, E. D.; Stick, R. V. *Org. Lett.* **2011**, *13*, 2514.

[13]Chan, T. R.; Hilgraf, R.; Sharpless, K. B.; Fokin, V. V. *Org. Lett.* **2004**, *6*, 2853-2855.

[14]Rodionov, V. O.; Fokin, V. V.; Finn, M. G. *Angew. Chem,. Int. Ed.* **2005**, *44*, 2210-2215.

[15]Donnelly, P. S.; Zanatta, S. D.; Zammit, S. C.; White, J. M. Williams, S. J. *Chem. Commun.* **2008**, 2459-2461.

[16]Lewis, W. G.; Magallon, F. G.; Fokin, V. V.; Finn, M. G. *J. Am. Chem. Soc.* **2004**, *126*, 9152-9153.

Chapter IV

PHYSICAL CHARACTERIZATION OF THE METALLOPEPTIDE DIMERS INCLUDING THE DETERMINATION OF DISSOCIATION CONSTANTS

A. Introduction

i. Choice of Ru^{II} and Os^{II} donor/acceptor positions for the metallopeptides

The importance of, and general considerations for, studying Ru^{II} to Os^{II} energy transfer were described in detail in Chapter I. The use of a dimeric coiled-coil peptide motif as a scaffold for studying Ru^{II} to Os^{II} energy transfer was introduced within Chapter II, along with the relevant design principles used for the selection of the parent sequences. The synthetic manipulations required for the preparation of the 2*b*-Ru, 2*e*-Ru, 2*f*-Ru, 2*c*-Os, 2*f*-Os, and 2*g*-Os metallopeptides were described in Chapter III. The specific substitution positions were chosen to provide a range of distances for the study of energy transfer, while not disrupting the coiled-coil structure of interest. The substitutions were made within the second heptad repeat unit of each coiled-coil parent sequence (Figure 4.1a). Substitutions near the peptide termini were avoided in order to prevent further disruption of the secondary structure due to end fraying (Chapter II). Avoiding Ru^{II}- and Os^{II}-substitution at the termini was also expected to provide more reliable donor/acceptor displacements during the energy transfer studies. The choices for the second heptad repeat unit versus the third heptad repeat unit were arbitrary. The choice to use the P2 parent sequence for the donor (Ru^{II})

metallopeptides and the P1 parent sequence for the acceptor (Os^{II}) metallopeptides was also arbitrary.

ii. Choice of metallopeptide pairs for analysis

Throughout the energy transfer studies discussed in Chapter V, the metallopeptides are examined as specific coiled-coil pairs. In this chapter the folding and association of the metallopeptides is examined for the same pairs in order to facilitate direct comparisons. Coiled-coil association and intermolecular energy transfer were studied for the 2*f*-Ru/2*f*-Os, 2*b*-Ru/2*c*-Os, and 2*e*-Ru/2*g*-Os metallopeptide pairs (Figure 4.1b). Although other metallopeptide partners could have potentially associated and facilitated energy transfer between the Ru^{II} and Os^{II} bipyridyl complexes, they were not specifically studied within this work.

The relative two-dimensional positioning of the different metallopeptide pairs is represented as a helical wheel diagram (Figure 4.1b). The relative three-dimensional positioning of the donor/acceptor bipyridyl complexes involves there longitudinal displacement as well, and may be roughly estimated from crystal structures of similar coiled-coil peptides (Figure 4.2). The 2*f*-Ru/2*f*-Os metallopeptide pair could be expected to provide the greatest donor/acceptor displacement with an approximate distance of 14.3 Å measured between the respective α-carbons. Distance measurements made between α-carbons could however be misleading due to the individual bond vectors (α-β) linking the bipyridyl complexes to the coiled-coil structure. For example, the 2*f*-Ru/2*f*-Os C_α-C_β bonds would project the donor/acceptor pairs even further apart. The expected distance between the 2*f*-Ru/2*f*-Os β-carbon atoms would increase to roughly 16.2 Å.

(a)

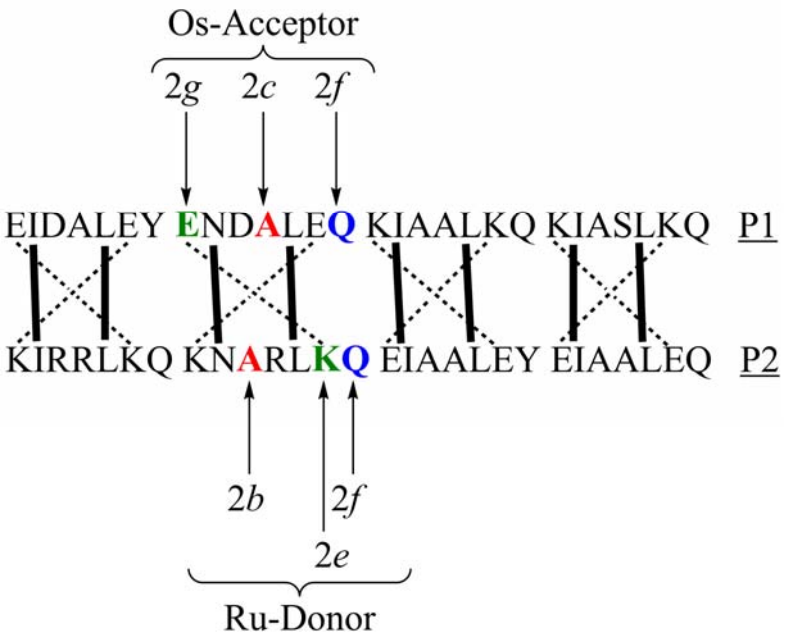

(b)

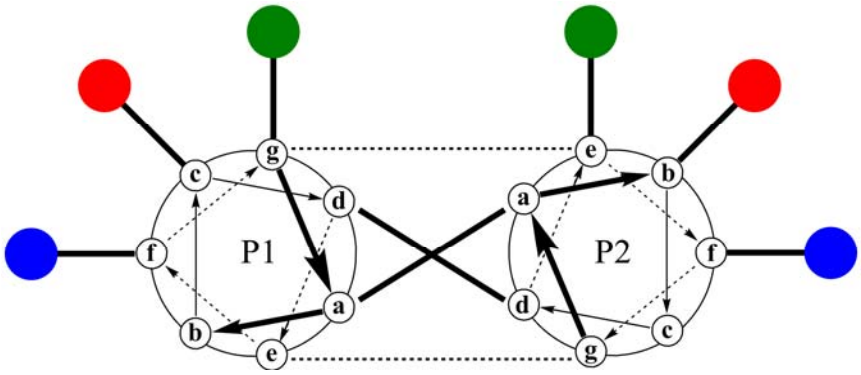

Figure 4.1 (a) The primary sequences for the P1 and P2 parent peptides showing the positions of modification for the 2*g*-Os, 2*c*-Os, 2*f*-Os, 2*b*-Ru, 2*e*-Ru, and 2*f*-Ru metallopeptides. Natural amino acids are designated using single letter codes. These positions are substituted with azidolysine in the azidopeptides, and in the metallopeptides they have been altered by attachment of either Ru^{II} (P2) or Os^{II} (P1) bipyridyl complexes as described in Chapter III. (b) A helical wheel diagram for the metallopeptide partners examined throughout the study. The 2*f*-Ru/2*f*-Os (blue), 2*b*-Ru/2*c*-Os (red), and 2*e*-Ru/2*g*-Os (green) metallopeptide pairs are shown, although the two-dimensional diagram is not necessarily representative of the actual donor/acceptor positions within the three-dimensional coiled-coil peptide scaffold.

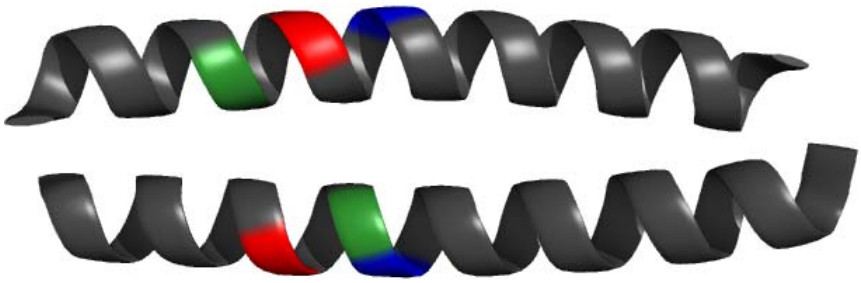

Figure 4.2 Crystal structure of a similar coiled-coil dimer (pdb code: 2ZTA). The relative positions corresponding to the 2*f*-Ru/2*f*-Os (blue), 2*b*-Ru/2*c*-Os (red), and 2*e*-Ru/2*g*-Os (green) metallopeptide pairs are shown.

The 2*b*-Ru/2*c*-Os metallopeptide pair could be expected to have a donor/acceptor displacement ranging from 12.7 to 14 Å, depending on whether the distance was measured from the α- or β-carbons. In the case of the 2*e*-Ru/2*g*-Os metallopeptide pair, the relative donor/acceptor displacement could be expected to decreases from 9.9 Å measured between the α-carbons to 9.1 Å measured between the β-carbons. This is due to the 2*g*-Os C_α-C_β bond directing the side chain towards the helical interface.

The ε-azido-L-lysine linker described in Chapter III was designed to provide a flexible four methylene tether for the Ru^{II} and Os^{II} bipyridyl complexes. The length and conformational freedom of the linker was predicted to prevent destabilization of the coiled-coil peptide structure, but also introduces a greater extent of ambiguity in determining precise donor/acceptor distances. For this reason the relative distances discussed above could not be assumed entirely representative of the donor/acceptor distances provided by the coiled-coil peptide scaffold until further analysis was performed.

The specific attachment points for the different metallopeptide pairs all have subtle effects on their observed structural stabilities. Circular dichroism spectroscopy and chemical denaturation analysis experiments are described throughout Chapter IV, in order to provide an understanding of the structural differences between the metallopeptide pairs.

Also described within this chapter is the computational modeling of the conformational states for the coiled-coil peptide backbones, the attached bipyridyl complexes, and the azido-L-lysine linkers for all three metallopeptide pairs using high-level molecular dynamics simulations. This work was performed in collaboration by Dr. Christopher Materese under the advisement of Professor Garyk Papoian.

B. Circular dichroism analysis of the metallopeptide pairs

Since the folding behavior of the coiled-coil metallopeptides is bimolecular, each pair has a related dissociation (K_d) constant that can be used to quantify and predict equilibrium concentrations of folded coiled-coil dimer and unfolded peptide monomer for any given preequilibrium concentration. Determination of a K_d for each metallopeptide pair is required to interpret the energy transfer behavior described in Chapter V.

Circular dichroism (CD) is a spectroscopic technique where the differential absorption of right and left circularly polarized light is measured for a sample.[1] Since right and left circularly polarized light are chiral, many biomolecules including peptides and oligonucleotides, interact differently with the polarized forms of light. These interactions lead to characteristic CD features that are typically expressed in terms of concentration corrected molar ellipticity values at specific wavelengths (θ_x).[1] For peptides these ellipticity measurements are also corrected for the number of amino acid residues and the measurement is referred to as the mean molar residue ellipticity ($[\theta]_x$). The standard ellipticity designation is bracketed to express this quantity with the units $deg \cdot cm^2 \cdot dmol^{-1}$.

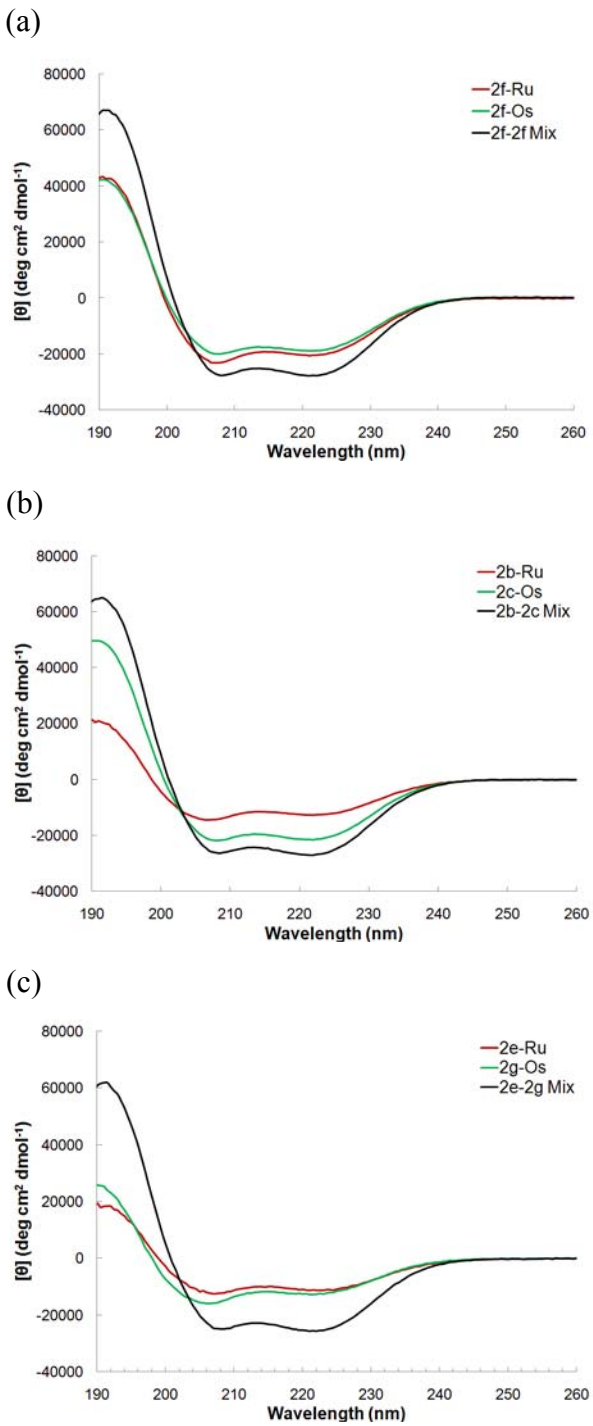

Figure 4.3. Circular dichroism (CD) spectra for all three metallopeptide pairs. (a) CD spectra for the 2*f*-Os (green) and 2*f*-Ru (red) peptides at 50 μM concentrations. A 1:1 mixture of the two peptides (black, 50 μM combined peptide concentration) shows a more intense negative signal at 222 nm indicating an increase in the α-helicity for the two peptides. (b) A similar analysis for the 2*c*-Os (green) and 2*b*-Ru (red) peptides at 50 μM concentrations. (c) A similar analysis for the 2*g*-Os (green) and 2*e*-Ru (red) peptides at 50 μM concentrations. All spectra were recorded at 25°C in 10 mM PO_4^{3-}, pH 7, buffer.

The CD spectra for all three heterodimeric metallopeptide pairs display features characteristic of α-helices, and more specifically to α-helical coiled-coils (Figure 4.3). These features include maxima below 200 nm, and pairs of minima at 208 and 222 nm.[1,2] The CD signals associated with the α-helical peptide secondary structure are concentration dependent for the metallopeptide pairs since folding and dimerization are coupled in these peptide structures. This concentration dependence qualitatively indicates that the metallopeptide pairs form coiled-coil structures when mixed in low μM concentrations. The ellipticity at 222 nm ($[\theta]_{222}$) corresponds to an *n*-π* transition and can be used as a quantitative measure of α-helicity, and therefore dimerization.[2] The ratio of the CD signals at 208 and 222 nm ($[\theta]_{222}/[\theta]_{208}$) also gives evidence for dimeric coiled-coil structures. The CD signal at 208 nm ($[\theta]_{208}$) is due to a π-π* transition parallel to the helix axis and is sensitive to whether the helix is single stranded or is part of a greater helical bundle.[2] The ellipticity ratio $[\theta]_{222}/[\theta]_{208}$ for the 2*f*-Os/2*f*-Ru metallopeptide pair is equal to 1.00. The 2*c*-Os/2*b*-Ru and 2*g*-Os/2*e*-Ru peptide pairs both have $[\theta]_{222}/[\theta]_{208}$ ratios equal to 1.03. Ratios of 1.0 or greater are characteristic of dimeric coil coil peptides, as single-stranded α-helices typically have values closer to 0.85.[3]

All three metallopeptide pairs were analyzed using continuous variation experiments. The different metallopeptides all display maximum α-helicity (minimum at $[\theta]_{222}$) when equimolar mixtures of the donor/acceptor metallopeptides are examined, indicating that heterodimeric coiled-coil structures are being formed in a 1:1 ratio (Figure 4.4). This is not unexpected since the sequences were designed to form dimeric species, but still important to confirm since trimeric species are often the default structure for α-helical coiled-coils when design features favoring the dimeric structure are not strongly reinforcing.[4]

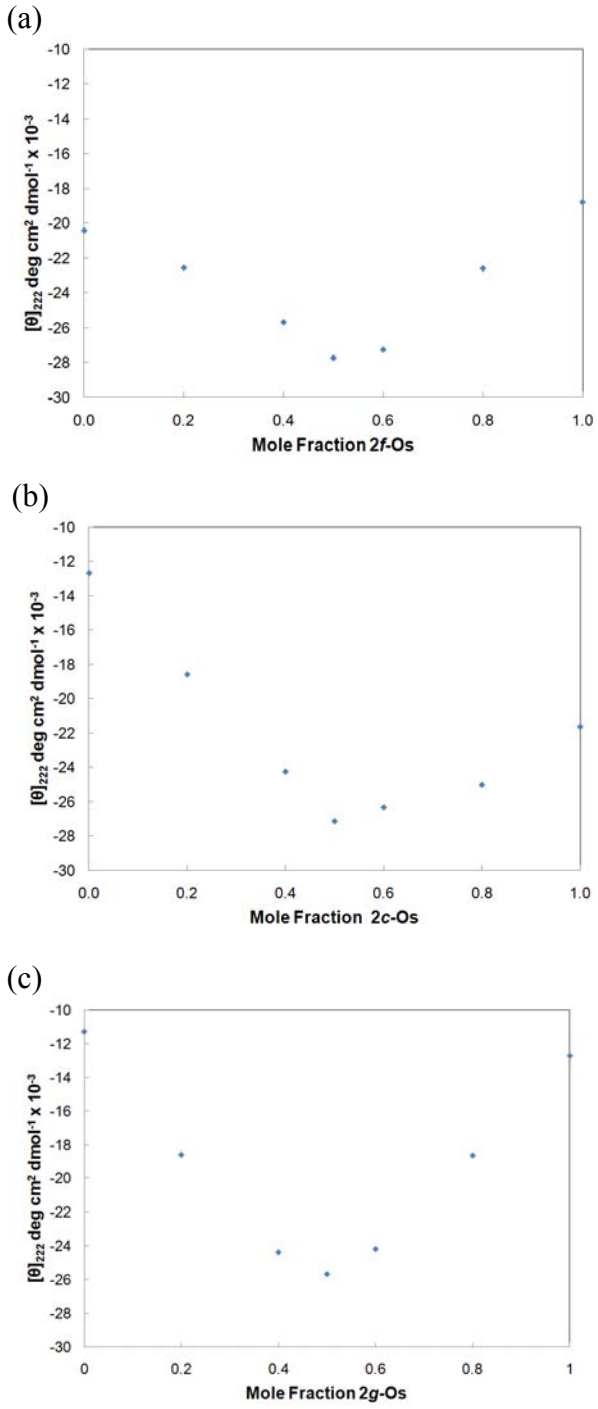

Figure 4.4 Continuous variation experiments (Job plot) for the metallopeptide pairs measured using the $[\theta]_{222}$ CD signal. (a) The 2*f*-Ru/2*f*-Os metallopeptide pair examined at a continuous concentration of 50 μM with variations made in the 2*f*-Os mole fraction. (b) The 2*b*-Ru/2*c*-Os metallopeptide pair examined at a continuous concentration of 50 μM with variations made in the 2*c*-Os mole fraction. (c) The 2*e*-Ru/2*g*-Os metallopeptide pair examined at a continuous concentration of 50 μM with variations made in the 2*g*-Os mole fraction. All spectra were recorded at 25°C in 10 mM PO_4^{3-}, pH 7, buffer.

C. Guanidinium chloride denaturation of the metallopeptide pairs

Chemical denaturation using guanidinium chloride (GndHCl) provides a reliable tool for measuring coiled-coil dissociation constants.[5] The method has been used to compare minute structural changes within families of similarly designed coiled-coils.[5c] Dissociation constants can also be measured directly from the concentration dependence of the $[\theta]_{222}$ signal,[6] however measuring dissociation constants by this method does have several disadvantages. Firstly, the ellipticity ($[\theta]_{222}$) must be accurately measured over a broad range of concentrations both above and below the dissociation constant. This requirement introduces technical complications since extremely high or low concentrations of peptides may not have the same solubility and/or may require cuvettes of different path lengths. Secondly, the method assumes that the individual monomers have a very low helical content and contribute only minimally to the $[\theta]_{222}$ signal. This assumption may not necessarily be true since many of the relevant amino acid residues may have a high helical propensity outside of the context of a coiled-coil peptide structure.[4] Alternatively, chemical denaturation experiments using GndHCl are performed at a single peptide concentration that is well above the dissociation constant for the coiled-coil pair. The assumption made during a GndHCl denaturation experiment is that at high peptide concentrations the coiled-coil is entirely associated and α-helical monomer concentrations are well below the detectable limit. Additionally, any peptide monomers that are not associated within a coiled-coil structure will be fully unfolded in the denaturing medium and will not contribute significantly to the observed $[\theta]_{222}$ signal.

Performed as a titration, GndHCl denaturation experiments track the unfolding of the coiled-coil structure as a function of the denaturant concentration. The fraction folded (F_F) at any denaturant concentration can be calculated using Equation 1 (Figure 4.5a):[5c]

$$F_F = ([\theta] - [\theta]_D)/([\theta]_F - [\theta]_D) \qquad Equation\ 1$$

where $[\theta]$ is the observed CD signal, $[\theta]_F$ is the CD signal for the fully folded coiled-coil at a denaturant concentration of zero, and $[\theta]_D$ is the CD signal for the fully denatured mixture. The fraction unfolded (F_U) can be calculated using Equation 2:[5c]

$$F_U = 1 - F_F \qquad Equation\ 2$$

Once the fraction folded and fraction unfolded have been calculated, the free energy of unfolding (ΔG_D) can be measured for all denaturant concentrations using Equation 3:[5c]

$$\Delta G_D = -RTln\left(\frac{2P_T F_U^2}{F_F}\right) \qquad Equation\ 3$$

where P_T is the total peptide concentration, R is the molar gas constant in units of cal·mol^{-1}·K^{-1} (1.986), and T is the temperature in Kelvin (298). The method of linear extrapolation is used to calculate the free energy of unfolding in the absence of denaturant (ΔG_{H20}), using Equation 4:[5c]

$$\Delta G_D = \Delta G_{H2O} - m[GdnHCl] \qquad Equation\ 4$$

where [GdnHCl] is the GndHCl denaturant concentration in units of molarity, m is the slope, and ΔG_{H20} is the y-intercept. The method of linear extrapolation is used to measure the y-intercept (ΔG_{H20}).[5a] The method assumes that the dependence of ΔG_D on the denaturant concentration observed throughout the transition period continues to be linear at denaturant

concentrations approaching zero. The GndHCl denaturation midpoint (C_m) is included in the linear extrapolation, along with adjacent points which produce a reliable linear fit (R^2 values close to unity).

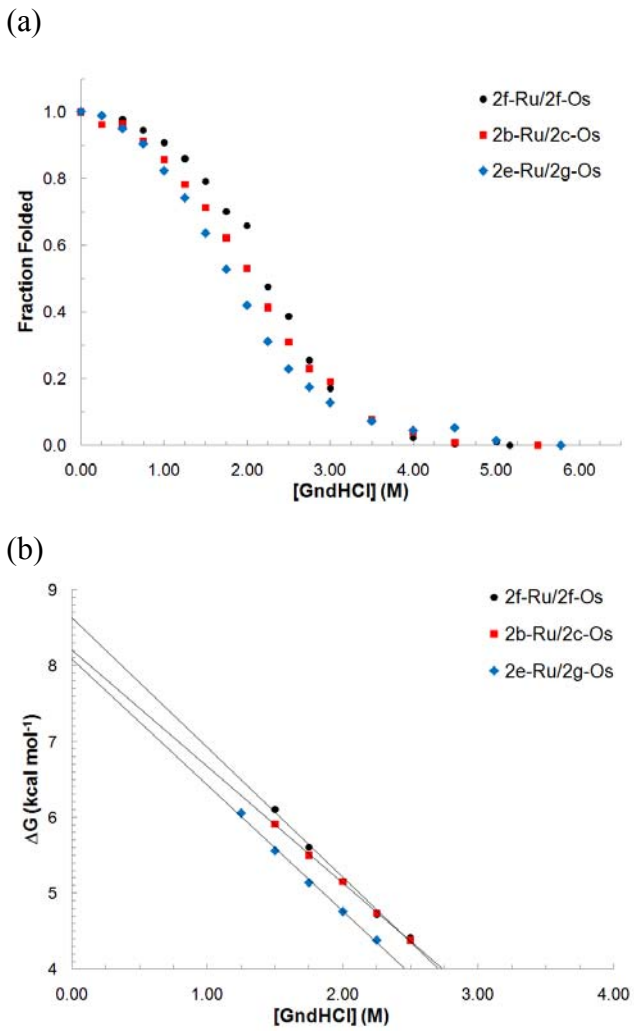

Figure 4.5 (a) GndHCl denaturation curves at 25 °C in 20 mM PO_4^{3-}, 100 mM NaCl, pH 7.4 buffer. Data shown for the 2*f*-Ru/2*f*-Os pair (black circles, 300 μM), the 2*b*-Ru /2*c*-Os pair (red squares, 200 μM), and the 2*e*-Ru/2*g*-Os pair (blue diamonds, 200 μM). The fraction folded (F_F) values were calculated using Equation 1. (b) Gibbs free energy of unfolding (ΔG_D) was calculated using Equation 3. Linear extrapolation using Equation 4 gives the value of the free energy of unfolding at zero denaturant concentration (ΔG_{H20}). Data shown for the 2*f*-Ru/2*f*-Os pair (black circles, m = -1.7 kcal·mol^{-1}·M^{-1}, R^2 =0.997), the 2*b*-Ru /2*c*-Os pair (red squares, m = -1.5 kcal·mol^{-1}·M^{-1}, R^2 =0.999), and the 2*e*-Ru/2*g*-Os pair (blue diamonds, m = -1.7 kcal·mol^{-1}·M^{-1}, R^2 =0.997).

Dissociation constants (Table 4.1.) for all three metallopeptide pairs were determined using the ΔG_{H20} values and Equation 5:

$$K_d = 10^{6} \cdot e^{-\left(\frac{\Delta G_{H2O}}{RT}\right)} \quad Equation\ 5$$

Dissociation constants could not be determined for the coiled-coil parent sequences due to solubility issues during the analysis. The 2*f*-Ru/2*f*-Os metallopeptide pair appeared to form the most thermodynamically stable coiled-coil peptide structure. The value of ΔG_{H20} measured for the 2*f*-Ru/2*f*-Os pair (8.6 ± 0.10 kcal·mol^{-1}) corresponds to a K_d of 0.49 ± 0.09 μM (Table 4.1).

Table 4.1. Folding parameters obtained from guanidinium denaturation experiments

Peptide Pair	**ΔG_{H2O} (kcal·mol^{-1})[a]**	**K_d (μM)[b]**	**C_m (M)[c]**	**% α-helicity[d]**
2*f*-Ru/2*f*-Os	8.6	0.49 ± 0.09	2.2	80%
2*b*-Ru/2*c*-Os	8.2	0.97 ± 0.2	2.0	74%
2*e*-Ru/2*g*-Os	8.0	1.4 ± 0.3	1.8	72%

[a]Values for ΔG_{H20} were calculated by the method of linear extrapolation using Equation 4. The error in the measurement of ΔG_{H20} was estimated to be less than 0.10 kcal·mol^{-1} for all. [b]The K_d values were calculated using Equation 5. Error estimates are included with the values and were calculated based on the observed error for ΔG_{H20}. [c]The GndHCl denaturation midpoints (C_m) were calculated based on the linear relationship between folded (F_F) and denaturant concentration ([GndHCl]) within the transition region and typically had an error of less than 0.05 M. [d]The percent α-helicity values are based on a value of -35,900 deg·cm^2·dmol^{-1} calculated for all three pairs using Equation 6.

The calculation of α-helical content has previously been described for similar *de novo* designed coiled-coils. The α-helical content can be estimated based on the theoretical maximum α-helicity for a 28-residue peptide. The maximum α-helicity for a peptide of any chain length can be calculated using Equation 6:[7]

$$[\theta]_{222}{}^{n} = ([\theta]_{222}{}^{\infty})\left(1 - {}^{k}/_{n}\right) \quad Equation\ 6$$

where n is the number of amino acid residues, $[\theta]_{222}^{\infty}$ is the mean molar residue ellipticity of an α-helix of infinite length taken to be -39,500 deg·cm^2·dmol^{-1}, and k is a wavelength-dependent factor taken to be 2.57 at 222 nm. Based on Equation 6, the maximum α-helicity for all three metallopeptide pairs would be -35,900 deg·cm^2·dmol^{-1}. The fully folded 2*f*-Ru/2*f*-Os dimer was calculated to be 80% α-helical based on the observed $[\theta]_{222}$ (-28,600 ± 800 deg·cm^2·dmol^{-1}). These values were measured at peptide concentrations where the fraction folded closely approaches unity. Measured values less than 100% do not imply the presence of monomeric species, but instead imply that the peptides within the coiled-coil dimer adopt nonideal α-helical conformations. The α-helical content reported for the 2*f*-Ru/2*f*-Os dimer falls within the range reported for peptides of similar length and sequence structure with values from 69-96% being common in the literature.[6,8]

The 2*b*-Ru/2*c*-Os peptide pair displays minor destabilization when compared to the 2*f*-Ru/2*f*-Os pair. The difference in ΔG_{H20} measured (8.2 ± 0.10 kcal·mol^{-1}) for the 2*b*-Ru/2*c*-Os dimer corresponds to an increase in the extrapolated K_d (0.97 ± 0.2 μM). The maximum ellipticity for the 2*b*-Ru/2*c*-Os peptide pair (-26,400 ± 700 deg·cm^2·dmol^{-1}) corresponded to 74% α-helicity, indicating slightly less α-helical character when compared to the 2*f*-Ru/2*f*-Os pair. The 2*e*-Ru/2*g*-Os peptide pair was found to be the most destabilized heterodimer, although the magnitude of the destabilization was again quite minimal. The extrapolated ΔG_{H20} (8.0 ± 0.10 kcal·mol^{-1}) value for the 2*e*-Ru/2*g*-Os peptide pair was within error of that reported for the 2*b*-Ru/2*c*-Os pair. The calculated K_d (1.4 ± 0.3 μM) value for 2*e*-Ru/2*g*-Os peptide pair was therefore also within error. The maximum ellipticity (-25,900 ± 300 deg·cm^2·dmol^{-1}) for the 2*e*-Ru/2*g*-Os peptide pair corresponded to 72% α-helicity. Although the thermodynamic parameters (ΔG_{H20}, K_d, and % α-helicity) for the 2*b*-Ru/2*c*-Os and 2*e*-

Ru/2*g*-Os metallopeptide pairs are all within error, the GndHCl denaturation midpoints (C_m = 2.0 M for the 2*b*-Ru/2*c*-Os and 1.8 M for the 2*e*-Ru/2*g*-Os) for the two pairs analyzed at the same total peptide concentrations are well outside of error. Chemical denaturation midpoints are often used to compare structurally similar peptide sequences since ΔG_{H20} values are extrapolated and inherently prone to large errors.[5c] The difference in free energy of unfolding between two peptides ($\Delta\Delta G_D$) can be calculate using Equation 7:[9]

$$\Delta\Delta G_D = (C_m^A - C_m^B)(m_A - m_B)(0.5) \quad Equation\ 7$$

where C_m^A and C_m^B are the GndHCl denaturation midpoints for two peptides A and B, and m_A and m_B are the slope values from Equation 4 applied to peptide A and B, respectively. The value of $\Delta\Delta G_D$ calculated for the 2*b*-Ru/2*c*-Os and 2*e*-Ru/2*g*-Os metallopeptide pairs is 0.3 kcal·mol^{-1}. This observation does indicate that the 2*e*-Ru/2*g*-Os peptide pair is somewhat destabilized when compared to the 2*b*-Ru/2*c*-Os pair. This result is not entirely unsurprising since the 2*e*-Ru and 2*g*-Os metallopeptides are substituted with bipyridyl complexes at the ***e*** and ***g*** positions, respectively. As discussed in Chapter II, amino acid residues at these positions are typically close to the hydrophobic core and are designed to provide attractive charge-charge interactions,[10] while the Ru^{II} and Os^{II} bipyridyl complexes may behave repulsively due to their identical positive charges.

The determination of K_d values for all three metallopeptide pairs is important for accurately measuring energy transfer in these systems since only the properties of donor/acceptor dimers are of interest. The energy transfer studies (Chapter V) for the different metallopeptide pairs were typically performed as titrations with the Ru^{II} peptide concentration fixed at 25 μM. The Os^{II} peptide concentrations employed were 6.25, 12.5, 18.75, 25.0, and 50.0 μM corresponding to 0.25, 0.5, 0.75, 1.0 and 2.0 equivalents compared

to the Ru^{II} peptide. Given the extinction coefficients of the bipyridyl complexes (~14,600 at 452 nm for $Ru(bpy)_3^{2+}$, and ~12,000 at 480 nm for $Os(bpy)_3^{2+}$) in water,[11,12] this concentration regime was appropriate for emission studies using a 0.2 cm optical path length cell. The K_d values allow for percent dimer and percent monomer to be calculated for each metallopeptide pair at the concentrations used during the energy transfer studies (Table 4.2). These values will be used later for comparison during the energy transfer studies.

Table 4.2. Percent dimer for the analyzed metallopeptides

Os^{II} Peptide Equivalents	Os^{II} Peptide Concentration[a] (μM)	2*f*-Ru/2*f*-Os Percent Dimer[b]	2*b*-Ru/2*c*-Os Percent Dimer[c]	2*e*-Ru/2*g*-Os Percent Dimer[d]
0.00	0.00	0	0	0
0.25	6.25	24	24	23
0.50	12.5	48	47	45
0.75	18.75	70	66	65
1.00	25.0	87	82	79
2.00	50.0	98	96	95

[a]The Ru^{II} peptide concentration is 25 μM for all three metallopeptide pairs. [b]The dimer concentration was calculated based on a K_d value of 0.49 μM for the 2*f*-Ru/2*f*-Os peptide pair. [c]The dimer concentration was calculated based on a K_d value of 0.97 μM for the 2*b*-Ru/2*c*-Os peptide pair. [d]The dimer concentration was calculated based on a K_d value of 1.4 μM for the 2*e*-Ru/2*g*-Os peptide pair. The percent dimer for each metallopeptide pair is calculated relative to the total Ru^{II} peptide concentration (25 μM).

Any equilibrium that can be described using a dissociation constant (K_d) can also be described as a ratio of association and dissociation rates as shown in equation 8:[6]

$$K_d = {k_{on}}/{k_{off}} \qquad Equation\ 8$$

where k_{on} is the rate of association to form the complex and k_{off} is the rate of dissociation that destroys the peptide-peptide complex. Although we have not directly measured the rates of k_{on} or k_{off}, comparison to other coiled-coil systems with low μM K_d values would imply that association occurs on the microsecond timescale and dissociation most likely occurs on the

millisecond to second timescale.[6] Since the decay of the $Ru(bpy)_3^{2+}$ ^{3}MLCT excited state (discussed in Chapter I) decays on the time scale of several hundred nanosecond in water,[11] one can tentatively conclude that coiled-coil strand exchange is unlikely to affect any energy transfer studies.

D. All-atom molecular dynamics simulations

As mentioned in the introductory section, the ε-azido-L-lysine amino acid residue used to incorporate the Ru^{II} and Os^{II} bipyridyl complexes is quite flexible. The length and flexibility of the linker may allow the metallopeptides to adopt a number of different conformational states in solution. A general trend may be anticipated based on the crystal structure analysis presented above (Figure 4.2), but an accurate depiction of metal complex displacement distances is certainly missing. All-atom molecular dynamics simulations were performed to better understand the possible solution-phase behaviors of the synthetic metallopeptide pairs. This work was performed by Dr. Christopher Materese under the advisement of Professor Garyk Papoian.

Similar to the structural analysis, the theoretical analysis was performed separately for the 2*f*-Ru/2*f*-Os, 2*b*-Ru/2*c*-Os, and 2*e*-Ru/2*g*-Os metallopeptide pairs. Both bipyridyl complexes were modeled as Ru^{II} in order to save computing space, and also because metallopeptide dynamics were of interest and energy transfer itself was not modeled. The designation for the metal identity is dropped throughout this section, and the metallopeptide pairs 2*f*-Ru/2*f*-Os, 2*b*-Ru/2*c*-Os, and 2*e*-Ru/2*g*-Os are instead referred to as the 2*f*/2*f*, 2*b*/2*c*, and 2*e*/2*g* pairs. The exact details for the simulations are provided within the experimental section.

The different simulations did indeed demonstrate dynamic behaviors for the metallopeptides, with many small local perturbations in the coiled-coil structure occurring at a very fast rate. These localized structural changes occur within the coiled-coil peptide scaffold, and also within the ε-azido-L-lysine linker. The vast majority of the dynamic movements did not lead to substantial displacement of the bipyridyl complexes, and would not be expected to affect energy transfer rates. In addition to the small structural changes the metallopeptide dimers experience, there are large scale movements of the bipyridyl complexes that do result in substantial changes in the displacements of the bipyridyl complexes. These larger scale movements allowed the metallopeptide pairs to occupy specific conformational states for extended periods of time during the simulation experiment. Histograms representing the relative time that the different metallopeptide pairs occupy different conformational states are presented below (Figure 4.6).

The simulation for the 2*f*/2*f* metallopeptide pair shows a relatively large metal-center displacement throughout the experiment. The metal-center distance distributions are very broad and non-Gaussian. The 2*f*/2*f* peptide pair exhibits the broadest range of metal-center distance distributions when compared to the 2*b*/2*c* and 2*e*/2*g* pairs (Figure 4.6a). Most of the conformations for the 2*f*/2*f* peptide pair place the bipyridyl complexes at distances greater than 2 nm. The relatively large metal-center displacements would imply that the 2*f*/2*f* peptide pair would be inefficient at promoting energy transfer compared to the 2*b*/2*c* and 2*e*/2*g* pairs, although it is possible that conformations with smaller metal-center displacements could exist and were simply not observed during the simulated time frame. One observation involving metallopeptide stability was made for the 2*f*/2*f* peptide pair. During the simulation experiment, conformations that brought the bipyridyl complexes and peptide termini in

proximity appeared to destabilize the coiled-coil structure. The interaction between the bipyridyl complexes and peptide scaffold would imply that the two have complementary attractive forces. Whether those interactions are hydrophobic, dipole-dipole, Van der Waals, Coulombic, or other in nature is difficult to determine but they do seem to affect coiled-coil stability near the peptide termini were the propensity for fraying is already increased.

The 2*b*/2*c* and 2*e*/2*g* metallopeptide pairs both exhibited conformations with significantly shorter metal-center displacements, demonstrating that some degree of positional control is exerted by the coiled-coil scaffold. The simulation for the 2*b*/2*c* pair shows the metallopeptides persistently occupying a conformation where the bipyridyl complexes are in close contact (Figure 4.6b). This conformation is characterized by a small metal-center displacement, close to 0.8 nm, and a close stacking of the bipyridyl ligands placing them in Van der Waals contact with each other (Figure 4.7a). The simulation for the 2*e*/2*g* pair shows the metallopeptide persistently occupying a conformation with a metal-center displacement closer to 1.2 nm (Figure 4.6c). This conformation is also characterized by fewer Van der Waals contacts between bipyridyl ligands coordinated to the metal centers (Figure 4.7b). The 2*e*/2*g* pair certainly is capable of accessing conformations similar to those observed almost exclusively for the 2*b*/2*c* pair, so it is unclear whether the preference for the conformation with the larger metal-center displacement would persist over longer periods of simulation. Both the 2*b*/2*c* and 2*e*/2*g* metallopeptide pairs occupy conformational states that allow the donor/acceptor bipyridyl complexes to access each other in solution, and are most likely both sufficient promoters of energy transfer when compared to the 2*f*/2*f* peptide pair.

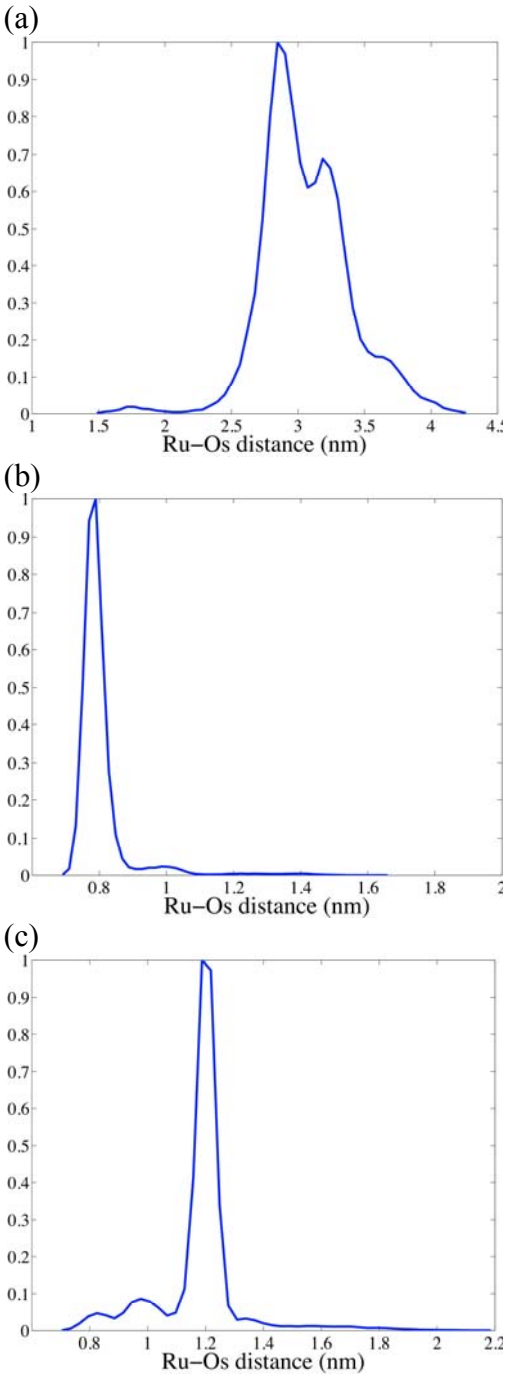

Figure 4.6. (a) Histogram showing the simulated metal-center distance distribution for the 2*f*-Ru/2*f*-Os peptide pair. (b) Histogram showing the simulated metal-center distance distribution for the 2*b*-Ru/2*c*-Os peptide pair. (c) Histogram showing the simulated metal-center distance distribution for the 2*e*-Ru/2*g*-Os peptide pair. The x-axis is the distance between the metal centers for the two metallopeptides for all. The y-axis is normalized for all and represents relative amounts of time that metal-center distances exist within the simulation.

(a)

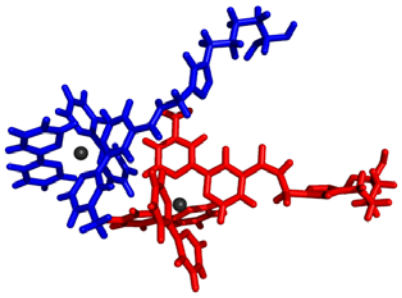

(b)

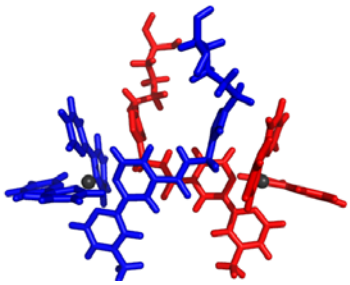

Figure 4.7 (a) The conformation that is a persistent arrangement in the 2*c*/2*b* metallopeptide pair only. The conformation is characterized by a small metal-center displacement (0.8 nm) and close contacts between bipyridyl ligands. The conformation appears only briefly in the simulation of the 2*g*/2*e* metallopeptide pair. (b) The conformation that is a persistent arrangement in the 2*g*/2*e* metallopeptide pair. The conformation is characterized by a slightly larger metal-center displacement (1.2 nm) and fewer contacts between bipyridyl ligands.

The simulations for the 2*b*/2*c* and 2*e*/2*g* metallopeptide pairs displayed an increasing destabilization of the coiled-coil structure, respectively, when compare to the 2*f*/2*f* peptide pair. This result is interesting when compared to the stability measurements made in section D, and probably relates to the attachment of the bipyridyl complexes closer to the termini of the metallopeptides. The observed trend for coiled-coil destabilization: 2*e*/2*g* > 2*b*/2*c* > 2*f*/2*f* matches the trend observed for all of the thermodynamic parameters measured previously (ΔG_{H20}, K_d, and % α-helicity) and implies that interactions between the bipyridyl complexes and the coiled-coil scaffold itself are most destabilizing, while steric interactions between bipyridyl complexes are less important in determining coiled-coil stability.

E. Conclusions

The selection of metallopeptides for energy transfer studies was discussed within Chapter IV. These selections, designed to provide a range of distances for energy transfer studies, were related to the current understanding of coiled-coil structure. The effects of Ru^{II} and Os^{II} substitution on coiled-coil structure was evaluated for the 2*f*-Ru/2*f*-Os, 2*b*-Ru/2*c*-Os, and 2*e*-Ru/2*g*-Os metallopeptide pairs using CD spectroscopy and chemical denaturant techniques. The flexible ε-azido-L-lysine amino acid residue used to incorporate the Ru^{II} and Os^{II} bipyridyl complexes was shown to allow coiled-coil formation for all three metallopeptide pairs, with only minor degrees of destabilization between them. A theoretical approach for understanding metallopeptide stability and dynamics is also presented in Chapter IV, performed by Dr. Christopher Materese. The Ru^{II} to Os^{II} energy transfer behaviors for the 2*f*-Ru/2*f*-Os, 2*b*-Ru/2*c*-Os, and 2*e*-Ru/2*g*-Os metallopeptide pairs is fully evaluated in Chapter V, using the structural analysis detailed within Chapter IV to reinforce the conclusions.

F. Experimental section

i. Circular dichroism and guanidinium denaturation experiments

CD spectra were recorded on a chirascan circular dichroism spectrometer. CD spectra were recorded from 185 to 260 nm using 10 mM sodium phosphate buffer, pH 7. CD spectra taken for GndHCl denaturation experiments were taken from 200 to 260 nm. All spectra were recorded at 25 °C (298.15 K) with an optical path length of 0.1 cm. All scans were corrected by subtracting the spectrum of the respective buffer used in the experiment. The results are expressed as mean molar residue ellipticity [θ] values with units of degrees$\cdot$cm$^2\cdot$dmol^{-1} as calculated using Equation 9:

$$[\theta] = \frac{(\theta_{obs})}{10 \cdot l \cdot c \cdot n} \qquad Equation\ 9$$

where θ_{obs} is the observed ellipticity at a specific wavelength in millidegrees, l is the path length in cm, c is the concentration in mol·L^{-1}, and n is the number of amino acid residues.

GndHCl denaturation experiments were conducted by monitoring $[\theta]_{222}$ as a function of GndHCl concentration. Samples were prepared from stock peptide solutions, buffer (20 mM sodium phosphate, 100 mM sodium chloride, pH 7.4), and 8M stock solutions of GndHCl. The GndHCl stock solution was prepared in the same buffer and adjusted to pH 7.4 before use. The GndHCl stock solution concentration was determined by mass using volumetric glassware. The concentrations for the Ru^{II} peptide stock solutions (2*b*-Ru, 2*e*-Ru, and 2*f*-Ru) were determined using the extinction coefficient for $Ru(bpy)_3^{2+}$ in water (14,600 at 452 nm).[11] The concentrations for the Os^{II} peptide stock solutions were determined using the extinction coefficient for $Os(bpy)_3^{2+}$ in water (12,000 at 480 nm).[12] All buffers and peptide stock solutions were prepared using MilliQ water. Metallopeptides used for the GndHCl denaturation experiments could typically be purified and used again after the removal of salts using polyacrylamide size-exclusion columns and separation using RP-HPLC.

The values for fraction folded (F_F) were calculated using Equation 1. The values for fraction unfolded (F_U) were calculated using Equation 2. The values for the free energy of unfolding (ΔG_D) were calculated using Equation 3. The values for the free energy of unfolding in the absence of denaturant (ΔG_{H20}) were extrapolated using Equation 4.

ii. All-atom molecular dynamics simulations

The computational details for the all-atom molecular dynamics simulations were provided by Dr. Christopher Materese. Since no crystal structure was available for the

system, the initial structure was generated using PyMOL,[13] which is a molecular visualization tool capable of constructing simple peptides. The P1 and P2 peptides were initially generated independently using PyMOL's helical parameters and were then manually aligned with care taken to avoid steric clashes and satisfy the hydrophobic interface. The ε-triazolo-L-lysine linker segment was constructed using Gaussview, part of the Gaussian 03 suite.[14] Ruthenium and osmium are very similar from an MD perspective. Since the primary focus of these simulations is peptide dynamics, ruthenium was used as the central atom in both chromophores and osmium was not explicitly included. In order to examine the effect of linker positioning on the chromophores, the following three systems were created: System 1, which corresponds to the 2*f*-Ru/2*f*-Os metallopeptide pair, System 2 which corresponds to the 2*b*-Ru/2*c*-Os metallopeptide pair, and System 3 which corresponds to the 2*e*-Ru/2*g*-Os metallopeptide pair.

The simulations were prepared using we use the AMBER[15] force field with the ff99SB[16] parameter set. Since the AMBER libraries do not possess parameters for the artificial amino acids used as tethers, or for the chromophores themselves, these values needed to be collected from literature or obtained through quantum calculations. Partial charges for the linker and chromophores were obtained from Gaussian calculations using restricted B3LYP[17] with the LANL2DZ[18] basis set. Charges derived using the restricted electrostatic potential (RESP) technique[19] gave spurious results for Ruthenium and the chelating nitrogen atoms in the bipyridyl ligands. RESP has difficulty predicting the correct charge for buried atoms since the charges are assigned in an effort to reproduce the external electrostatic potential.[19] Because of this, Mulliken charges were used in lieu of RESP charges. In general, Mulliken charges tend to be slightly more exaggerated than RESP

charges with an average difference in predicted charge of 0.1(±0.1)**e** for all atom excluding from the Ruthenium and those atoms immediately surrounding it. There was insufficient memory to compute partial charges for the entire linker and chromophore. In order to deal with this issue, the partial charges for the base of the peptide up to the γ-carbon of the side chain were extracted from the standard lysine amino acid residue. Force constants for Ru-N stretches, N-Ru-N (*cis*/*trans*) bends, C-C-N-Ru dihedrals, H-C-N-Ru dihedrals and van der Waals parameters were obtained from Brandt et al.[20] Since AMBER does not explicitly support Octahedral geometry, chelating nitrogen atoms were divided into three distinctly named but chemically identical types in order to establish different bending force constants for cis and trans positions. Each of the three simulations were performed with ~13000 explicit TIP3P water molecules in a box with the dimensions ~ 75 × 75 × 75 Å under periodic boundary conditions. The charge of each system was neutralized by the addition of sodium counter ions, followed by the subsequent introduction of an additional 10mM NaCl. Each system was held at constant volume, and the peptides were frozen in place while the water and ions were minimized for 200,000 steps. Subsequently, all constraints were removed from the systems and they were minimized for an additional 200,000 steps. The systems were gradually heated via Langevin temperature control to 300 K in incremental steps of 5 K every 50 ps. The production runs proceeded under the constant pressure, moderated by Langevin piston (set to 1 atm), with 2 fs time steps using the SHAKE algorithm and Ewald summation for long-range interactions. Short-range non-bonded interactions were calculated at each step, long-range interactions were only calculated on even steps and the pair list was updated every 10 steps. System coordinates were saved every 1000 steps (2 ps) for analysis for a total simulation length of 500 ns.

The individual trajectories of the Ru^{II} bipyridyl complexes for each simulation are shown (Figure 4.7). The trajectories serve only as an oversimplified report of the peptide dynamics. They represent the relatively metal-center displacements but do represent other dynamic portions of the metallopeptide scaffolds. The histograms shown in Figure 4.6 were generated from these trajectories, with the first 20 ns being discarded as relaxation time for the system.

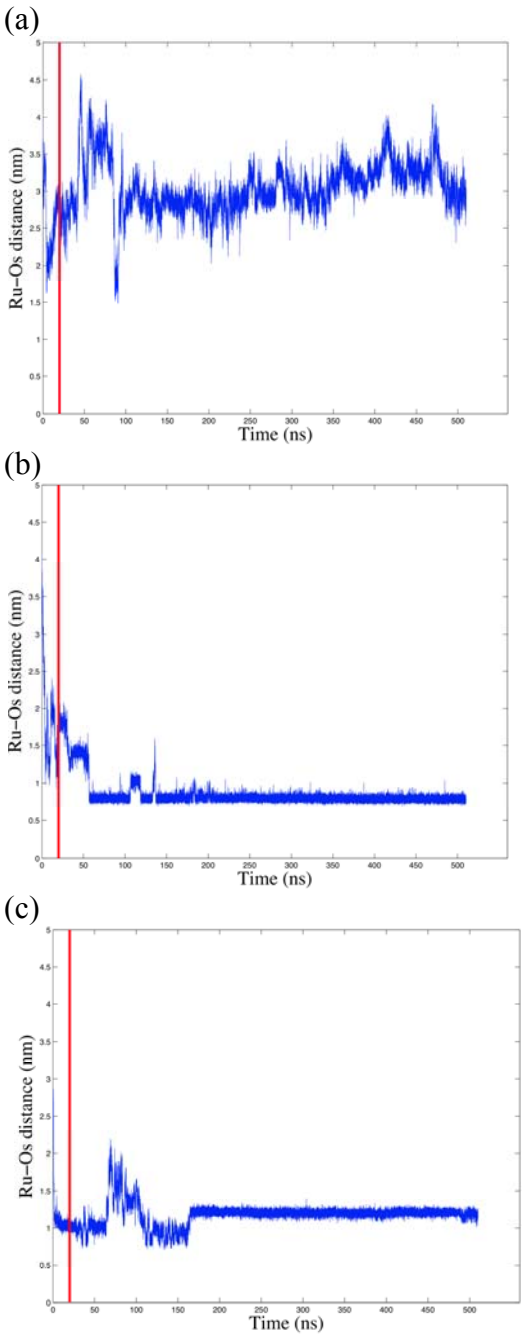

Figure 4.8 (a) Metal-center displacement distance for the 2*f*/2*f* metallopeptide pair as a function of time. (b) Metal-center displacement distance for the 2*b*/2*c* metallopeptide pair as a function of time. (c) Metal-center displacement distance for the 2*e*/2*g* metallopeptide pair as a function of time. The red lines signify the cutoff point before which data is discarded as part of the system relaxation.

References

[1](a) Woody, R. W. *Methods Enzymol.* **1995**, *246*, 34-71. (b) Greenfield, N. J. *Nature Protocols* **2006**, *1*, 2876-2890.

[2](a) Hodges, R. S. *Biochem. Cell Biol.* **1996**, *74*, 133-154. (b) Zhou, N. E.; Zhu, B. Y.; Kay, C. M.; Hodges, R. S. *Biopolymers* **1992**, *32*, 419-426.

[3](a) Zhou, N. E.; Kay, C. M.; Hodges, R. S. *Biochemistry* **1992**, *31*, 5739-5746. (b) Zhou, N. E.; Kay, C. M.; Hodges, R. S. *J. Biol. Chem.* **1992**, *267*, 2664-2670. (c) Su, J. Y.; Hodges, R. S.; Kay, C. M. *Biochemistry* **1994**, *33*, 15501-15510.

[4]Woolfson, D. K. *Adv. Protein Chem.* **2005**, *70*, 79-112.

[5](a) Pace, C. N. *Methods Enzymol.* **1986**, *131*, 266-280. (b) De Francesco, R.; Pastore, A.; Vecchio, G.; Cortese, R. *Biochemistry* **1991**, *30*, 143-147. (c) Litowski, J. R.; Hodges, R. S. *J. Biol. Chem.* **2002**, *277*, 37272-37279.

[6]Wendt, H.; Berger, C.; Baici, A.; Thomas, R. M. Bossard, H. R. *Biochemistry* **1995**, *34*, 4097-4107.

[7](a) Chen, Y.-H.; Yang, J. T.; Chau, K. H. *Biochemistry* **1974**, *13*, 3350-3359. (b) Scholtz, J. M.; Qian, H.; York, E. J.; Stewart, J. M.; Baldwin, R. L. *Biopolymers* **1991**, *31*, 1463-1470.

[8](a) Kozlov, G. V.; Ogawa, M. Y. *J. Am. Chem. Soc.* **1997**, *119*, 8377-8378. (b) Kornilova, A. Y.; Wishart, J. F.; Xiao, W.; Lasey, R. C.; Fedorova, A.; Shin, Y.-K.; Ogawa, M. Y. *J. Am. Chem. Soc.* **2000**, *122*, 7999-8006. (c) Kornilova, A. Y.; Wishart, J. F.; Ogawa, M. Y. *Biochemistry* **2001**, *40*, 12186-12192.

[9](a) Kohn, W. D.; Kay, C. M.; Hodges, R. S. *Protein Sci.* **1995**, *4*, 237-250. (b) Serrano, J.; Horovitz, A.; Avron, B.; Bycroft, M.; Fersht, A. R. *Biochemistry* **1990**, *29*, 9343-9352.

[10](a) O'Shea, E. K.; Rutkowski, R.; Kim, P. S. *Cell* **1992**, *68*, 699-708. (b) Kohn, W. D.; Kay, C. M.; Hodges, R. S. *J. Mol. Biol.* **1998**, *283*, 993-1012. (c) Litowski, J. R.; Hodges, R. S. *J. Biol. Chem.* **2002**, *277*, 37272-37279. (d) Zhou, N. E.; Kay, C. M.; Hodges, R. S, *J. Mol. Biol.* **1994**, *237*, 500-512.

[11]Juris, A.; Balzani, V.; Barigelletti, F.; Campagna, S.; Belser, P.; Von Zelewski, A. *Coord. Chem. Rev.* **1988**, *84*, 85-277.

[12]Creutz, C.; Chou, M.; Netzel, T. L.; Okumura, M.; Sutin, N. *J. Am. Chem. Soc.* **1980**, *102*, 1309-1319.

[13]The PyMOL Molecular Graphics System, Version 1.2r3pre, Schrödinger, LLC.

[14]Gaussian 03, Revision C.02, Frisch, M. J.; Trucks, G. W.; Schlegel, H. B.; Scuseria, G. E.; Robb, M. A.; Cheeseman, J. R.; Montgomery, Jr., J. A.; Vreven, T.; Kudin, K. N.; Burant, J. C.; Millam, J. M.; Iyengar, S. S.; Tomasi, J.; Barone, V.; Mennucci, B.; Cossi, M.; Scalmani, G.; Rega, N.; Petersson, G. A.; Nakatsuji, H.; Hada, M.; Ehara, M.; Toyota, K.; Fukuda, R.; Hasegawa, J.; Ishida, M.; Nakajima, T.; Honda, Y.; Kitao, O.; Nakai, H.; Klene, M.; Li, X.;

Knox, J. E.; Hratchian, H. P.; Cross, J. B.; Bakken, V.; Adamo, C.; Jaramillo, J.; Gomperts, R.; Stratmann, R. E.; Yazyev, O.; Austin, A. J.; Cammi, R.; Pomelli, C.; Ochterski, J. W.; Ayala, P. Y.; Morokuma, K.; Voth, G. A.; Salvador, P.; Dannenberg, J. J.; Zakrzewski, V. G.; Dapprich, S.; Daniels, A. D.; Strain, M. C.; Farkas, O.; Malick, D. K.; Rabuck, A. D.; Raghavachari, K.; Foresman, J. B.; Ortiz, J. V.; Cui, Q.; Baboul, A. G.; Clifford, S.; Cioslowski, J.; Stefanov, B. B.; Liu, G.; Liashenko, A.; Piskorz, P.; Komaromi, I.; Martin, R. L.; Fox, D. J.; Keith, T.; Al-Laham, M. A.; Peng, C. Y.; Nanayakkara, A.; Challacombe, M.; Gill, P. M. W.; Johnson, B.; Chen, W.; Wong, M. W.; Gonzalez, C.; and Pople, J. A.; Gaussian, Inc., Wallingford CT, 2004.

[15]Case, D. A.; Darden, T. A.; Cheatham, III, T. E.; Simmerling, C. L.; Wang, J.; Duke, R. E.; Luo, L.; Crowley, M.; Walker, R. C.; Zhang, W.; Merz, K. M.; Wang, B.; Hayik, S.; Roitberg, A.; Seabra, G.; Kolossváry, I.; Wong, K. F.; Paesani, F.; Vanicek, J.; Wu, X.; Brozell, S. R.; Steinbrecher, T.; Gohlke, H.; Yang, L.; Tan, C.; Mongan, J.; Hornak, V.; Cui, G.; Mathews, D. H.; Seetin, M. G.; Sagui, C.; Babin, V.; Kollman, P. A. AMBER 10, University of California, San Francisco, 2008.

[16]Hornak, V.; Abel, R.; Okur, A.; Strockbine, B.; Roitberg, A.; Simmerling, C. *Proteins* **2006**, *65*, 712– 725.

[17]Lee, C.; Yang, W.; Parr, R. *Phys. Rev. B* **1988**, *37*, 785–789.

[18](a) Hay, P. J.; Wadt, W. R. *J. Chem. Phys.* **1985**, *82*, 270-283. (b) Hay, P. J.; Wadt, W. R. *J. Chem. Phys.* **1985**, *82*, 284-298. (c) Hay, P. J.; Wadt, W. R. *Chem. Phys.* **1985**, *82*, 299-310.

[19]Bayly, C. I.; Cieplak, P.; Cornell, W. D.; Kollman, P. A. *J. Phys. Chem.* **1993**, *97*, 10269–10280.

[20]Brandt, P.; Norrby, T.; Akermark, B.; Norrby, P.-O. *Inorg. Chem.* **1998**, *37*, 4120–4127.

Chapter V

THE STUDY OF POSITION-DEPENDENT ENERGY TRANSFER WITHIN COILED-COIL METALLOPEPTIDE HETERODIMERS

A. Introduction

As mentioned in Chapter 1, the phenomena of Ru^{II} to Os^{II} energy transfer has been studied using a number of covalent linkages,[1] high molecular weight polymers,[2] and DNA scaffolds.[3] The coiled-coil peptide motif has not previously been used as an organizational structure for Ru^{II} to Os^{II} energy transfer. The general structure and dynamic monomer-dimer equilibrium behavior of these novel coiled-coil metallopeptides were presented in Chapter IV using a combination of CD spectroscopy and GndHCl denaturation experiments. General trends that may be expected for the displacement distances of Ru^{II} and Os^{II} bipyridyl complexes attached at different positions within the coiled-coil peptide scaffold were also discussed. The discussion was based on reported crystal structures for similar coiled-coil dimers, and on existing knowledge within the field of *de novo* protein design.[4] Another interpretation of the coiled-coil peptide structure was provided by Dr. Christpher Materese using all-atom molecular dynamics simulations under the advisement of professor Garyk Papoian.

Despite the extensive characterization provided within Chapter IV, the exact energy transfer behavior that should have been expected for the coiled-coil metallopeptides was not intuitively obvious at the outset. The metallopeptides that form the

focus of the preceding chapter do indeed exhibit position-dependent Ru^{II} to Os^{II} energy transfer. The steps taken to determine and fully characterize this energy transfer are described throughout Chapter V. This work was performed in collaboration with Stephanie Bettis under the advisement of Professor John Papanikolas. All time-resolved emission measurements were collected by Stephanie Bettis.

B. General energy transfer behavior and control experiments

Similar to the measurements of thermodynamic stability made in Chapter IV, energy transfer studies were performed specifically on the 2*f*-Ru/2*f*-Os, 2*b*-Ru/2*c*-Os, and 2*e*-Ru/2*g*-Os coiled-coil metallopeptide heterodimers (Figure 5.1). Based on the equilibrium behavior described in Chapter IV, energy transfer within the coiled-coil metallopeptides would be expected to be concentration dependent. Energy transfer from the Ru^{II}-containing metallopeptides was expected to vary with the concentration of the Os^{II}-containing metallopeptide. For this reason, all of the energy transfer experiments were performed as titrations where the Ru^{II} metallopeptide concentration was held constant and the lifetime of Ru^{II} excited-state emission was examined as a function of both substoichiometric and superstoichiometric concentrations of the Os^{II} metallopeptide. Time-resolved measurements of the Ru^{II} metallopeptide emission allowed correlations to be made with the physical model of the coiled-coil system that would have been more difficult using steady-state emission techniques alone. The emissive lifetimes were measured using time-correlated single photon counting (TCSPC)[2e] experiments. The metallopeptide samples were excited at 450 nm and emission data was collected at 660 nm. The general spectroscopy setup used to make the TCSPC measurements is diagramed in the experimental section.

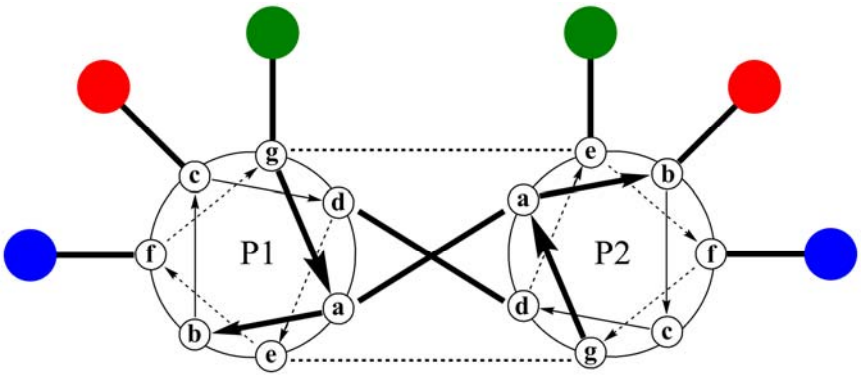

Figure 5.1. A helical wheel diagram for the metallopeptide partners examined throughout the study. The 2*f*-Ru/2*f*-Os (blue), 2*b*-Ru/2*c*-Os (red), and 2*e*-Ru/2*g*-Os (green) metallopeptide pairs are shown. The approximate distances between attachment points based on crystal structures (pdb code: 2ZTA) measured between the the respective α-carbons are 14.3, 12.7, and 9.9 Å for the 2*f*-Ru/2*f*-Os, 2*b*-Ru/2*c*-Os, and 2*e*-Ru/2*g*-Os metallopeptide pairs, respectively.

When considering potential energy transfer behaviors, the 2*b*-Ru/2*c*-Os and 2*e*-Ru/2*g*-Os metallopeptide pairs were expected to provide the most favorable energy transfer if any were observed at all. Indeed, titration of the 2*b*-Ru or 2*e*-Ru metallopeptides with the 2*c*-Os or 2*g*-Os peptides, respectively, resulted in a significant decrease in the observed lifetime of Ru^{II} emission. Quenching of the $Ru(bpy)_3^{2+}$ excited-state emission by $Os(bpy)_3^{2+}$ was reported by Cruetz and coworkers, although the bimolecular rate constant (1.5×10^9 $M^{-1}\cdot s^{-1}$) would imply that diffusional quenching would be inefficient at the concentrations the 2*b*-Ru and 2*e*-Ru peptides were titrated at (low μM for both donor and acceptor).[5] Although it was believed that diffusion controlled quenching was unlikely in the absence of the peptide scaffold, a control experiment was designed to test such an occurrence. The 2*b*-Ru peptide was titrated with an Os^{II} complex (**13**) designed to mimic the attachment linker, while not providing any strong noncovalent interactions that would encourage association with the peptide scaffold (Figure 5.2a). The addition of Os^{II} complex **13** to the 2*b*-Ru peptide had no

measurable effect on the Ru^{II} excited-state lifetime at concentrations greater than those required for measurable quenching compared to the 2*c*-Os metallopeptide (Figure 5.2b). This result indicates that noncovalent association is required for quenching and is in contrast to the report by Tor and coworkers where the addition of $Os(bpy)_2(phen)^{2+}$ to solutions containing a Ru^{II}-modified oligonucleotide resulted is subtle quenching of the Ru^{II}-based phosphorescence, even at much lower concentrations.[3c] Tor's result could be due to the longer emissive lifetime of the Ru^{II}-modified oligonucleotide used in the study. The result could also be attributed to the fact that, while oligonucleotides are polyanionic molecules, the 2*b*-Ru peptide contained a net positive (+5) charge at pH 7. The 2*b*-Ru peptide may have had repulsive charge-charge interactions with **13** that were less important or even attractive when compared to Tor's oligonucleotide system. It is also possible that the $Os(bpy)_2(phen)^{2+}$ complex used as a control in Tor's study interacted with the DNA scaffold via classical intercalation or surface binding, both phenomena known for Ru^{II} complexes that contain phenanthroline ligands.[6]

(a)

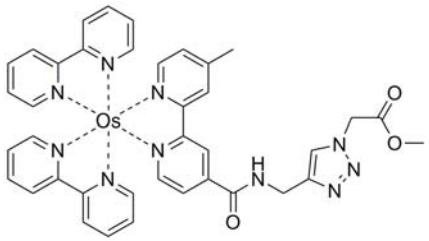

(b)

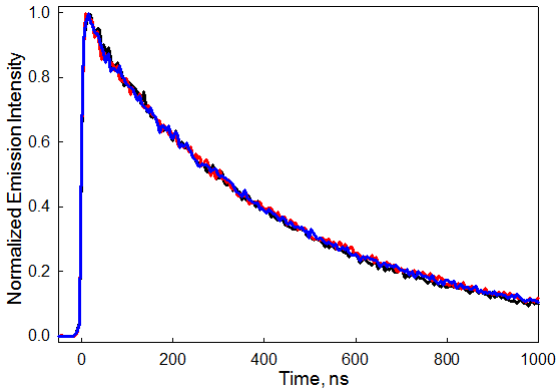

Figure 5.2 (a) The chemical structure of the osmium complex **13** is shown. (b) The time-resolved emission experiment showing that the 2*b*-Ru monoexponential lifetime τ (red: 25 μM 2*b*-Ru peptide and 50 μM P1 peptide) at 660 nm is not measurably affected by either one (blue: 25 μM 2*b*-Ru peptide and 25 μM **13**), or two (black: 25 μM 2*b*-Ru peptide and 50 μM **13**) equivalents of **13.**

A second control experiment was designed to demonstrate that the coiled-coil structure was directly responsible for promoting the observed quenching behavior in the manner predicted. The GndHCl denaturation experiments used to determine dissociation constants within Chapter IV provided a convenient strategy for disrupting the structure of the coiled-coil scaffold, even when the complementary Os^{II}-containing peptide was present in excess. The emissive lifetimes for both the 2*b*-Ru and 2*e*-Ru metallopeptides increased considerably when examined in buffered media containing 5 M GndHCl (Figure 5.3). However, the lifetimes for Ru^{II} decay in both the 2*b*-Ru/2*c*-Os or 2*e*-Ru/2*g*-Os

metallopeptide heterodimers were identical to those for the 2*b*-Ru and 2*e*-Ru peptides, respectively, when examined in the denaturing media. Both experiments were good indicators of the role the coiled-coil scaffold performed during energy transfer.

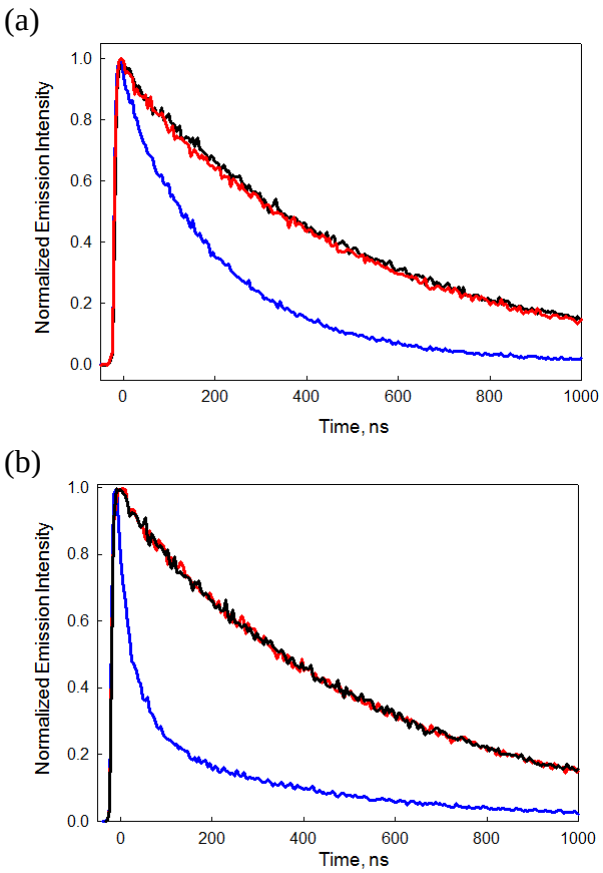

Figure 5.3 (a) Time-resolved emission trace for the 2*b*-Ru/2*c*-Os GndHCl denaturation experiment (blue: 25 μM 2*b*-Ru peptide and 50 μM 2*c*-Os peptide in 10 mM sodium phosphate buffer, pH 7, red: 25 μM 2*b*-Ru peptide and 50 μM 2*c*-Os peptide in 5 M GndHCl buffer, pH 7). The emission lifetime of the 2*b*-Ru peptide is longer in the denaturing buffer (black: 25 μM 2*b*-Ru peptide only in 5 M GndHCl buffer, pH 7), but is unaffected by the presence of the 2*c*-Os peptide. (b) Time-resolved emission trace for the 2*e*-Ru/2*g*-Os GndHCl denaturation experiment (blue: 25 μM 2*e*-Ru peptide and 50 μM 2*g*-Os peptide in 10 mM sodium phosphate buffer, pH 7, red: 25 μM 2*e*-Ru peptide and 50 μM 2*g*-Os peptide in 5 M GndHCl buffer, pH 7). The emission lifetime of the 2*e*-Ru peptide is longer in the denaturing buffer (black: 25 μM 2*e*-Ru peptide only in 5 M GndHCl buffer, pH 7), but is unaffected by the presence of the 2*g*-Os peptide.

C. Titration experiments

Once control experiments had confirmed that the observed Ru^{II}-based emission quenching was due to coiled-coil formation with the Os^{II}-containing metallopeptides, detailed analyses of the different heterodimers were performed. Interestingly, all three Ru^{II} metallopeptides have excited-state lifetimes that differ slightly when measured in isolation from the Os^{II}-containing peptides. This fact demonstrates the sensitivity of the Ru^{II} excited-state lifetime to environment, a phenomenon typically observed in the context of solvatochromism.[7] The lifetimes of the 2*b*-Ru, 2*e*-Ru, and 2*f*-Ru metallopeptides are, however, unaffected by the presence of the P1 parent peptide, even in an excess. This too is in contrast to the reports by Tor and coworkers who observed a significant change in the emissive lifetime of Ru^{II}-containing oligonucleotides when duplexed with complementary DNA oligonucleotides which did not contain Os^{II} bipyridyl complexes.[3c] This observation was attributed to the fact that DNA oligonucleotides are highly disordered in isolation and go through a considerable degree of structural reorganization when they are duplexed with complementary oligonucleotides. In contrast, peptides designed to form coiled-coil structures can contain a considerable degree of α-helical character in the monomeric state, and may also be bound to a small extent as α-helical homodimers in the absence of the complementary unit. Both characteristics could explain why the 2*b*-Ru, 2*e*-Ru, and 2*f*-Ru metallopeptides are insensitive to complementary peptide sequences which did not contain Os^{II}.

The excited state decay of the 2*b*-Ru, 2*e*-Ru, and 2*f*-Ru metallopeptides are all monoexponential in isolation, but became biexponential when the complementary 2*c*-Os, 2*g*-

Os, or 2*f*-Os metallopeptides are added (Figure 5.3). In all cases, the biexponential behavior can be described using Equation 1:

$$\langle\tau\rangle = A_1 \cdot \tau_1 + A_2 \cdot \tau_2 \qquad Equation\ 1$$

where $\langle\tau\rangle$ is the weighted average lifetime observed for the mixture, τ_1 is the lifetime of the slower component, τ_2 is the lifetime of the faster component, and A_1 and A_2 are the amplitudes of the slower lifetime and faster lifetime components, respectively. The slower lifetime component for each metallopeptide pair corresponds to the lifetime of the Ru^{II} peptide in isolation. For example, the 2*e*-Ru/2*g*-Os metallopeptide pair has a slower excited-state decay component (τ_1) that corresponds to the lifetime of the 2*e*-Ru peptide measured in isolation. By implication, the amplitude (A_1) of this slower component is found to be unity when no 2*g*-Os metallopeptide was added. While the τ_1 component measured for the different Ru^{II}-containing peptides vary by less than 10%, the τ_2 components measured for the different metallopeptide pairs vary to a greater extent. The amplitude of the faster lifetime component (A_2) varies with the concentration of the Os^{II}-containing peptide and was assigned as Ru^{II} to Os^{II} energy transfer. The results of the time-resolved emission experiments are shown (Figure5.4).

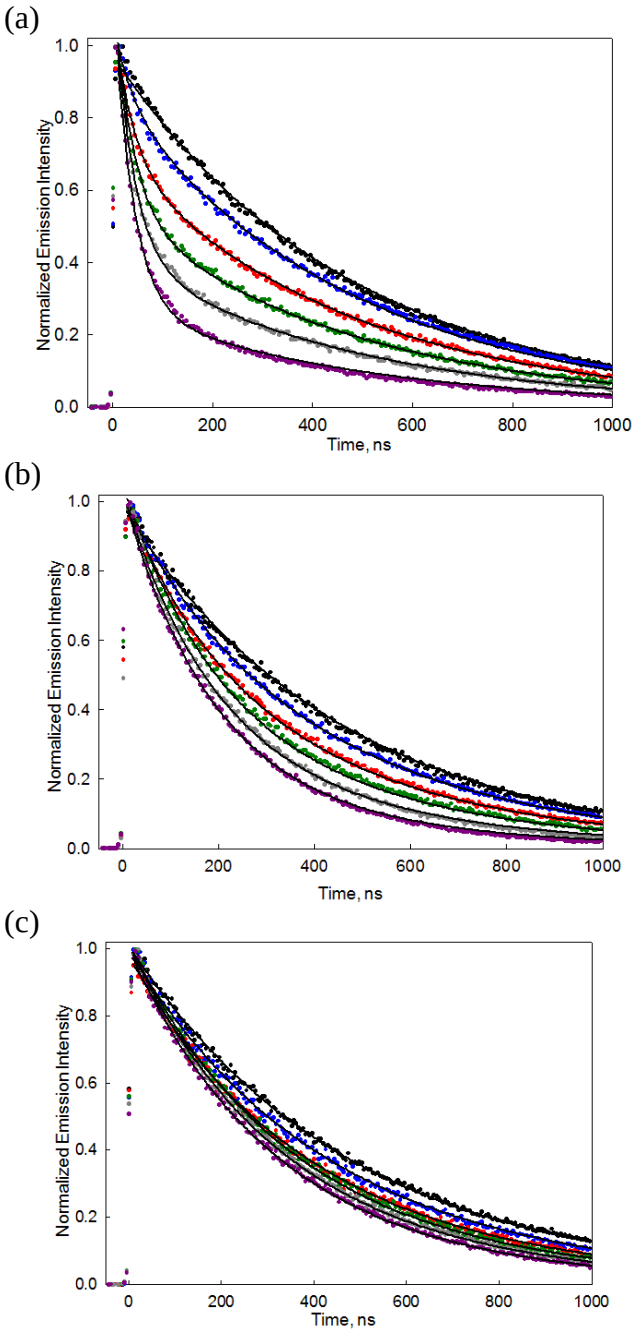

Figure 5.4 (a) The time-resolved emission trace at 660 nm for the 2*e*-Ru/2*g*-Os metallopeptide pair. (b) The time-resolved emission trace at 660 nm for the 2*b*-Ru/2*c*-Os metallopeptide pair. (c) The time-resolved emission trace at 660 nm for the 2*f*-Ru/2*f*-Os metallopeptide pair. The concentration of the Ru^{II}-containing peptide was 25 μM for each. The following titration experiments are shown for each: 0 μM (black), 6.25 μM (blue, 0.25 equiv), 12.5 μM (red, 0.5 equiv), 18.75 μM (green, 0.75 equiv), 25 μM (grey, 1.0 equiv), and 50 μM (violet, 2.0 equiv) Os^{II}-containing peptide concentration. All samples analyzed at 25°C in 10 mM PO_4^{3-}, pH 7, buffer. The computer generated fit is shown as a solid line in each.

The concentration-dependence of the faster lifetime component can be described using a dissociation constant (K_d) similar to that measured for the metallopeptide pairs by GndHCl denaturation (Chapter IV). The dissociation constants for the different metallopeptide pairs can all be expressed using Equation 2:

$$K_d = \frac{[Ru][Os]}{[Ru \cdot Os]} \qquad Equation\ 2$$

where [*Ru*] is the concentration of the Ru^{II}-containing peptide at equilibrium, [*Os*] is the concentration of the Os^{II}-containing peptide at equilibrium, and [*Ru·Os*] is the concentration of the coiled-coil metallopeptide dimer at equilibrium. The quantities, [*Ru*] and [*Os*], can be expressed in terms of the dimer concentration [*Ru·Os*] using Equation 3 and Equation 4:

$$[Ru] = [Ru]_0 - [Ru \cdot Os] \qquad Equation\ 3$$

$$[Os] = [Os]_0 - [Ru \cdot Os] \qquad Equation\ 4$$

where $[Ru]_0$ is the total Ru^{II}-containing peptide concentration and $[Os]_0$ is the total Os^{II}-containing peptide concentration. Substitution of Equation 3 and Equation 4 into Equation 2 gives Equation 5:

$$K_d = \frac{([Ru]_0 - [Ru \cdot Os])([Os]_0 - [Ru \cdot Os])}{[Ru \cdot Os]} \qquad Equation\ 5$$

where the dissociation constant (K_d) is expressed in terms of the known quantities $[Ru]_0$ and $[Os]_0$. Equation 5 was rearranged to express the metallopeptide heterodimer concentration ($[Ru{\cdot}Os]$) in terms of the K_d, $[Ru]_0$, and $[Os]_0$ resulting in Equation 6:

$$[Ru \cdot Os] = \frac{[Ru]_0 + [Os]_0 + K_d - \sqrt{([Ru]_0 + [Os]_0 + K_d)^2 - 4[Ru]_0[Os]_0}}{2} \quad Equation\ 6$$

The relative emission intensity (I) measured for the emission experiments can be expressed as a time-dependent function using Equation 7:

$$I(t) = \left[\left(\frac{[Ru \cdot Os]}{[Ru]_0}\right) e^{-(k_{Ru}+k_{EnT})t} + \left(\frac{[Ru]_0 - [Ru \cdot Os]}{[Ru]_0}\right) e^{-k_{Ru}t}\right] \quad Equation\ 7$$

where k_{Ru} is the emission lifetime for the Ru^{II}-containing peptide in isolation, k_{EnT} is the rate of energy transfer to the Os^{II}-containing peptide, and t is time. Since the preexponential terms $[Ru{\cdot}Os]/[Ru]_0$ and $([Ru]_0\text{-}[Ru{\cdot}Os])/[Ru]_0$ represent the fractions of the Ru^{II} peptide contained in the heterodimer and monomer states (F_F and F_U), respectively, they can be used to calculate the K_d values of interest. The lifetimes and dissociation constants derived from these titration experiments are given in Table 5.1. The K_d values determined for the metallopeptides by time-resolved emission (Table 5.1) agree extremely well with the K_d values determined by chemical denaturation (Chapter IV). The correlation between the values is important to our hypothesis that the structure of the coiled-coil peptide scaffold is responsible for promoting the observed energy transfer since chemical denaturation is monitored by CD signal ($[\theta]_{222}$) and is dependent only on the peptide secondary structure.

Table 5.1. Lifetimes and amplitudes generated from the titration experiments

	2*e*-Ru/2*g*-Os	**2*b*-Ru/2*c*-Os**	**2*f*-Ru/2*f*-Os**
τ_1[a] (ns)	468.2 ± 0.4	450.0 ± 0.5	478.7 ± 0.5
τ_{EnT}[b] (ns)	42.0 ± 0.2	304 ± 2	816 ± 14
K_d[c] (μM)	1.127 ± 0.001	1.088 ± 0.002	1.101 ±0.006
K_d (GndHCl)[d] (μM)	1.4 ± 0.3	0.97 ± 0.2	0.49 ± 0.09

[a]The slower excited-state decay component τ_1 is attributed to Ru^{II} emission in the absence of quenching. [b]The rates of energy transfer for the metallopeptide heterodimers are reported as lifetimes ($\tau_{EnT} = 1/k_{EnT}$) for comparison. [c]The dissociation constants were calculated using Equation 6 and Equation 7. [d]The dissociation constants were measured in Chapter IV.

D. Results and discussion

The 2*e*-Ru/2*g*-Os metallopeptide pair is predicted to be the best promoter of Ru^{II} to Os^{II} energy transfer based on the discussion of coiled-coil structure presented in Chapter IV. Indeed, the lifetime of energy transfer (τ_{EnT}) measured for the 2*e*-Ru/2*g*-Os metallopeptide pair is 42 ns. This value was considerably faster than that for either the 2*b*-Ru/2*c*-Os or 2*f*-Ru/2*f*-Os pairs. The molecular dynamics simulations of the 2*e*-Ru/2*g*-Os pair presented in Chapter IV showed a number of conformations where the bipyridyl complexes were able to come in close contact with each other.

Comparing τ_{EnT} for the 2*e*-Ru/2*g*-Os metallopeptide pair to the subnanosecond rates observed within the Ru^{II}- and Os^{II}-modified polystyrene systems studied by Fleming and coworkers indicated that the metallopeptide system is a less efficient promoter of Ru^{II} to Os^{II} energy transfer.[2e] This is almost certainly due to the Ru^{II} and Os^{II} bipyridyl complexes occupying, on average, conformations that are less conducive (greater metal complex displacement) to excited-state energy transfer compared to the polystyrene-based systems where the donor and acceptor complexes are forced into van der Waals contact with each other.[2e] There is also the possibility that the effect is due to the different chemical structure of the Ru^{II}-bipyridyl complexes used within the polystyrene-based system.

Based on the discussion presented in Chapter IV, a number of results could be expected for the 2*b*-Ru/2*c*-Os metallopeptide system. The 2*b*-Ru/2*c*-Os pair could be expected to promote energy transfer less efficiently than the 2*e*-Ru/2*g*-Os pair based on an analysis of the helical positions within similar coiled-coil peptide structures (Figure 5.1). Conversely, the molecular dynamics simulation of the 2*b*-Ru/2*c*-Os metallopeptide pair implies that it could promote energy transfer in a manner very similar to the 2*e*-Ru/2*g*-Os pair. The titration experiments using time-resolved emission indicated that the 2*b*-Ru/2*c*-Os metallopeptide pair give an energy transfer lifetime of 304 ns. Although the 2*b*-Ru/2*c*-Os metallopeptide pair is less efficient at promoting energy transfer compared to the 2*e*-Ru/2*g*-Os pair, the structural differences between the two metallopeptide heterodimers may not be that great. As described in Chapter I, the efficiency of Dexter energy transfer decreases exponentially with distance and the displacement between metal centers in the two metallopeptide systems may therefore be similar.[8] It is reasonable to assume a Dexter mechanism is operative in both the 2*b*-Ru/2*c*-Os and 2*e*-Ru/2*g*-Os metallopeptide systems since the analysis of coiled-coil crystal structures presented in Chapter IV indicate that the attachment positions for the two scaffolds are very similar in distance to the radius of the metal complexes themselves and would likely allow for the Ru^{II} and Os^{II} bipyridyl complexes to come in van der Waals contact.[9] Tor and coworkers concluded that Ru^{II} to Os^{II} energy transfer in the oligonucleotide-based system was primarily due to a Förster mechanism with contributions from the Dexter mechanism being important at smaller donor/acceptor separations. A similar conclusion could likely be made for the 2*b*-Ru/2*c*-Os and 2*e*-Ru/2*g*-Os metallopeptide sytems where both Dexter and Förster mechanisms may play a role in determining energy transfer rates, but to different extents.[3c]

The 2*f*-Ru/2*f*-Os metallopeptide pair was, not surprisingly, the least efficient promoter of Ru^{II} to Os^{II} energy transfer energy. At the outset it was difficult to even predict that the 2*f*-Ru/2*f*-Os metallopeptide pair would promote energy transfer. The different analyses of the coiled-coil structures presented in Chapter IV all imply that the attachment positions on the peptide scaffold are sufficiently displaced to prevent any contact between the bipyridyl complexes. The energy transfer lifetime for the 2*f*-Ru/2*f*-Os metallopeptide system (816 ns) is fairly long compared to the 2*b*-Ru/2*c*-Os and 2*e*-Ru/2*g*-Os systems, but the fact that energy transfer is observed at all is likely an indicator that a Förster mechanism is involved. Again, this would agree with the conclusion reached both by Tor and by other researchers where a Förster mechanism is operative at greater donor/acceptor distances, but a Dexter mechanism is possible for the same energy transfer pair at closer distances.[1,3]

E. Conclusions

The coiled-coil peptide scaffold presented throughout this report has been shown to be an efficient promoter of Ru^{II} to Os^{II} energy transfer. The 2*e*-Ru/2*g*-Os, 2*b*-Ru/2*c*-Os, and 2*f*-Ru/2*f*-Os metallopeptide systems exhibit different energy transfer rates that correlate with the structural model presented for the coiled-coil peptide scaffold. Control experiments performed on the systems indicate the peptide scaffold is critical for promoting energy transfer. Equilibrium constants for the metallopeptides, measured by time-ressolved emission titration experiments, agree extremely well with those measured by chemical denaturation (Chapter IV), and reinforce the importance of the peptide scaffold for promoting Ru^{II} to Os^{II} energy transfer. Although the mechanism of energy transfer could not be assigned exactly, the analyses of the metallopeptide system would imply that both Dexter and Förster components may play a role in determining the observed energy transfer rates. The exact

mechanism may be identified if additional metallopeptides representing a wider range of donor-acceptor displacements were examined. It is important to recognize that the position-dependent energy transfer observed for the different metallopeptide pairs most likely does not represent a static displacement of bipyridyl complexes but instead is a measure of the average distances observed for the systems as a result of dynamic solution conformations. Inspired by the widespread use of the coiled-coil peptide scaffold throughout natural systems, a number of researchers have already investigated them for potential materials applications.[10] The metallopeptide systems described throughout this report could be applied to a number of productive applications including the construction of synthetic light-harvesting antenna,[11] or as a sensitizer for dye-sensitized solar cells.[12] It is the latter that forms the focus of Chapter VI where the initial efforts for developing Ru^{II}-containing peptides capable of performing excited-state electron injection with metal-oxide semiconductors is described.

F. Time-resolved emission experimental section

Ground state absorbance measurements were conducted with a Hewlett Packard 8453 UV-VIS-NIR absorption spectrophotometer. Steady state emission (SSE) data were collected using an Edinburgh Instruments FLS920 equipped with a 450 W Xenon lamp and photomultiplier tube (Hamamatsu 2658P). SSE data were collected using a bandwidth no larger than 4.0 nm and, once collected, were corrected for the emission spectrophotometer's spectral response. The FLS920 was also used for time-resolved measurements by the time-correlated single photon counting (TCSPC) technique with an instrument response of <100 ps. TCSPC excitation came from a 444.2 nm diode laser (Edinburgh Instruments EPL- 445, 73 ps FWHM pulsewidth) operated at 200 kHz. A 495 nm long pass color filter was used for emission experiments. A diagram showing the basic experimental set up for time-resolved

emission measurements by time-correlated sinlge photon counting (TCSPC) is shown (Figure 5.5).

The samples were placed in a 2.0 mm cuvette and placed at 45 degree angle from the incident laser beam. The samples were purged in Argon for >25 minutes prior to emission experiments. All experiments were performed with $Abs_{444\ nm}$< 0.2 OD. The solvent for each sample was 10 mM phosphate buffer at pH 7.

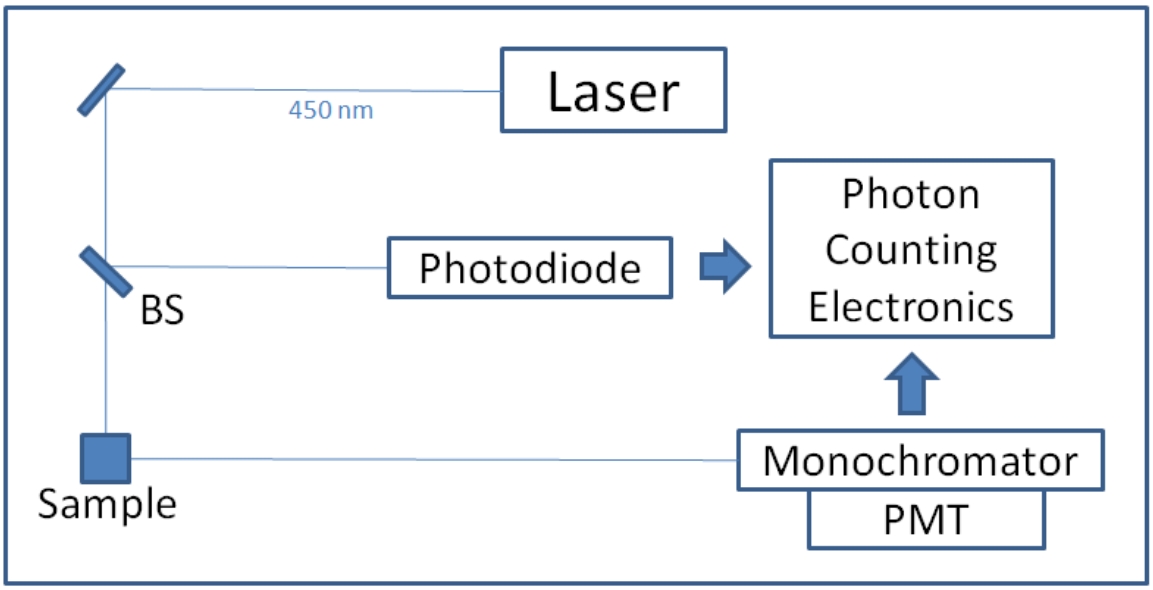

Figure 5.5. Diagram showing the experimental set up for time-resolved emission measurements by time-correlated sinlge photon counting (TCSPC).

References

[1](a) Furue, M.; Kinoshita, S.; Kushida, T. *Chem. Lett.* **1987**, 2355-2358. (b) Furue, M.; Yoshidzumi, T.; Kinoshita, S.; Kushida, T.; Nozakura, S.; Kamachi, M. *Bull. Chem. Soc. Jpn.* **1991**, *64*, 1632-1640. (c) Gholamkhass, B.; Nazaki, K.; Ohno, T. *J. Phys. Chem. B* **1997**, *101*, 9010-9021.

[2](a) Jones, Jr., W. E.; Baxter, S. M.; Strouse, G. F.; Meyer, T. J. *J. Am. Chem. Soc.* **1993**, *115*, 7363-7373. (b) Dupray, L. M.; Meyer, T. J. *Inorg. Chem.* **1996**, *35*, 6299-6307. (c) Dupray, L. M.; Devenney, M.; Striplin, D. R.; Meyer, T. J. *J. Am. Chem. Soc.* **1997**, *119*, 10243-10244. (d) Friesen, D. A.; Kajita, T.; Danielson, E.; Meyer, T. J. *Inorg. Chem.* **1998**, *37*, 2756-2762. (e) Fleming, C. N.; Maxwell, K. A.; DeSimone, J. M.; Meyer, T. J.; Papanikolas, J. M. *J. Am. Chem. Soc.* **2001**, *123*, 10336-10347.

[3](a) Hurley, D. J.; Tor, Y. *J. Am. Chem. Soc.* **1998**, *120*, 2194-2195. (b) Hurley, D. J.; Tor, Y. *J. Am. Chem. Soc.* **2002**, *124*, 3749-3762. (c) Hurley, D. J.; Tor, Y. *J. Am. Chem. Soc.* **2002**, *124*, 13231-13241.

[4]Woolfson, D. K. *Adv. Protein Chem.* **2005**, *70*, 79-112.

[5]Creutz, C.; Chou, M.; Netzel, T. L.; Okumura, M.; Sutin, N. *J. Am. Chem. Soc.* **1980**, *102*, 1309-1319.

[6](a) Satyanarayana, S.; Dabrowiak, J. C.; Chaires, J. B. *Biochemistry* **1993**, *32*, 2573-2584. (b) Coury, J. E.; Anderson, J. R.; MsFail-Isom, L.; Williams, L. D.; Bottomley, L. A. *J. Am. Chem. Soc.* **1997**, *119*, 3792-3796.

[7]Caspar, J. V.; Meyer, T. J. *J. Am. Chem. Soc.* **1983**, *105*, 5583-5590.

[8]Dexter, D. L. *J. Chem. Phys.* **1953**, *21*, 836-850.

[9]Rillema, D. P.; Jones, D. S.; Levy, H. A. *J. Chem. Soc., Chem. Commun.* **1979**, 849-851.

[10](a) Pandya, M. J.; Spooner, G. M.; Sunde, M.; Thorpe, J. R.; Rodger, A.; Woolfson, D. N. *Biochemistry* **2000**, *39*, 8728-8734. (b) Ryadnov, M. G.; Woolfson, D. N. *Nat. Mater.* **2003**, *2*, 329-332. (c) Ryadnov, M. G.; Woolfson, D. N. *Angew. Chem., Int. Ed. Engl.* **2003**, *42*, 3021-3023. (d) Ryadnov, M. G.; Woolfson, D. N. *J. Am. Chem. Soc.* **2004**, *126*, 7454-7455. (e) Mahmoud, Z. N.; Gunnoo, S. B.; Thomson, A. R.; Fletcher, J. M.; Woolfson, D. N. *Biomat.* **2011**, *32*, 3712-3720.

[11]Alstrum-Acevedo, J. H.; Brennaman, M. K.; Meyer, T. J. *Inorg. Chem.* **2005**, *44*, 6802-6827.

[12](a) O'Regan, B.; Grätzel, M. *Nature* **1991**, *353*, 737-740. (b) Ardo, S.; Meyer, G. J. *Chem. Soc. Rev.* **2009**, *38*, 115-164.

Chapter VI

THE STUDY OF METALLOPEPTIDE SENSITIZERS FOR NANOCRYSTALLINE SEMICONDUCTORS

A. Introduction

Chapter I described the importance and general considerations for studying excited-state energy transfer phenomena. The chemistry required to synthesize Ru^{II}-containing metallopeptides for the study of Ru^{II} to Os^{II} energy transfer was described within Chapter III. Chapter VI will now describe the utilization of that synthetic chemistry to developed a series of metallopeptide-based sensitizers for nanocrystalline semiconductors. This work focused on synthesis, surface attachment, photophysics and excited-state electron transfer dynamics of these metallopeptide-based sensitizers on nanocrystalline semiconductor surfaces. This work was performed in close collaboration with Dr. Kenneth Hanson using the EFRC spectroscopy facility under the advisement of Professor Thomas J. Meyer.

B. Background

Interest in excited-state electron transfer across heterogeneous surfaces has accelerated since the invention of the dye-sensitized solar cell (DSSC).[1] Although the exact mechanisms of action for DSSCs differ, several key steps are generally involved (Figure 6.1).[2] These elementary steps include: (*a*) the absorption of light which creates an electronically-excited state localized on the sensitizer molecule; (*b*) electron injection from the excited state molecule into the semiconductor conduction band known as photoinjection;

(*c*) the reduction of the oxidized sensitizer molecule by a charge-transporting electrolyte; and (*d*) the return of the injected electron through an external circuit, performing useful work on a load, with reduction of oxidized electrolyte occuring at a counter electrode. In addition to the processes described above that are required for efficient DSSC performance there are competitive detrimental processes that include but are not limited to back electron transfer (BET, *e*). BET is the process of charge recombination between the oxidized sensitizer and electrons localized in the semiconductor. The process described above is, as a whole, completely regenerative, meaning no net chemical reaction occurs. The general process of creating an interfacial charge-separated state from a photoexcited state can be thought of as biomimetic, as excited-state electron transfer drives the generation of useful redox equivalents in natural photosynthetic systems as well.[3] Although early studies indicated sensitizers dissolved in the electrolyte solution could be used, it was quickly realized that the direct attachment of sensitizers to semiconductor surfaces was a more practical approach.[2]

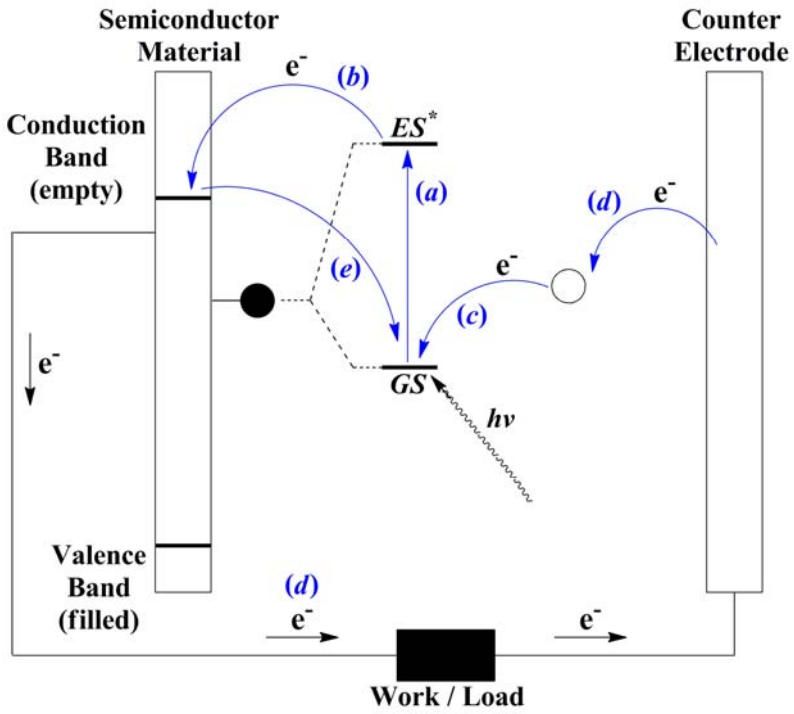

Figure 6.1 A schematic representation of a DSSC is given. The elementary processes involved: (*a*) absorption of light by a sensitizer (filled black sphere); (*b*) electron transfer into the semiconductor conduction band; (*c*) reduction of the oxidized sensitizer by a charge-transporting electrolyte (empty sphere); (*d*) current traveling through the external circuit and successively reducing the oxidized electrolyte; and (*e*) nonproductive BET from the semiconductor to the oxidized sensitizer.

DSSCs are distinguished from other semiconductor-based solar cells by the separation of light absorption and charge transport functions between two different molecular components. DSSCs of the design presented above are typically referred to as Grätzel cells, since Michael Grätzel made significant contributions to their design by employing high surface area colloidal TiO_2 films as the semiconductor component.[1] Grätzel's use of a high surface area semiconductor allowed for increased surface loading of sensitizer molecules and therefore higher absorbance of incident light, an absolute requirement for increased solar harvesting efficiency. A general description of the monochromatic current yield (η_i) possible for a DSSC is given by Equation 1:[1]

$$\eta_i(\lambda) = LHE(\lambda) \cdot \Phi_{inj} \cdot \eta_e \qquad Equation\ 1$$

where LHE is the light harvesting efficiency of the cell at a specific wavelength (λ), Φ_{inj} is the quantum yield for charge injection into the semiconductor, and η_e is the charge collection efficiency. The LHE is the fraction of the incident photons that are absorbed by the sensitizer, also commonly referred to as the absorptance (α (λ)). The LHE of a DSSC is related to transmittance and absorbance by Equation 2:[2]

$$LHE(\lambda) = \alpha(\lambda) = 1 - \frac{I(\lambda)}{I_0(\lambda)} = 1 - 10^{-A(\lambda)} \qquad Equation\ 2$$

where I_0 is the intensity of incident light, I is the intensity of light transmitted through the sample, and A is the absorbance of light at a specific wavelength (λ). The efficiency of light absorption, and therefore the DSSC as a whole, will depend directly on the extinction coefficient of the sensitizer, and on the ability to adsorb high local concentrations of sensitizer molecules on the surface. The surface area required to bind a sensitizer is known as the footprint (A_S).

Polypyridyl complexes of the transition metals Fe^{II}, Ru^{II}, Os^{II}, and Re^{I} have properties well equipped for use in DSSCs.[4] As described in Chapter I, the MLCT absorbance bands for $Ru(bpy)_3^{2+}$ and the related M^{II} bipyridyl complexes have relatively high extinction coefficients over broad ranges of the visible spectrum. While the $Ru(bpy)_3^{2+}$ ground state is relatively inert, photoexcitation produces a ^{3}MLCT state sufficiently reducing compared to the conduction band of TiO_2.[5] Photoinjection into TiO_2 typically occurs on the subnanosecond timescale.[4] The excited-state lifetimes of the bipyridyl complexes can be tens or even hundreds of nanoseconds, and result in photoinjection yields that are quite high when sensitizer molecules are attached close to the semiconductor surface.[4]

Any number of functional groups have been used to anchor Ru^{II} polypyridyl complexes to semiconductor surfaces including carboxylic acids, esters, amides, alcohols, and silyl chlorides.[4] Carboxylic acid and phosphonic acid groups are typically considered superior attachment groups (Figure 6.2).[4] Ru^{II} complexes containing bipyridyl ligands with two carboxylic acid groups serving as anchors have been the most commonly employed in DSSCs, and are known to exhibit high device performances (Figure 6.2a).[5] Bipyridyl ligands containing multiple phosphonic acid groups have more recently been shown to provide greater surface attachment stability under conditions of irradiance in aqueous environments (Figure 6.2b,c).[6] The phosphonic acid group also provides better surface stability over a broader range of pH values.

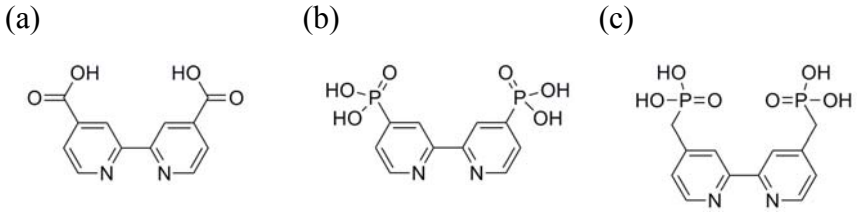

Figure 6.2 (a) A bipyridyl ligand with two carboxylic acid groups. (b) A bipyridyl ligand with two phosphonic acid groups attached directly to the pyridine ring. (c) A bipyridyl ligand with two phosphonic acid groups attached to the pyridine ring through a methylene group.

C. System design

Phosphoserine is a naturally occurring amino acid in proteins, although it is a post-translational modification and is not synthesized during normal translation of the genetic code (Figure 6.3).[7] The post-translational phosphorylation of amino acids such as serine, threonine, and tyrosine by protien kinases is one of the most important regulatory mechanisms within cellular signaling pathways.[7] Similar to the phosphonic acid groups used within the bipyridyl ligands discussed above, phosphoserine is known to provide coordinative binding to TiO_2 surfaces when included in short peptide sequences.[8] An

attachment strategy for Ru^{II}-based sensitizers and TiO_2 surfaces based on phosphoserine anchoring groups was designed and tested. To the best of our knowledge phosphoserine has not been used for the anchoring of sensitizers to semiconductor surfaces.

Several possible advantages were anticipated with Ru^{II}-containing phosphopeptides as compared to traditional polypyridyl Ru^{II} complexes as sensitizers. The possible advantages include: (1) the ease of system redesign due to the high throughput nature of solid-phase peptide synthesis; (2) the ability to incorporate a number of phosphoserine groups in sequence in order to provide high-affinity anchoring of the Ru^{II} sensitizer; (3) the attachment of the Ru^{II} complexes to the phosphopeptides through a single bipyridyl ligand; (4) the ability to attach multiple Ru^{II} complexes to a single anchoring motif; and also (5) the tunable distance between the Ru^{II} bipyridyl complexes and the semiconductor surface. More explicitly, the ability to attach multiple Ru^{II} complexes to a single anchoring motif would allow for high extinction coefficient sensitizers with relatively small footprints, and would also allow for systematic distance dependence studies.

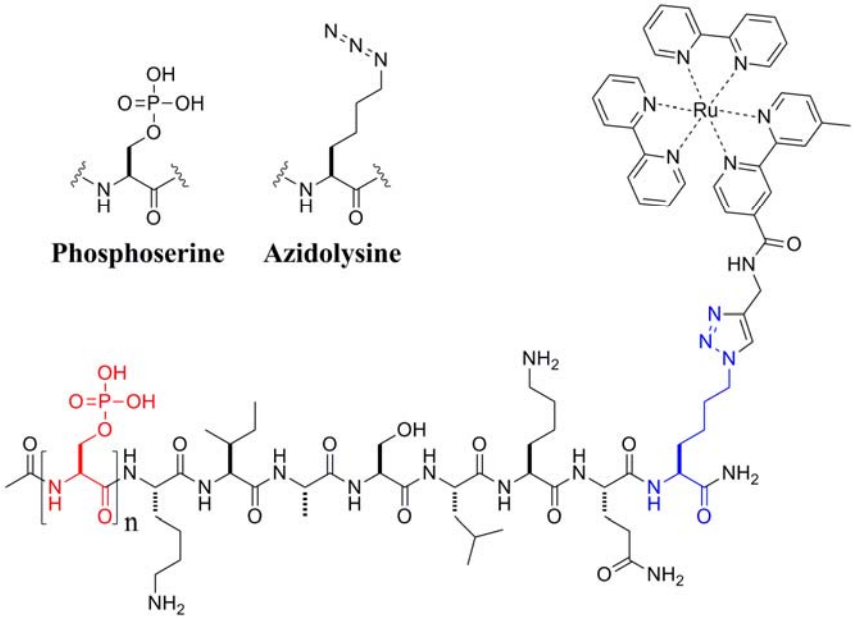

Figure 6.3 System design for the Ru^{II}-containing phosphopeptides 2pS (n = 2) and 3pS (n = 3). The structure of both phosphoserine and azidolysine are shown.

A phosphopeptide system was designed based on a single heptad repeat unit (KIASLKQ) from the P1 peptide sequence in Chapter II (Figure 6.3). The initial system design contained either two (2pS) or three (3pS) phosphoserine residues for surface anchoring, and a Ru^{II} bipyridyl complex (**11a**) attached using an azidolysine residue. The synthesis of and conjugation strategies for using α-Fmoc-ε-azido-L-lysine (**8**) are presented in Chapter III. Ru^{II} complexes typically gain high affinity for semiconductor surfaces when multiple ligands are derivatized with anchoring groups.[2,4] It was hoped that using only one alkyne-functionalized ligand for the attachment of the phosphopeptide anchoring group to the Ru^{II} bipyridyl complex would allow for the chromophoric and electrochemical properties of the other two bipyridyl ligands to be varied more easily.

The relative anchoring stability of the 2pS and 3pS phosphopeptides was tested by first adsorbing the phospopeptides onto high surface area TiO_2 films, and then tracking the surface coverage over time using absorbance measurements. Thin-film TiO_2 slides were

soaked for 48 hours in solutions containg 100 μM phosphopeptide at pH 4 and 7 (phosphate buffer). The TiO_2 adsorption of Ru^{II} bipyridyl complexes derivatized with phosphonic acid groups is known to be highly pH dependent, with more acidic media favoring higher adsorption levels.[6c] The surface coverages of the different slides were measured by absorbance at 452 nm. The slides were stored in identical buffers that did not contain the phosphopeptides so that the surface stabilities could be monitored periodically. Since the thickness of the TiO_2 slides was somewhat nonhomogeneous, the absorbance of the individual uncoated slides was subtracted from the measurements and ΔA values were reported (Figure 6.4). The 3pS phosphopeptide anchoring group was found to be superior to the 2pS anchoring group both with regard to initial loading and also long term surface stability. As expected the lower pH buffer provided better surface anchoring stability for the 3pS phosphopeptide.

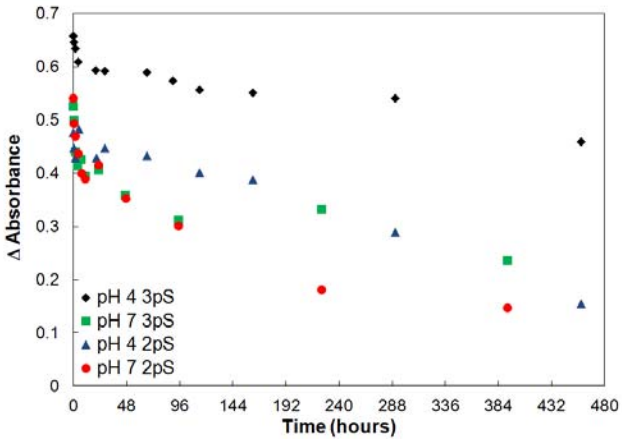

Figure 6.4 Relative surface stability of the 2pS and 3pS phosphopeptides on TiO_2. Slides were coated for 48 hours in 100 μM phosphopeptide solutions in 10 mM phosphate buffer, pH 4 or pH 7, and surface stability was evaluated in buffers that did not contain the phosphopeptides.

D. Photophysical measurements

Once the 3pS phosphopeptide design had been established as a platform for attaching Ru^{II}-containing sensitizers, the length of the phosphopeptide anchor was investigated. It was unknown from the outset whether the phosphopeptide anchor would provide the intimate contact with the TiO_2 surface required for excited-state electron transfer to occur. It was anticipated that if photoinjection from the phosphopeptides did occur, the length of the peptide structure could be used to tune both photoinjection (Figure 6.1, *b*) and BET (Figure 6.1, *e*) rates. A second generation of phosphopeptide anchors was designed in order to test the influence that peptide structure had (Figure 6.5). Compared to the 3pS phosphopeptide, the 3pS-P3 and 3pS-P0 phosphopetides contain fewer amino acid residues between the phosphoserine anchor motif and the azidolysine residue used for Ru^{II} attachment. The general peptide sequence remains the same throughout in order to provide similar solubillity properties and aid in purification. A Ru^{II} complex containing a bis-phosphonated bipyridyl

ligand (**14**) was used for comparison. The complex **14** has previously been used by the Meyer group to study interfacial electron transfer dynamics.[9]

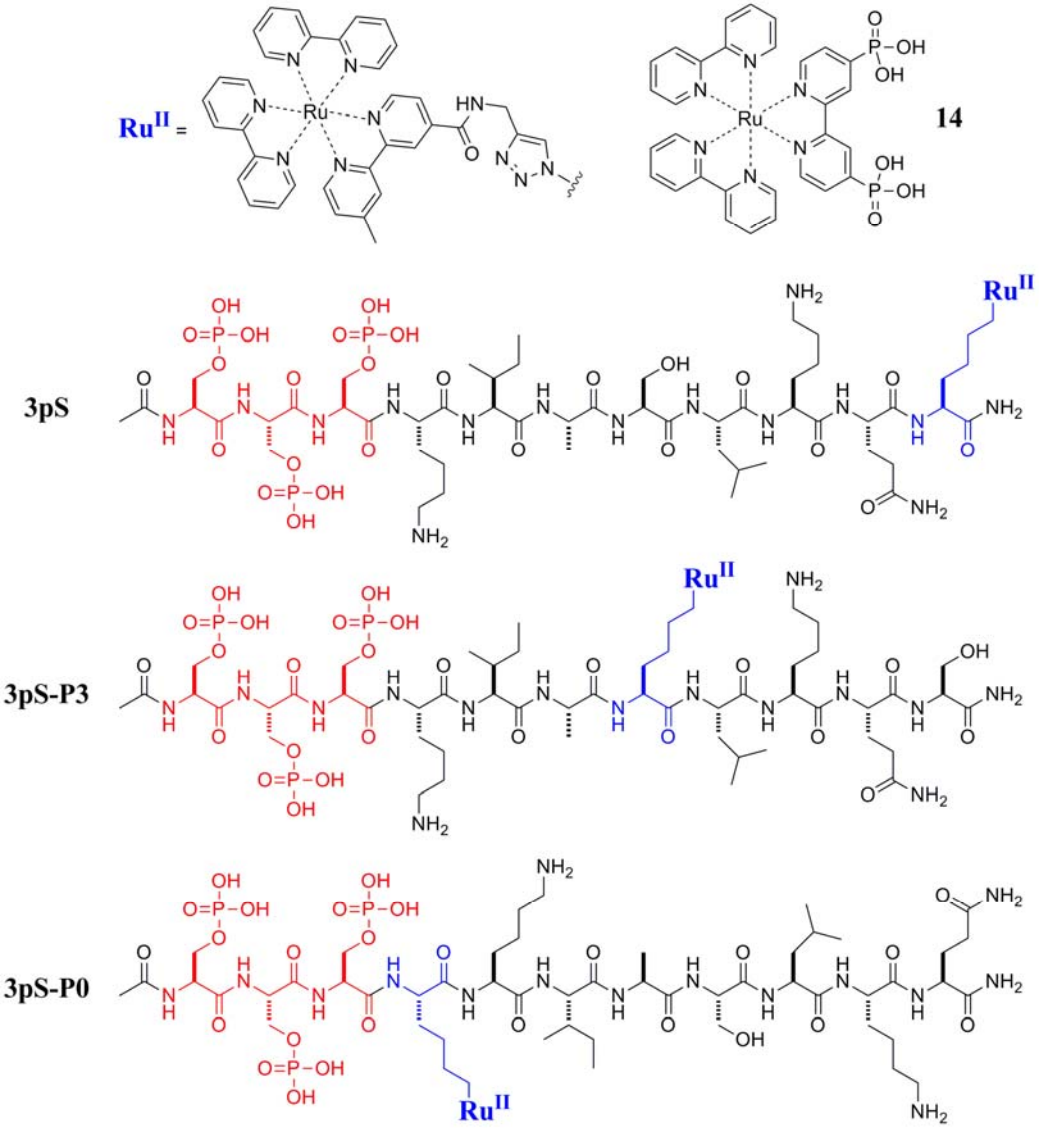

Figure 6.5 Structure of the phosphopeptides used to test the effects of anchor length on photoinjection with TiO_2. The 3pS peptide was optimized for surface coverage and stabillity. The second-generation phosphopeptides 3pS-P3 and 3pS-P0 have shorter peptide linkers between the phosphoserine anchoring motif and the Ru^{II}-containing sensitizer complex. The phosphonate-based complex $[Ru(bpy)_2((4,4'\text{-}PO_3H_2)_2bpy)]^{2+}$ (**14**) was used for comparison when photoinjection was examined.

(a)

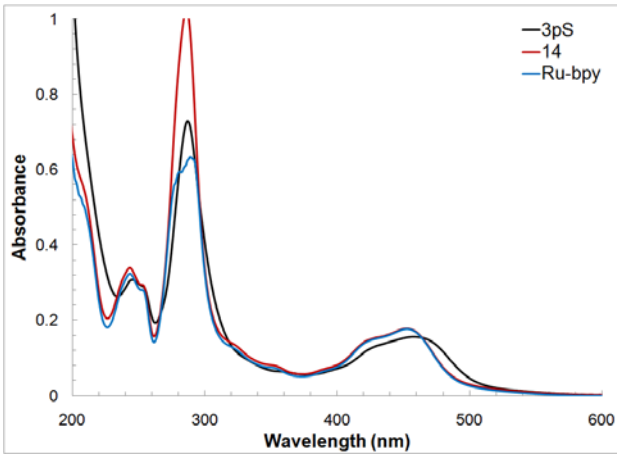

(b)

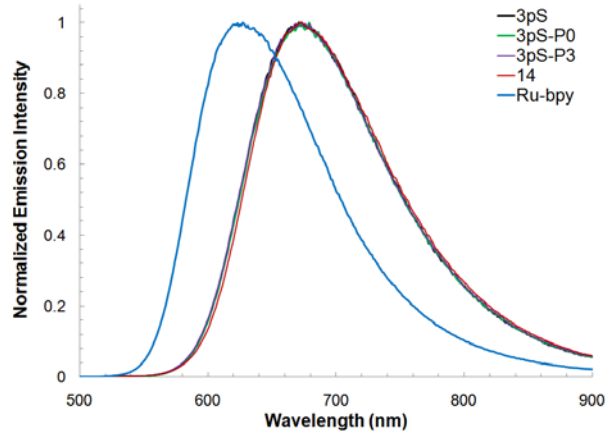

Figure 6.6 (a) Absorbance spectra are shown for the phosphopeptides 3pS (black), the bis-phosphonated complex **14** (red), and $Ru(bpy)_3^{2+}$ (blue). (b) Normalized emission spectra are shown for the phosphopeptides 3pS (black), 3pS-P0 (green), 3pS-P3 (violet). Also shown for comparison are the normalized emission spectra for the bis-phosphonated complex **14** (red), and $Ru(bpy)_3^{2+}$ (blue).

The Ru^{II}-containing phosphopeptides have photophysical properties very similar to the bis-phosphonated complex **14** when measured in solution. The absorbance spectra for the three phosphopeptides and **14** are typical of Ru^{II} bipyridyl complexes (Figure 6.6), displaying intense bands due to the π-π* (ligand-centered) and MLCT transitions.[10] The electron withdrawing character of the amide substituent in the 3pS, 3pS-P0, and 3pS-P3 phosphopeptides results in a hypsochromic shift in their emission spectra (λ_{max} = 674 nm)

relative to $Ru(bpy)_3^{2+}$ (λ_{max} = 626 nm). The shift is similar to that observed for the bis-phosphonated complex **14** (λ_{max} = 675 nm). The three phosphopeptides also have excited-state lifetimes (τ) that are similar to **14** when measured in 0.1 M aqueous $HClO_4$ (Table 6.1).

Table 6.1. Photophysical properties of the phosphopeptides 3pS, 3pS-P0, and 3pS-P3.

	Absorbance (MLCT) λ_{max} (nm)[a]	**Emission λ_{max} (nm)**[b]	**Lifetime (ns)**[b]
3pS	459	674	302
3pS-P3	459	674	282
3pS-P0	459	674	280
14	453	675	306
$Ru(bpy)_3^{2+}$	454	626	554

[a]Measured in 0.1 M $HClO_4$. [b]Measured in 0.1 M $HClO_4$ after degassing with Ar for 30 minutes.

The lowest conduction band of zirconium dioxide (ZrO_2) semiconductors is considerably higher in energy than the excited state reduction potential of most Ru^{II} bipyridyl complexes and therefore precludes photoinjection.[11] For this reason ZrO_2 films have been used for comparative studies where the surface-bound photophysical properties of potenitial sensitizers are examined in the absence of quenching due to electron injection. While the the solution-phase emission lifetimes for the three phosphopeptides were single exponential in character, their surface-bound excited-state lifetimes are biexponential (Table 6.2). The time-resolved emission traces for each phosphopeptide displayed one component that was similar in lifetime to that observed in the solution phase (τ_1) and one component that was of considerably longer lifetime (τ_2). The longer lifetime component (τ_2) had a greater amplitude for all three phosphopeptides.

Table 6.2. Photophysical properties of the phosphopeptides on ZrO_2.

	Emission λ_{max} (nm)[a]	**τ_1 (A_1) ns (%)[a]**	**τ_2 (A_2) ns (%)[a]**	**$<\tau>$ ns[a]**
3pS	665	280 (19)	630 (81)	470
3pS-P3	665	290 (23)	600 (77)	410
3pS-P0	665	280 (23)	560 (77)	380
14	665	150 (13)	400 (87)	370

[a]Measured in 0.1 M $HClO_4$ after degassing with Ar for 30 minutes.

The surface-bound excited-state lifetimes of the phosphopeptides became triexponential after adsorption on TiO_2 films (Table 6.3). Again, the emission spectra for each phosphopeptide displayed one component that was similar in lifetime to that observed in the solution-phase (τ_1) and one component that was of considerably longer lifetime (τ_2). The time-resolved emission traces for the phosphopeptides adsorbed on TiO_2 displayed an additional component that was of considerably shorter lifetime (τ_3) when compared to that observed in the solution phase. The short lifetime (τ_3) component could be related to photoinjection from the Ru^{II} phosphopeptide excited state into TiO_2. The relative amplitude of this component was less than 10% for all three phosphopeptides. The decrease in the average lifetimes of the phosphopeptides adsorbed on TiO_2 indicate emission quenching due to photoinjection, although the degree of this quenching is minimal. Transient absorption analysis, to be reported elsewhere, indicate that the quantum yields for photoinjection (Φ_{inj}) do not exceed 12% for the phosphopeptides adsorbed onto TiO_2.

Table 3. Photophysical properties of the phosphopeptides on TiO_2.

	Emission λ_{max} (nm)[a]	**τ_1 (A_1) ns (%)[a]**	**τ_2 (A_2) ns (%)[a]**	**τ_3 (A_3) ns (%)[a]**	**$<\tau>$ ns[a]**
3pS	664	290 (23)	590 (76)	40 (1)	400
3pS-P3	664	280 (35)	550 (61)	50 (3)	280
3pS-P0	664	230 (54)	490 (37)	50 (9)	160
14	676	*b*	*b*	*b*	*b*

[a]Measured in 0.1 M $HClO_4$ after degassing with Ar for 30 minutes. [b]Values were not obtained due to the instrument response.

E. Conclusions

The phosphopeptides designed and tested throughout Chapter VI were shown to be efficient anchoring modules for Ru^{II} bipyridyl complexes. The 3pS, 3pS-P0, and 3pS-P3 phosphopeptides were compared to the previously studied bis-phosphonated complex **14** using a number spectroscopic techniques. The complex **14** is intimately bound to the TiO_2 surface after adsorption and provides efficient photoinjection ($\Phi_{inj} = 1$). The phosphopeptides described in Chapter VI do not provide efficient photoinjection and are unlikely to be useful as primary sensitizers for nanocrystalline semiconductors. It is likely that the distance between the TiO_2 surface and the Ru^{II} bipyridyl complexes is too large for the phosphopeptides to exhibit photoinjection on a timescale comparable to **14**. There does appear to be a subtle distance dependence for the photoinjection observed in the phosphopeptides. The decrease in the average lifetime for each phosphopeptide roughly correlates with the number of amino acid residues between the Ru^{II} complex and the phosphoserine motif. Photoinjection yields measured by transient absorption also roughly correlate with this parameter. Although the 3pS, 3pS-P0, and 3pS-P3 phosphopeptides do not provide photoinjection yields that would make them attractive for use as primary sensitizers, they may be useful as secondary sensitizers capable of slowing BET (Figure 6.1, *e*) rates.

F. Experimental section

Synthesis of phosphopeptides using α-Fmoc-ε-azido-L-lysine and α-Fmoc-O-benzyl-L-serine. Standard procedures for synthesizing peptides and azidopeptides using an automated synthesizer are described in detail in Chapter III. α-Fmoc-ε-azido-L-lysine (**8)** was synthesized and employed in automated coupling reactions by manual injection. α-Fmoc-O-benzyl-L-serine was purchased from Novabiochem and was also manually injected during automated peptide synthesis. The phosphopeptides were cleaved from the resin, and purified as described in Chapter III. Azidopeptide identities were confirmed by ESI-MS. M was calculated as 1315.61 (exact) for **2pS-N$_3$** ($C_{49}H_{91}N_{17}O_{21}P_2$). MS *m/z* observed: 1316.4 ($[M + H^+]^+$), 658.8 ($[M + 2H^+]^{2+}$); M was calculated as 1482.60 (exact) for **3pS-N$_3$** ($C_{52}H_{97}N_{18}O_{26}P_3$). MS *m/z* observed: 1483.5 ($[M + H^+]^+$), 742.3 ($[M + 2H^+]^{2+}$); M was calculated as 1482.60 (exact) for **3pS-P3-N$_3$** ($C_{52}H_{97}N_{18}O_{26}P_3$). MS *m/z* observed: 1483.3 ($[M + H^+]^+$), 742.2 ($[M + 2H^+]^{2+}$); M was calculated as 1482.60 (exact) for **3pS-P0-N$_3$** ($C_{52}H_{97}N_{18}O_{26}P_3$). MS *m/z* observed: 1483.4 ($[M + H^+]^+$), 742.2 ($[M + 2H^+]^{2+}$).

Synthesis of Ru^{II}-containing phosphopeptides using the CuAAC reaction. Standard procedures for synthesizing Ru^{II}-containing peptides by way of the CuAAC reaction are described in detail in Chapter III. Ru^{II}-containing phosphopeptides were synthesized and purified using identical procedures. M^{2+} was calculated as 1980.75 (exact) for **2pS** ($C_{84}H_{120}N_{24}O_{22}P_2Ru$). MS *m/z* observed: 990.2 ($[M^{2+}]$), 660.5 ($[M^{2+} + H^+]^{3+}$); M^{2+} was calculated as 2147.75 (exact) for **3pS** ($C_{87}H_{126}N_{25}O_{27}P_3Ru$). MS *m/z* observed: 1073.8 ($[M^{2+}]$), 716.2 ($[M^{2+} + H^+]^{3+}$); M^{2+} was calculated as 2147.75 (exact) for **3pS-P3** ($C_{87}H_{126}N_{25}O_{27}P_3Ru$). MS *m/z* observed: 1073.7 ($[M^{2+}]$), 716.2 ($[M^{2+} + H^+]^{3+}$); M^{2+} was

calculated as 2147.75 (exact) for **3pS-P0** ($C_{87}H_{126}N_{25}O_{27}P_3Ru$). MS *m/z* observed: 1073.8 ($[M^{2+}]$), 716.2 ($[M^{2+} + H^+]^{3+}$).

References

[1]O'Regan, B.; Grätzel, M. *Nature* **1991**, *353*, 737-740.

[2]Ardo, S.; Meyer, G. J. *Chem. Soc. Rev.* **2009**, *38*, 115-164.

[3]Gust, D.; Moore, T. A.; Moore, A. L. *Acc. Chem. Res.* **2001**, *34*, 40-48.

[4](a) Galoppini, E. *Coord. Chem. Rev.* **2004**, *248*, 1283-1297. (b) Kalyanasundaram, K, Grätzel, M. *Coord. Chem. Rev.* **1998**, *77*, 347-414. (c) Meyer, G. J. *Inorg. Chem.* **2005**, *44*, 6852-6864.

[5](a) Desilvestro, J.; Grätzel, M.; Kavan, L.; Moser, J. *J. Am. Chem. Soc.* **1985**, *107*, 2988-2990. (b) Vlachopoulos, N.; Liska, P.; Augustynski, J.; Grätzel, M. *J. Am. Chem. Soc.* **1988**, *110*, 1216-1220.

[6](a) Gillaizeau-Gauthier, I.; Odobel, F.; Alebbi, M.; Argazzi, R.; Costa, E.; Bignozzi, C. A.; Qu, P.; Meyer, G. J. *Inorg. Chem.* **2001**, *40*, 6073-6079. (b) Caramori, S.; Cristino, V.; Argazzi, R.; Meda, L.; Bignozzi, C. A. *Inorg. Chem.* **2010**, *49*, 3320-3328. (c) Bae, E.; Choi, W. *J. Phys. Chem. B.* **2006**, *110*, 14792-14799. (d) Park, H.; Bae, E.; Lee, J.-J.; Park, J.; Choi, W. *J. Phys. Chem. B* **2006**, *110*, 8740-8749.

[7](a) Adams, J. A. *Chem. Rev.* **2001**, *101*, 2271-2290. (b) Hunter, T. *Cell* **1995**, *80*, 225-236.

[8](a) Gertler, G.; Fleminger, G.; Rapaport, H. *Langmuir* **2010**, *26*, 6457-6463. (b) Schmidt, S. R.; Schweikart, F.; Anderson, M. E. *J. Chromatogr., B.* **2007**, *849*, 154-162. (c) Sano, A.; Nakamura, H. *Anal. Sci.* **2004**, *20*, 861-864. (d) Sano, A.; Nakamura, H. *Anal. Sci.* **2004**, *20*, 565-566. (e) Pinkse, M. W. H.; Uitto, P. M.; Hilhorst, M. J.; Ooms, B.; Heck, A. J. R. *Anal. Chem.* **2004**, *76*, 3935-3943.

[9]Song, W.; Brennaman, M. K.; Concepcion, J. J.; Jurss, J. W.; Hoertz, P. G.; Luo, H.; Chen, C.; Hanson, K.; Meyer, T. J. *J. Phys. Chem. C.* **2011**, *115*, 7081-7091.

[10]Juris, A.; Balzani, V.; Barigelletti, F.; Campagna, S.; Belser, P.; Von Zelewski, A. *Coord. Chem. Rev.* **1988**, *84*, 85-277.

[11]Katoh, R.; Furube, A.; Yoshihara, T.; Hara, K.; Fujihashi, G.; Takano, S.; Murata, S.; Arakawa, H.; Tachiya, M. *J. Phys. Chem. B.* **2004**, *108*, 4818-4822.

Chapter VII

OLIGOPROLINE RECOGNITION BY A β-HAIRPIN PEPTIDE

A. Introduction and significance

i. Proline is a structurally unique amino acid

Amongst the canonical amino acids, proline holds a distinguished position. Proline is the only amino acid that contains a cyclic side chain attached directly to its α-amino group. This property makes proline the most conformationally restricted amino acid and renders it incapable of donating hydrogen bonds when it forms tertiary amide linkages within peptide structures. Proline occupies a very narrow region of the Ramachandran plot as a direct consequence of the pyrrolidine-containing side chain, and the conformational constraints that it imposes on the peptide backbone (Φ = -75º, Ψ = +145º, approximately).[1] Proline typically plays a highly specialized role in proteins, whether it is incorporated in polyproline structures, or within structures containing the other proteinogenic amino acids.

The unique chemical properties of proline allow it to interact with the other amino acids in very distinctive ways. One of these distinct interactions is the aromatic-prolyl interaction.[2] Interactions between proline and the aromatic amino acids have been well studied in the context of both protein folding and protein-protein interactions.[2] An important manifestation of the aromatic-prolyl interaction is its effect on determining the *cis-trans* isomerisation state for amide bonds in many proteins.

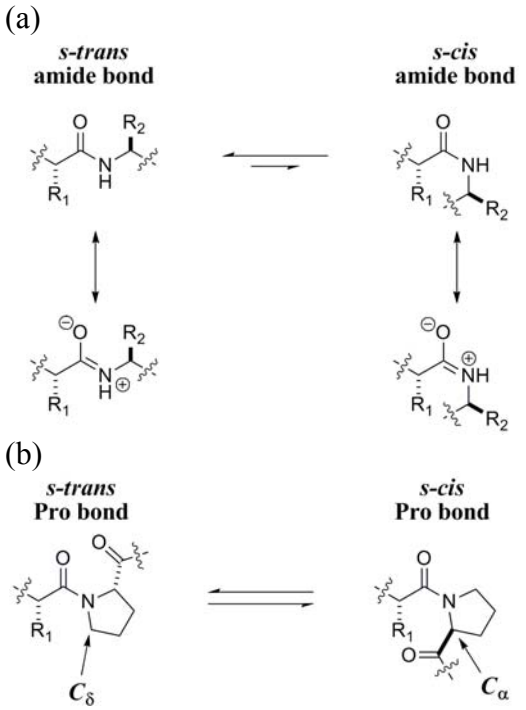

Figure 7.1 (a) The *s-trans* and *s-cis* amide bond conformations for peptides are shown. Steric repulsions between the C_α substituents lead to destabilization of the *s-cis* amide bond conformation. (b) The *s-trans* and *s-cis* conformations for X_{aa}-Pro amide bonds are closer in energy due to competing steric repulsions from the C_α and C_δ substituents (X_{aa} is any nonproline amino acid).

There is a significant degree of electron delocalization in amide bonds which results in considerable double-bond character (Figure 7.1a). This double-bond character results in a roughly 20 kcal·mol^{-1} barrier to rotation around the C-N amide bond.[2a] In the majority of amino acid peptides the *s-trans* conformation ($\omega = 180°$) is favored by roughly 2.5 kcal·mol^{-1} relative to the *s-cis* conformation ($\omega = 0°$) due to the steric restrictions present in secondary amides (Figure 7.1a). In peptides containing X_{aa}-Pro tertiary amide bonds the preference for the *s-trans* conformation is considerably decreased since steric restrictions presented by the C_α and C_δ substituents are more similar. The *s-trans* conformation is closer to 0.5 kcal·mol^{-1} more stable compared to the *s-cis* conformation in these amide bonds containing proline. The barrier to rotation in proline-containing amide bonds is also decreased to roughly 13

kcal·mol^{-1}.[2a] The relatively low barrier to rotation and increased energy in the *s-trans* conformation results in X_{aa}-Pro amide bonds adopting an *s-cis* conformation in more than 5% occurrence in natural proteins.[2d] This is significantly more often than any of the other proteinogenic amino acids which on average occupy the *s-cis* conformation in less than 1% of amide bonds. Aromatic residues directly preceding proline confer stability to the *s-cis* conformation due to favorable aromatic-prolyl interactions, with tryptophan being the most *s-cis*-stabilizing non-proline residue. These interactions were first recognized through the analysis of protein data banks in which many aromatic residues stack against proline side chains. Most often, the proline H_α, H_β, or H_δ show the shortest contact distances (roughly 4 Å) with the aromatic ring (Figure 7.2a).

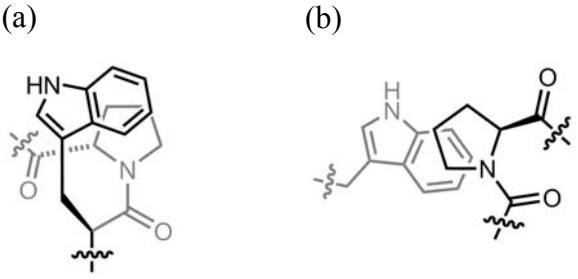

Figure 7.2 (a) A tryptophan-proline amide bond is shown. The *s-cis* conformation is stabilized by an aromatic-prolyl interaction. (b) An aromatic-prolyl interaction between tryptophan and proline residues located within different protein domains. Many aromatic-prolyl interactions are important in protein-protein recognition events.

ii. Proline-rich motifs

The aromatic-prolyl interaction has also been recognized in the context of the interdomain contacts made between proteins (Figure 7.2b). There are many protein domains that recognize proline-rich motifs (PRMs) during complex signaling events (Figure 7.3).[2e,f] PRM-binding domains all contain highly conserved clusters of surface-exposed aromatic residues, referred to as “aromatic cradles”. PRM-binding domains typically recognize ligands

that are peptide segments 5-10 amino acids in length. PRM-binding domains recognize specific 3-6 amino acid residue "core motifs" within these ligand peptides. The core motifs often repeat in tandem within the ligand peptides. Currently, six distinct families of PRM-binding domains have been distinguished based on their respective structure and ligand binding preferences. The SH3 domains,[3] the WW domains,[4] the EVH1 domains,[5] the GYF domains,[6] the UEV domains,[7] and the single-domain profilin proteins[8] all interact with specific "core motifs". The different families recognize their respective PRMs with K_d values that typically range from 1 to 500 μM. Interactions of non-proline residues within the motifs provide specificity. PRM-binding domains are typically found in larger multidomain proteins and are involved in a number of cellular processes including cytoskeletal rearrangement, cell growth, postsynaptic signaling, and transcription.[2e,f] There are more than 400 PRM-binding domains found in the human genome, and PRMs are the most common sequence motifs in many simple organisms including *Drosophila melanogaster* and *Caenorhabditis elegans*.[2f] It is believed that many PRMs are associated with multiple PRM-binding domains with varying affinities, a property that would allow them to perform multiple signaling functions orthogonally.[2e]

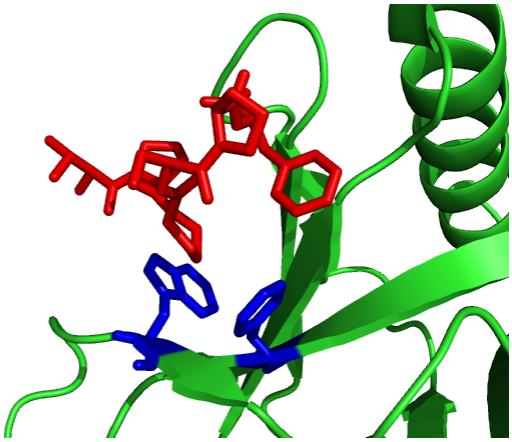

Figure 7.3 The PRM-binding EVH1 domain from Homer 1a is shown (green) bound to its natural ligand peptide (red) which has the sequence TPPSPF (pdb: 1DDV). The "aromatic cradle" that is required for binding is also highlighted (blue) within the EVH1 domain. The two aromatic residues, tryptophan and tyrosine, are shown making close contacts with proline residues in the ligand.

iii. The polyproline type II (PPII) helix

It is widely believed that the ubiquitous use of proline as a recognition element for signaling modules is a the result of the unique polyproline type II (PPII) helix structure that repetitive proline-rich sequences adopt in an aqueous environment (Figure 7.4). The PPII helix is a left-handed helical structure that lacks the intramolecular hydrogen bonds that stabilize the more common peptide secondary structures including α-helices and β-sheets. The PPII helix has a pitch greater than 9 Å and contains 3 residues per turn making it considerably more extended than the α-helix which has a pitch of only 5.4 Å and 3.6 residues per turn. The structure of the PPII helix is the result of previously mentioned conformational constraints imposed by the annular side chain. All amide bonds within PPII helices are in the *s-trans* conformation. The PPII helix is typically considered rigid and it is believed that the preorganization of recognition elements within the PPII helix reduces the entropic cost of binding PRM ligands.[2e] Since PRMs all share the PPII helix as their conserved secondary structure, it is not surprising that the different families of PRM-binding domains exhibit

structural homology as well. The previously mentioned aromatic cradles are most commonly found on the surface of a β-sheet and consist of two diagonal (i, j+2) aromatic residues. The overall shape of the PPII helix resembles that of a triangular prism, and most PRM-binding domains have a cleft arrangement that is complementary to this shape.[2f] The absence of intramolecular hydrogen bonding within PPII helices leaves the electron-rich proline carbonyl groups free to accept hydrogen bonds donated from amino acids present within PRM-binding domains. Hydrogen bonds to PRMs are typically donated from aromatic residues such as Trp or Tyr, although Asn, Thr, Ser, Gln, and His can also contribute in this fashion.[2e,f]

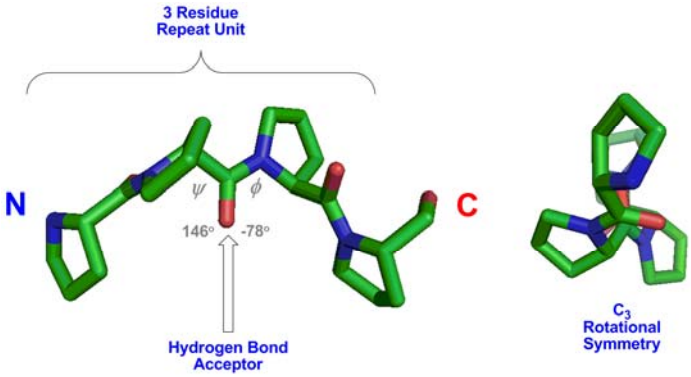

Figure 7.4 The conformation of the polyproline type II (PPII) helix viewed both perpendicular (left) and parallel (right) to the helical axis. The helix has a pseudo C_3 rotational axis and contains three residues per turn with torsion angles that are dictated by the pyrrolidine-containing side chain (Φ = -78º, Ψ = +146º). The tertiary amide groups are very good hydrogen-bond acceptors and serve as an additional recognition element in addition to the aromatic-prolyl interaction.

The aromatic-prolyl interactions that stabilize *s-cis* amide bond conformations in many proteins and allow PRMs to coordinate multiprotein signalling cascades are thought to be driven by a combination of enthalpic C-H-π interactions and the classical hydrophobic effect.[9] Zondlo and co-workers have helped elucidate the enthalpic contribution to aromatic-

prolyl interactions from studies on peptide model systems using ^{1}H NMR.[10] They were able to modulate the preference for the *s-cis* versus *s-trans* amide bond conformation in a simple tetrapeptide model system. The results indicated that more electron rich aromatic amino acids favored the *s-cis* conformation for enthalpic reasons and showed that tryptophan and deprotonated tyrosine were the most efficient in this regard. This result is interesting since tryptophan and tyrosine are the residues selected most often by evolutionary processes for binding PRMs.

B. The tryptophan zipper peptides as models for aromatic-prolyl interactions

i. The tryptophan zipper peptides

The tryptophan zipper peptides were originally reported by Cochran and coworkers (Figure 7.5a).[11a] The tryptophan zipper (trpzip) structural motif greatly stabilizes the β-hairpin conformation and was first demonstrated for a series of 12 to 16 residue peptides with different turn sequences. Cochran and coworkers determined an experimental energy scale for the stabilizing contributions of amino acid residues as nonhydrogen-bonded positions within β-hairpin peptides.[11b,c] There results indicated that cross-strand tryptophan residues were the most stabilizing pair at nonhydrogen bonding positions and went on to develop the trpzip peptides as stable monomeric β-structure mimics. The trpzip β-hairpins all exhibit cooperative thermal unfolding transitions and nonzero changes in heat capacity. The Gibbs free energy change of unfolding (ΔG_F = 0.6-1.7 kcal·mol^{-1}) for the β-hairpins are comparable as per-residue values to those measured for large natural proteins. NMR structures deposited for the trpzip peptides show an interdigitating pattern for the tryptophan side chains (Figure 7.5b). The nearly perpendicular conformation of the side chains is not unlike that of the aromatic cradles discussed for PRM-binding domains. The three-dimensional disposition of

the aromatic residues led to the hypothesis that the trpzip peptides may serve as good model systems for studying aromatic-prolyl interactions. Indeed, overlay images of trpzip NMR structures and crystal structures of the aromatic cradles located within natural PRM-binding domains show a close concordance.

(a)

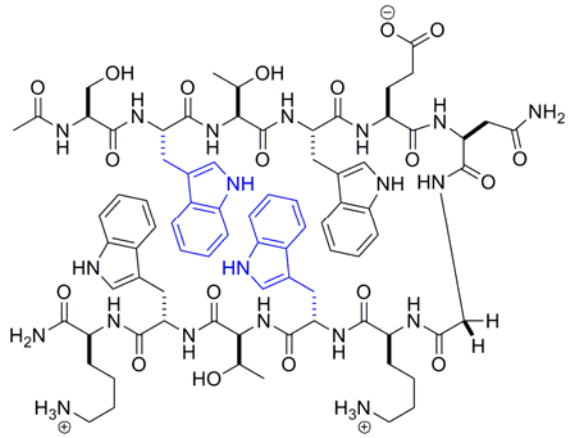

(b)

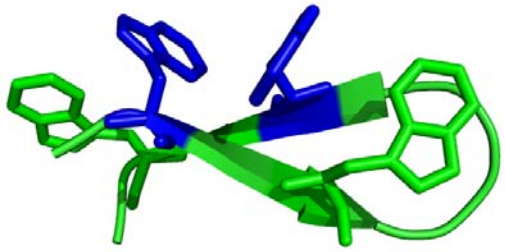

Figure 7.5 (a) The structure of a trpzip β-hairpin peptide is rendered in a two-dimensional fashion. (b) The three-dimensional NMR structure generated for the trpzip β-hairpin peptide is shown (pdb: 1LE1). The two tryptophan residues that form a cleft arrangement similar to that observed within natural PRM-binding domains are highlighted (blue) in each structural representation.

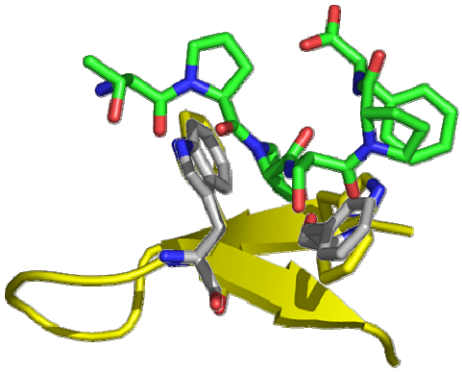

Figure 7.6 The aromatic binding residues (tryptophan and tyrosine, gray) from the Homer 1a EVH1 domain bound to the natural ligand sequence (green) (pdb: 1DDV) overlaid with a trpzip peptide (yellow) containing a type II' turn sequence (pdb: 1LE0). The aromatic residues from each structure occupy very similar conformations.

ii. System design

It was hypothesized that the trpzip peptide scaffold originally reported by Cochran could be modified so that thermodynamic measurements of aromatic-prolyl interactions could be made via disulfide exchange experiments. Exchange reactions under thermodynamic equilibrium conditions have previously been employed in measuring the strength of non-covalent interactions between peptide segments.[12] Thiol-disulfide exchange has proven particularly advantageous in defining important, but subtle, structural features during *de novo* protein design.[12a-c] When performing exchange reactions, favorable interactions manifest themselves as perturbations in the observed equilibrium constant (K_{EQ} differs from the value expected for a statistical distribution with $\Delta G = 0$). Essentially a competition experiment, analysis is performed under "native" conditions and is highly beneficial for assessing relatively weak non-covalent interactions since they are measured as a ratio of covalent species. Other methods for assessing binding strength such as ITC or

fluorescence anisotropy may be too insensitive or otherwise less suited for measuring weaker attractive forces like the aromatic-prolyl interaction.

The trpzip β-hairpin peptide motif was ultimately redesigned so as to be compatible with disulfide exchange conditions (Figure 7.7a). [12a-c] The addition of Cys-Gly-Gly to the N terminus provides a flexible tether for thiol-disulfide exchange. The Gly-Asn turn sequence in Cochran's peptide was replaced with a D-Pro-Gly sequence in order to provide the peptide with greater chemical stability under the experimental conditions which require equilibration for several days in neutral to basic media. The D-Pro-Gly sequence has been shown a superior promoter for β-turn structures when compared to sequences containing only L amino acids.[11b,13] Two additional Lys residues were appended to the C terminus of the β-hairpin to encourage solubility of all disulfide species and discourage aggregation. A series of oligoproline peptides were designed, varying in length from five to seven Pro residues (Figure 7.7b). The oligoproline peptide contained a tryptophan residue for concentration determinations, and a flexible Cys-Gly-Gly tether for disulfide exchange measurements.

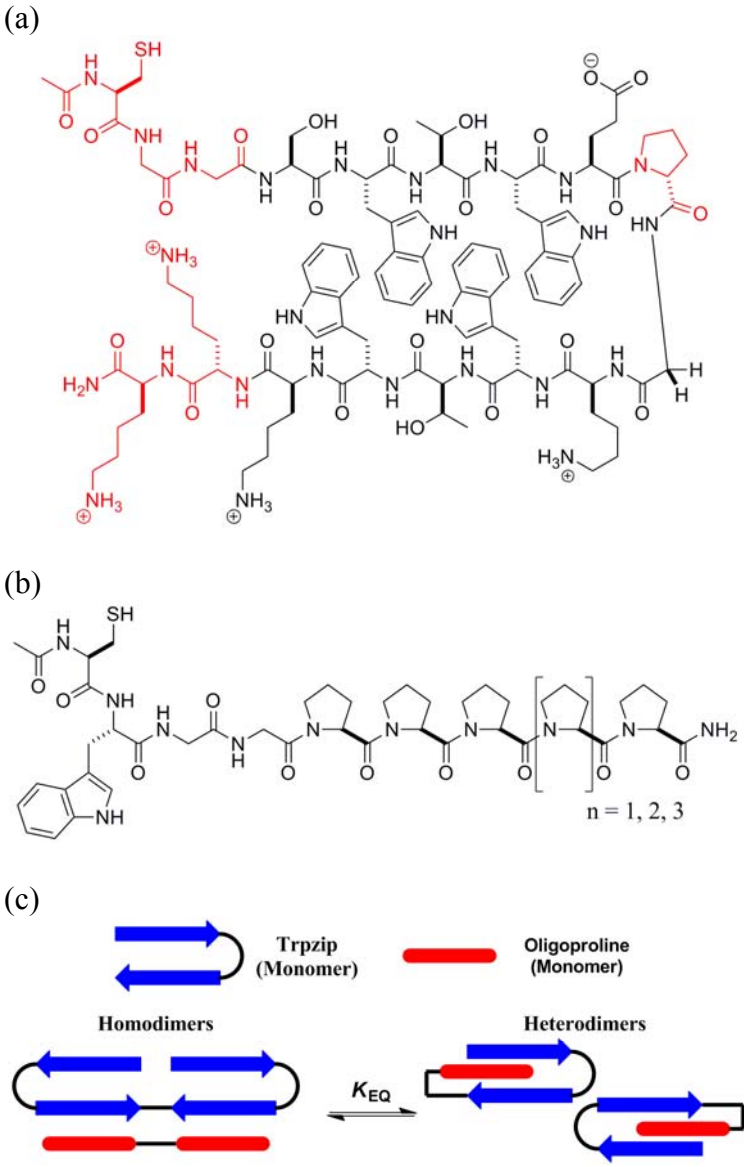

Figure 7.7 (a) The trpzip β-hairpin peptide redesigned for disulfide exchange experiments is shown. The residues that have been changed from the original design are shown in red. (b) The oligoproline peptides used for the disulfide exchange experiments are shown. The length of the oligoproline segment ranges from five to seven Pro residues. (c) A simple schematic representation of the designed disulfide exchange experiments.

It was anticipated that, by mixing the trpzip peptide with an appropriate oligoproline peptide, a number of disulfide species could be produced (Figure 7.7c). The oxidized mixture would contain oligoproline homodimers, β-hairpin homodimers, and heterodimers composed of each peptide. At equilibrium the relative concentration of the heterodimer would be twice that of either homodimer if a statistical mixture were produced ($\Delta G = 0$). The equilibrium constant (K_{EQ}) for a statistical mixture would therefore be equal to 4 using Equation 1:

$$K_{EQ} = \frac{[Heterodimer]^2}{[Pro\ Homodimer][Hairpin\ Homodimer]} = \frac{[2]^2}{[1][1]} = 4 \qquad Equation\ 1$$

where [Heterodimer] is the equilibrium concentration of the heterodimer containing both an oligoproline peptide and a β-hairpin peptide, [Pro Homodimer] is the equilibrium concentration of the homodimer containing two oligoproline peptides, and [Hairpin Homodimer] is the equilibrium concentration of the homodimer containing two β-hairpin peptides. Any attractive or repulsive interactions between the β-hairpin peptide and/or the oligoproline peptide would manifest as an equilibrium constant deviating from 4. The magnitude of the net thermodynamic driving force for the interactions ($\Delta G_{[HP]}$) can be measured using Equation 2:

$$\Delta G_{[HP]} = -RTLn\left(\frac{K_{EQ}}{4}\right) \qquad Equation\ 2$$

where K_{EQ} is the equilibrium constant calculated using Equation 1, R is the molar gas constant in units of $cal \cdot mol^{-1} \cdot K^{-1}$ (1.986), and T is the temperature in Kelvin (298).

Since the distinctive shape of the trpzip β-hairpin peptide motif was hypothesized to be favorable for providing aromatic-prolyl interactions, a negative control was designed based on another β-hairpin peptide motif used for molecular recognition. The WKWK β-hairpin peptide was designed as a synthetic receptor for ATP and has a binding cleft comprised of two tryptophan residues (Figure 7.8a).[14] The NMR structure of the WKWK peptide indicates that the tryptophan residues present a much flatter surface when compared to natural PRM binding domains and the trpzip peptides (Figure 7.8b).[15] The turn sequence for the WKWK peptide was also converted to D-Pro-Gly in order to provide greater chemical stability. The sequences for the peptides used throughout the disulfide exchange experiments are shown in Table 1.

(a)

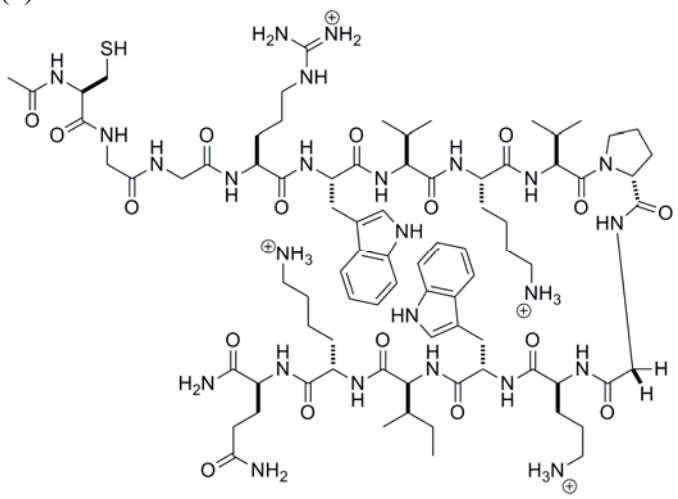

(b)

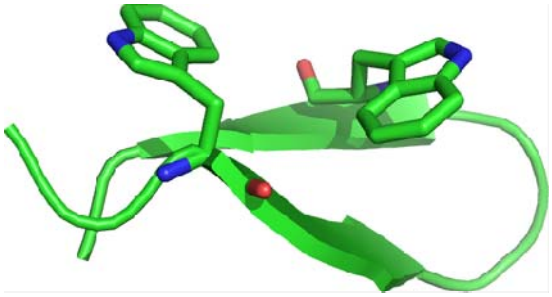

Figure 7.8 (a) The WKWK β-hairpin peptide redesigned for disulfide exchange experiments is shown. (b) The NMR structure for the WKWK peptides shows the aromatic residues adopts a much flatter conformation when compared to the trpzip β-hairpin peptide motif.

Table 7.1. Primary sequences for the peptides used in disulfide exchange experiments

Peptide Name	Sequence[a]
Trpzip	Ac-Cys-Gly-Gly-Ser-Trp-Thr-Trp-Glu- D-Pro-Gly-Lys-Trp-Thr-Trp-Lys-Lys- Lys-NH_2
CW-Pro5	Ac-Cys-Trp-Gly-Gly-Pro-Pro-Pro-Pro- Pro-NH_2
CW-Pro6	Ac-Cys-Trp-Gly-Gly-Pro-Pro-Pro-Pro- Pro-Pro-NH_2
CW-Pro7	Ac-Cys-Trp-Gly-Gly-Pro-Pro-Pro-Pro- Pro-Pro-Pro-NH_2
CWGG	Ac-Cys-Trp-Gly-Gly
C-Pro7-W	Ac-Cys-Gly-Gly-Gly-Pro-Pro-Pro-Pro-Pro-Pro-Pro-Trp- NH_2
WC-Pro7	Ac-Trp-Cys-Gly-Gly-Gly-Pro-Pro-Pro-Pro-Pro-Pro-Pro- NH_2
WKWK	Ac-Cys-Gly-Gly-Arg-Trp-Val-Lys-Val- D-Pro-Gly-Orn-Trp-Ile-Lys-Gln-NH_2

[a]Primary sequences for all peptides are designated by the standard three letter amino acid code. Orn is ornithine. All amino acids are L amino acids, except D-Pro.

iii. CD analysis of trpzip β-hairpin and oligoproline peptides

The trpzip β-hairpin, oligoproline peptides, and WKWK β-hairpin were analyzed using CD spectroscopy before disulfide exchange analysis. As desired, the oligoproline peptides all form PPII helices in buffer (Figure 7.9a) as indicated by intense minima at 205 nm, with less intense maxima at 228 nm. Both spectral features are closely associated with the PPII helix secondary structure.[16] Decreasing the number of residues within the oligoproline series results in a hypsochromic shift of the maxima which is likely indicative of a subtle decrease in the PPII helical content of the peptide (Figure 7.9a).[16b]

The CD spectrum for the trpzip peptide displays strong exciton-coupled bands at 215 and 230 nm that are characteristic for the tryptophan zipper motif (7.9b).[11a,17] CD spectra for the trpzip peptide were taken under reducing conditions to prevent the formation of homodimers. When the trpzip peptide is allowed to oxidize in the standard phosphate buffers used for CD analysis, the spectra show an approximately 30% decrease in the intensity of the exciton-coupled CD bands compared to the monomeric peptide (not shown). This

observation indicates that the trpzip peptide is probably distorted from the structure reported by Cochran when bound in the homodimer state, and also implies some interaction between the two trpzip peptides that compose the homodimer. The CD spectrum for the WKWK peptide has a minimum between 210 and 220 nm and a positive signal below 200 nm. Both spectral features can be attributed to an antiparallel β-structure,[18] and indicate the D-Pro-Gly sequence is a competent nucleator of a β-turn structure in this sequence.

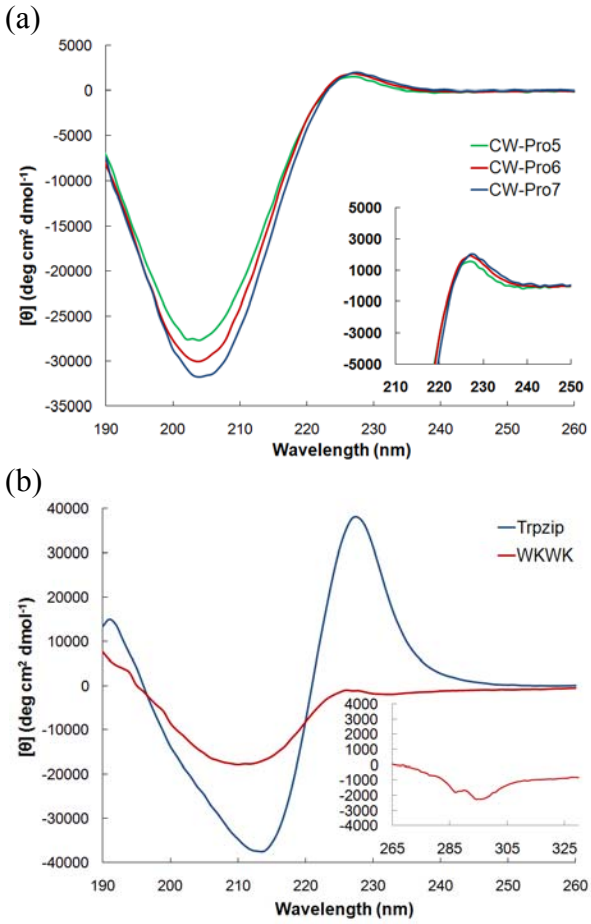

Figure 7.9 (a) CD spectra of the oligoproline peptides at 100 μM are shown. All three oligoproline peptides show signals at approximately 205 and 228 nm characteristic to the PPII helix secondary structure. Spectra were recorded at 25°C in 10 mM PO_4^{3-}, pH 7, buffer. (b) CD spectra of the trpzip and WKWK β-hairpin peptides at 50 μM are shown. The spectrum for the trpzip peptide was taken at 25°C in 10 mM PO_4^{3-}, 2 mM TCEP, pH 7, buffer, and shows signals at 215 and 230 nm characteristic to structural motif. The spectrum for the WKWK peptide was taken at 25°C in 10 mM PO_4^{3-}, pH 7, buffer, and shows a minimum at 210 nm characteristic to β-structures.

iv. Analysis of the disulfide exchange experiments

Disulfide exchange experiments were performed by mixing approximately equal proportions of an oligoproline peptide and the trpzip β-hairpin peptide in basic aqueous buffer with no effort made to exclude oxygen. The presence of molecular oxygen oxidized all of the thiol-containing peptides to disulfide species within a matter of hours or days. As previously mentioned, once all of the peptide thiols were oxidized, the mixture contained a number of homodimer and heterodimer species. The equilibration of those species was monitored for several days by HPLC analysis (Figure 7.10). Although reactions were monitored at multiple wavelengths during the equilibration period, the absorbance at 280 nm was used for quantification since all of the designed peptides contained a tryptophan residue.

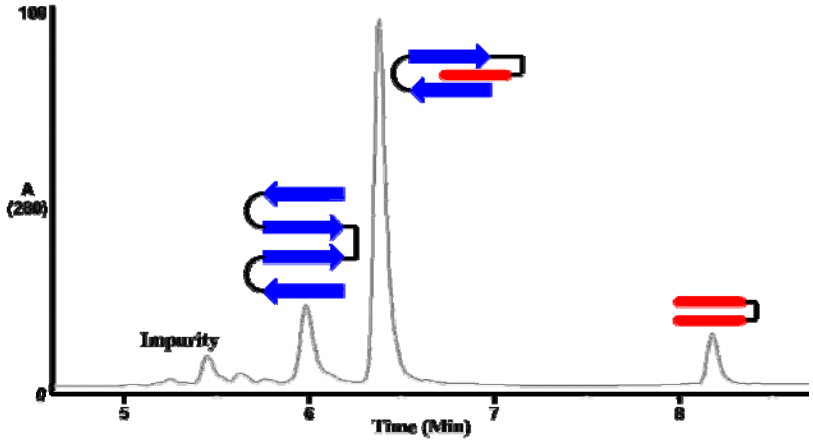

Figure 7.10 An HPLC chromatogram at 280 nm is shown for the analysis of a typical disulfide exchange reaction. The equilibrated mixture contains a trpzip β-hairpin homodimer (blue), an oligoproline homodimer (red), and a heterodimer (blue and red) containing both a trpzip β-hairpin and oligoproline motif.

All three of the oligoproline peptides equilibrated with the trpzip β-hairpin to give nonstatistical distributions of species. The CW-Pro7 peptide gave the largest relative concentration of heterodimer at equilibrium, implying a substantial stabilizing interaction between the trpzip β-hairpin and the oligoproline. Likewise, the CW-Pro5 peptide gave the

smallest relative concentration of heterodimer species, with the concentration still being well above that predicted for a statistical mixture. The WKWK peptide was equilibrated with the CW-Pro7 peptide only, and gave a heterodimer concentration above that expected for a statistical mixture as well. The equilibrium constants (K_{EQ}) calculated for the different disulfide exchange experiments according to Equation 1 are given in Table 2.

Table 7.2. Equilibrium constants generated from the disulfide exchange experiments

β-hairpin	**Oligoproline**	K_{EQ}[a]
Trpzip	CW-Pro5	18 ± 1
Trpzip	CW-Pro6	47 ± 2
Trpzip	CW-Pro7	68 ± 3
WKWK	CW-Pro7	15 ± 2

[a]Equilibrium constants (K_{EQ}) are averaged from at least two separate trials. Error estimates provided are based on the peak resolution for the different trials.

Based on the results of the disulfide exchange experiments it seemed likely that favorable aromatic-prolyl interactions could be measured through disulfide exchange experiments. It was, however, observed that during sample preparation the trpzip peptide formed homodimer species at an accelerated rate relative to the oligoproline and WKWK peptides. Coupled with the previously mentioned CD analysis, the observation of the accelerated homodimer formation led to the hypothesis that the trpzip peptide has a favorable homodimer interactions. Cochran reported no intermolecular aggregation for the trpzip peptides based on concentration-dependent NMR experiments and analytical ultracentrifugation (AUC), but a favorable intramolecular trpzip-trpzip interaction in the homodimer is not unreasonable given the number of tryptophan residues that could contribute π-stacking interactions when covalently linked. These interactions could be too weak to manifest as an intermolecular association, while still easily being measured during a disulfide exchange experiment.

A favorable trpzip-trpzip homodimer interaction would manifest itself as a decrease in the observed K_{EQ} values measured by disulfide exchange since heterodimer formation would have to overcome an energetic penalty corresponding to the disruption of the trpzip-trpzip interactions. In order to test this hypothesis, the two β-hairpin peptides were both subjected to disulfide exchange experiments with a short peptide comprised only of the linker sequence (CWGG) used for the oligoproline peptides. Both the trpzip and WKWK peptides exhibited nonstatisitcal values for K_{EQ} when equilibrated with CWGG. For WKWK, the K_{EQ} values (14 ± 1) were within error of that reported for the interaction with CW-Pro7. This implies that the WKWK peptide does not have any favorable aromatic-prolyl interactions. The nonstatisitical K_{EQ} value measured for the β-hairpin and the CW-Pro7 peptide (15 ± 2) are most likely due to interactions between amino acid residues in WKWK and on the tether sequence (CWGG).

The disulfide exchange experiments with the trpzip peptide and the linker sequence CWGG display K_{EQ} values below 4, a result that would be expected if homodimer formation were thermodynamically favorable. The K_{EQ} values for the trpzip-CWGG exchange experiments (1.3 ± 0.15) corresponds to a free energy change ($\Delta G_{[HP]}$) of 0.67 ± 0.07 kcal·mol^{-1}. Equation 2 was modified using the average K_{EQ} value measured for the trpzip-CWGG exchange experiments. The modification provides the corrected free energy change for heterodimer formation between the trpzip and the oligoproline peptides ($\Delta G^*_{[HP]}$) in the form of Equation 3:

$$\Delta G *_{[HP]} = -RTLn\left(\frac{K_{EQ}}{1.3}\right) \qquad Equation\ 3$$

The corrected $\Delta G^*_{[HP]}$ values for the trpzip, WKWK, and oligoproline peptides are given in Table 3. The $\Delta G^*_{[HP]}$ value calculated for the exchange reaction between WKWK and CW-Pro7 was zero since the K_{EQ} value reported for the pair was within error of that reported for the WKWK-CWGG exchange reaction (14 ±1). The value ($\Delta G^{**}_{[HP]}$) was calculated using the similarly modified Equation 4:

$$\Delta G\ {}^{**}_{[HP]} = -RTLn\left(\frac{K_{EQ}}{14}\right) \qquad Equation\ 4$$

Table 7.3. Corrected values for Gibb's free energy change of heterodimer formation

β-hairpin	Oligoproline	K_{EQ}[a]	$\Delta G^*_{[HP]}$[b] (kcal·mol^{-1})
Trpzip	CW-Pro5	18 ± 1	-1.6
Trpzip	CW-Pro6	47 ± 2	-2.1
Trpzip	CW-Pro7	68 ± 3	-2.3
WKWK	CW-Pro7	15 ± 2	0

[a]Equilibrium constants (K_{EQ}) and error estimates are the same as those reported in Table 2. [b]The corrected Gibbs free energy change for the disulfide exchange reactions ($\Delta G^*_{[HP]}$) were calculated using Equation 3. The error estimated for each was less than 0.07 kcal·mol^{-1} based on the error reported for the K_{EQ} value measured for CWGG and the trpzip peptide.

The corrected $\Delta G^*_{[HP]}$ values given in Table 3 are representative of the aromatic-prolyl interactions in these systems if the assumption is made that no other attractive forces are cooperatively contributing to heterodimer formation during the exchange reactions. The oligoproline peptides used within the experiments all contain a single tryptophan residue used for concentration determination and quantitation during the disulfide exchange experiments. Since an aromatic-aromatic interaction could contribute to heterodimer formation in the trpzip-CWGG exchange reaction control experiments were designed to probe this possibility. Based on the observation that increasing the length of the oligoproline peptides from CW-Pro5 to CW-Pro7 resulted in an increase in heterodimer formation, it was hypothesized that the trpzip peptide primarily interacts with the oligoproline peptides near

their C termini. The peptide C-Pro7-W has a tryptophan residue at the C terminus where interactions between the trpzip β-hairpin and the oligoproline peptides were thought to occur (Table 7.1). Indeed, when the C-Pro7-W peptide is subjected to disulfide exchange experiments with the trpzip peptide, the observed K_{EQ} value was extremely large and difficult to measure by HPLC integration ($K_{EQ} > 150$). This result suggested strongly that moving the tryptophan residue closer to the C terminus allows binding of the residue to the β-hairpin moiety through aromatic-aromatic interactions. The peptide WC-Pro7 has a tryptophan residue included on the N terminal side of the cysteine residue, displaced two residue positions relative to the CW-Pro7 peptide (Table 7.1). When the WC-Pro7 peptide is equilibrated with the trpzip β-hairpin the measured K_{EQ} value (69 ± 3) was within error of that reported for CW-Pro7. If the tryptophan residue in either the CW-Pro7 or WC-Pro7 peptides significantly contributed to binding it would be highly unlikely that the peptides would have identical K_{EQ} values. Therefore this suggests that the attractive interactions measured for the oligoproline peptides ($\Delta G^*_{[HP]}$) are due to aromatic-prolyl interactions and are not due to interactions between the linker sequence and the trpzip β-hairpin motif. 2D NMR experiments performed on the CW-Pro7-trpzip heterodimer indicated that NOE signals were present between Trp residues in the β-hairpin structure and Pro residues in the oligoproline moiety. There were, however, no NOE signals present between the Trp residue on the oligoproline (CWGG linker) and the β-hairpin.

C. Conclusions

The tryptophan-zipper peptide motif reported by Cochran and coworkers was shown to provide favorable interactions with a series of oligoproline peptides. To the best of our knowledge, this is the first example of a small β-hairpin peptide demonstrating affinity for

peptides which adopt the PPII helix secondary structure. The energetics of the aromatic-prolyl interactions in the system were measured, with the most favorable reaching -2.3 kcal·mol^{-1}. A related β-hairpin peptide, WKWK, does not show affinity for oligoproline helices. This subtlety demonstrates the importance of structure when examining aromatic-prolyl interactions in peptide model systems. Due to the structural similarities between the trpzip peptide family and natural PRM-binding domains, the disulfide exchange system described herein could be used to further understanding of how natural recognition domains bind to their ligand core motifs.

D. Experimental Section

i. Peptide synthesis and purification

Peptides were typically synthesized by standard automated SPPS using a Thuramed tetras synthesizer. Fmoc-protected amino acids were used along with a CLEAR-Amide resin from Peptides International, Inc. Amino acid residues were activated with HBTU, HOBt, and DIPEA in DMF. Amino acids were deprotected twice with 2% DBU and 2% piperidine in DMF for 15 minutes each step. Amino acids were coupled using double coupling cycles of 30-60 minutes each. The N-terminus of each peptide was acetylated using 5% acetic anhydride and 6% lutidine in DMF for 30 minutes. Cleavage of the peptides from the resin was performed in 95.0% TFA, 2.5% water, and 2.5% TIPS. TFA was evaporated with a stream of nitrogen and diethyl ether was added to precipitate the cleavage products. The peptides were extracted with water or collected as solids by centrifugation and lyophilized to dryness. Peptides were purified by RP-HPLC using an Atlantis Prep OBD dC-18 semi-preparative column, with a gradient of 0-100% solvent B over 40 minutes, where solvent A

was 95:5 water:ACN, 0.1% TFA, and solvent B was 95:5 ACN:water, 0.1% TFA. Purified samples were lyophilized and the peptide sequence was confirmed by ESI-MS.

ii. Circular dichroism measurements

CD measurements were performed on an Aviv 62DS Circular Dichroism Spectrometer, using quartz cells with a path length of 0.1 cm. CD data was obtained for the trpzip and WKWK peptides at 50 μM concentrations in 10 mM sodium phosphate buffer, 2 mM TCEP, pH 7. Wavelength scans were performed in triplicate and averaged. Scans were typically performed from 260-190 nm, although spectra for trpzip were collected up to 330 nm at times. CD data was obtained for the oligoproline sequences at 100 μM concentration in 10 mM sodium phosphate buffer (no TCEP), pH 7. All spectra were recorded at 25ºC (298 K), and a 30 second averaging time was used for all scans. All scans were corrected by subtracting the spectrum of the respective buffer used in the experiment. The results of the CD experiments are reported as mean molar residue ellipticity [θ] with the units of degrees·cm^2·dmol^{-1} and were calculated using Equation 5:

$$[\theta] = \frac{(\theta_{obs})}{10 \cdot l \cdot c \cdot n} \qquad Equation\ 5$$

where θ_{obs} is the observed ellipticity in millidegrees, c is concentration in mol·L^{-1}, l is the path length in cm, and n is the number of amino acid residues in the peptide.

iii. Disulfide exchange experiments

Disulfide exchange experiments were typically initiated by mixing an oligoproline peptide (CW-Pro5, CW-Pro6, CW-Pro7, C-Pro7-W, or WC-Pro7) with either the trpzip or WKWK peptide in approximately equal proportions in 10 mM sodium phosphate buffer (pH 8.1-8.5) with no effort made to exclude oxygen. The total peptide concnetrations were

typically 250 μM. Peptide concentrations were determined prior to sample preparation by recording the absorbance of Trp at 280 nm (ε = 5690 M^{-1} cm^{-1}) in 5 M GndHCl dilutions. LC-MS analysis of the exchange reactions was accomplished using an Agilent Series 1200 instrument, equipped with an Agilent Zorbax Eclipse XDB-C18 column (4.6 x 50 mm, 1.8 μm). Various gradient methods were employed (water/methanol containing 0.2% formic acid), ranging from 15-30 minutes at a flow rates of 0.8-1.0 mL/min (column temperature, 35ºC). The injection volumes were typically 2.0-4.0 μL for both 100 μM and 250 μM exchange reactions. The reactions were monitored at 280 nm, and integrated areas were adjusted for the number of Trp residues. Equilibrium constants (K_{EQ}), reported in Table 2 and Table 3, were calculated using Equation 1:

$$K_{EQ} = \frac{[Heterodimer]^2}{[Pro\ Homodimer][Hairpin\ Homodimer]} \qquad Equation\ 1$$

where [Heterodimer] is the equilibrium concentration of the heterodimer containing both an oligoproline peptide and a β-hairpin peptide, [Pro Homodimer] is the equilibrium concentration of the homodimer containing two oligoproline peptides, and [Hairpin Homodimer] is the equilibrium concentration of the homodimer containing two β-hairpin peptides. The values for $\Delta G_{[HP]}$, $\Delta G^*_{[HP]}$, and $\Delta G^{**}_{[HP]}$ reported in Table 7.2 and Table 7.3 were calculated using Equation 2, Equation 3, and Equation 4:

$$\Delta G_{[HP]} = -RTLn\left(\frac{K_{EQ}}{4}\right) \qquad Equation\ 2$$

$$\Delta G *_{[HP]} = -RTLn\left(\frac{K_{EQ}}{1.3}\right) \quad Equation\ 3$$

$$\Delta G **_{[HP]} = -RTLn\left(\frac{K_{EQ}}{14}\right) \quad Equation\ 4$$

where K_{EQ} is the equilibrium constant calculated using Equation 1, R is the molar gas constant in units of cal·mol^{-1}·K^{-1} (1.986), and T is the temperature in Kelvin (298.15). A sample set of data and provided in Table 4. A sample calculation of $\Delta G_{[HP]}$ for the exchange experiment with CWGG and the trpzip β-hairpin is presented below.

Table 7.4. Sample data set for trpzip/CWGG exchange experiment

	Retention Time (min)	**Area (mAU*sec)**	**Number of Trp Residues**	**Corrected Area**
trpzip Homodimer	14.415	328	8	41
trpzip-CWGG Heterodimer	15.872	255	5	51
CWGG Homodimer	19.902	109	2	55

$$K_{EQ} = \frac{[51]^2}{[55][41]} \quad Equation\ 1b$$

$$K_{EQ} = 1.15 \quad Equation\ 1c$$

$$K_{EQ}(average) = 1.3\ (\pm 0.15) \quad Equation\ 1d$$

The values reported in Table 2 and Table 3 are the average for many trials with error describing the absolute range of values observed, not the standard deviation of the set (Equation 1d).

$$\Delta G_{[HP]} = -RTLn\left(\frac{1.3}{4}\right) \quad Equation\ 2b$$

$$\Delta G_{[HP]} = -(0.5921) Ln\left(\frac{1.3}{4}\right) \qquad Equation\ 2c$$

$$\Delta G_{[HP]} = 0.67\ (\pm 0.07)\ kcal \cdot mol^{-1} \qquad Equation\ 2c$$

iv. Sample chromatograms

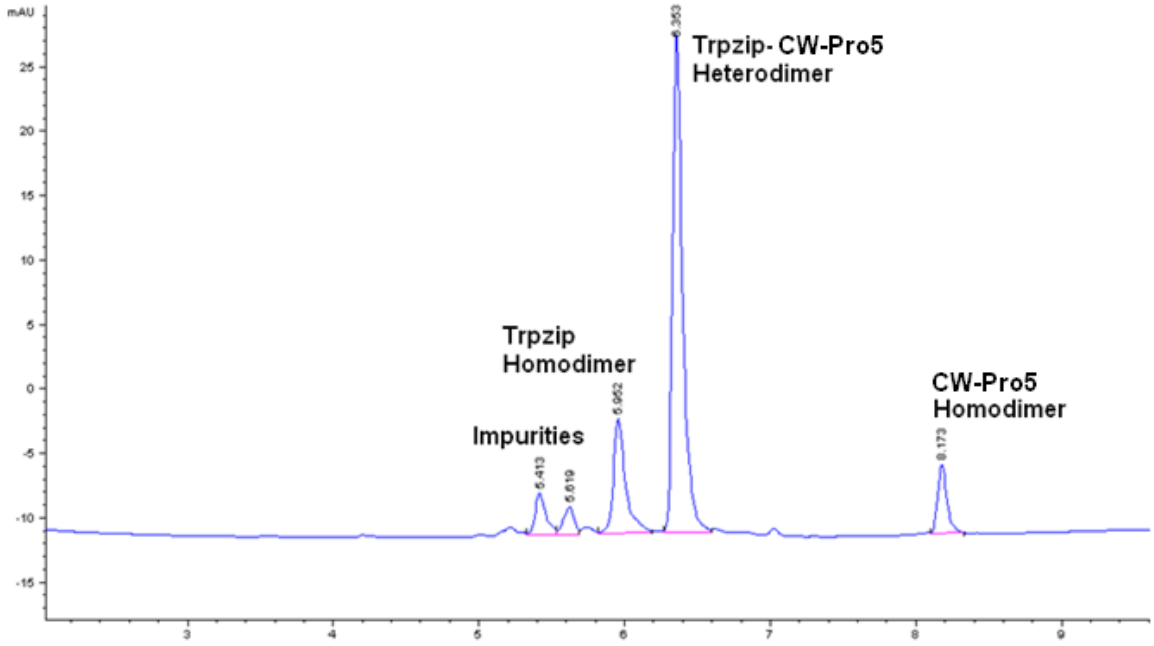

Figure 7.11 Sample chromatogram at 280 nm for the disulfide exchange experiment with the trpzip β-hairpin and the CW-Pro5 peptide.

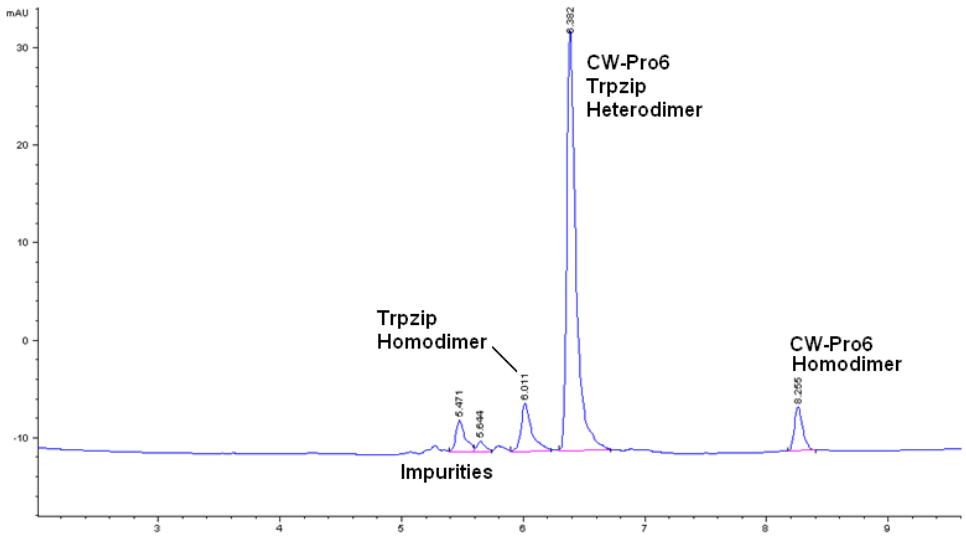

Figure 7.12 Sample chromatogram at 280 nm for the disulfide exchange experiment with the trpzip β-hairpin and the CW-Pro6 peptide.

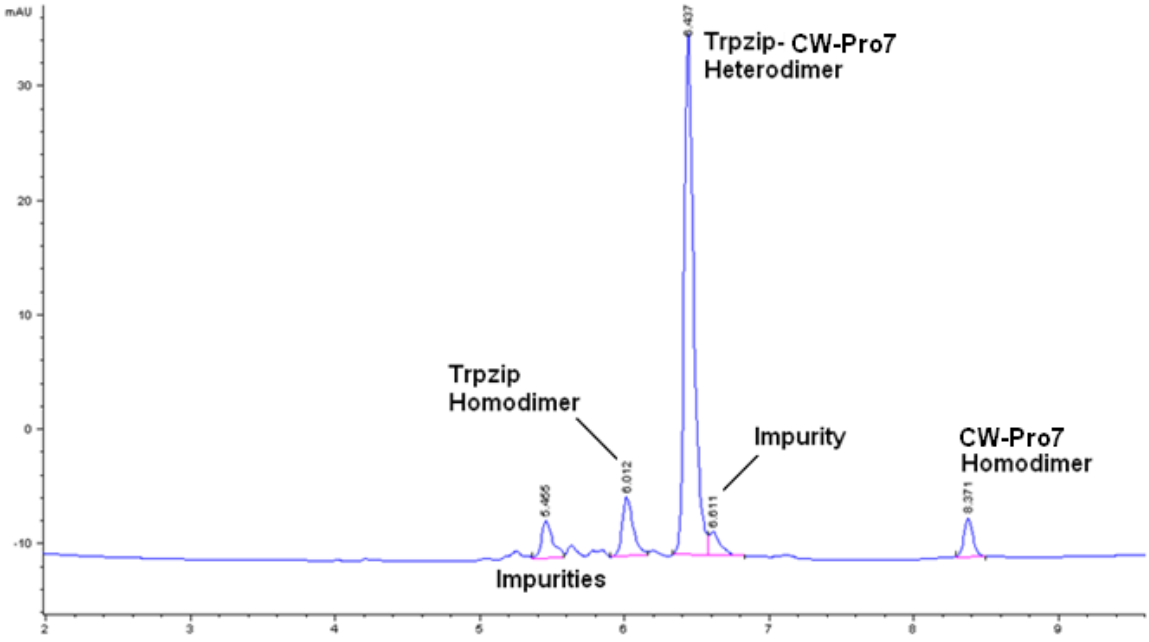

Figure 7.13 Sample chromatogram at 280 nm for the disulfide exchange experiment with the trpzip β-hairpin and the CW-Pro7 peptide.

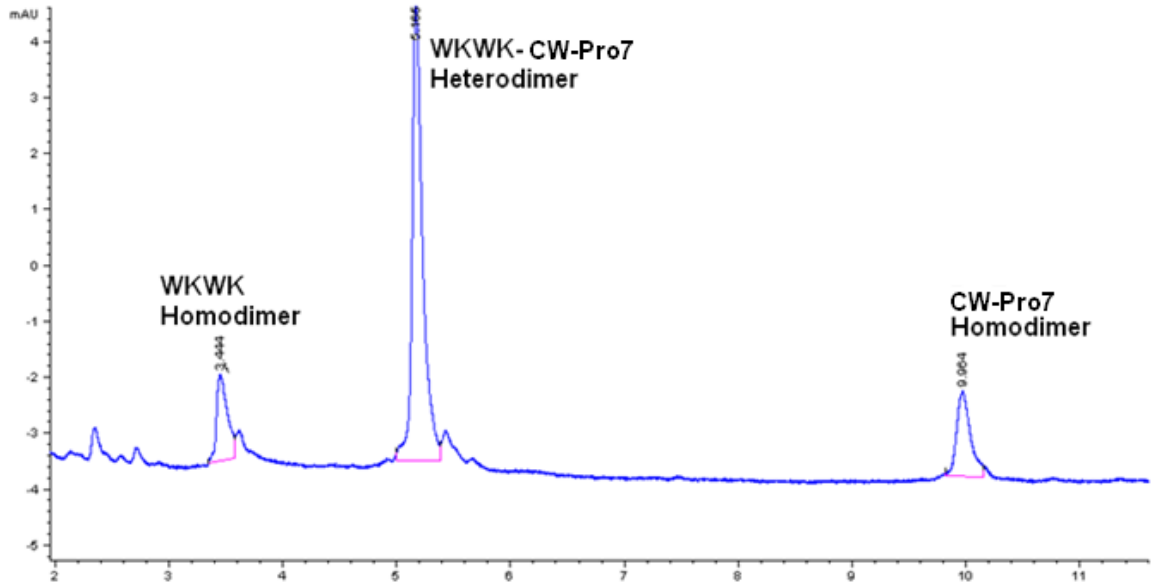

Figure 7.14 Sample chromatogram at 280 nm for the disulfide exchange experiment with the WKWK β-hairpin and the CW-Pro7 peptide.

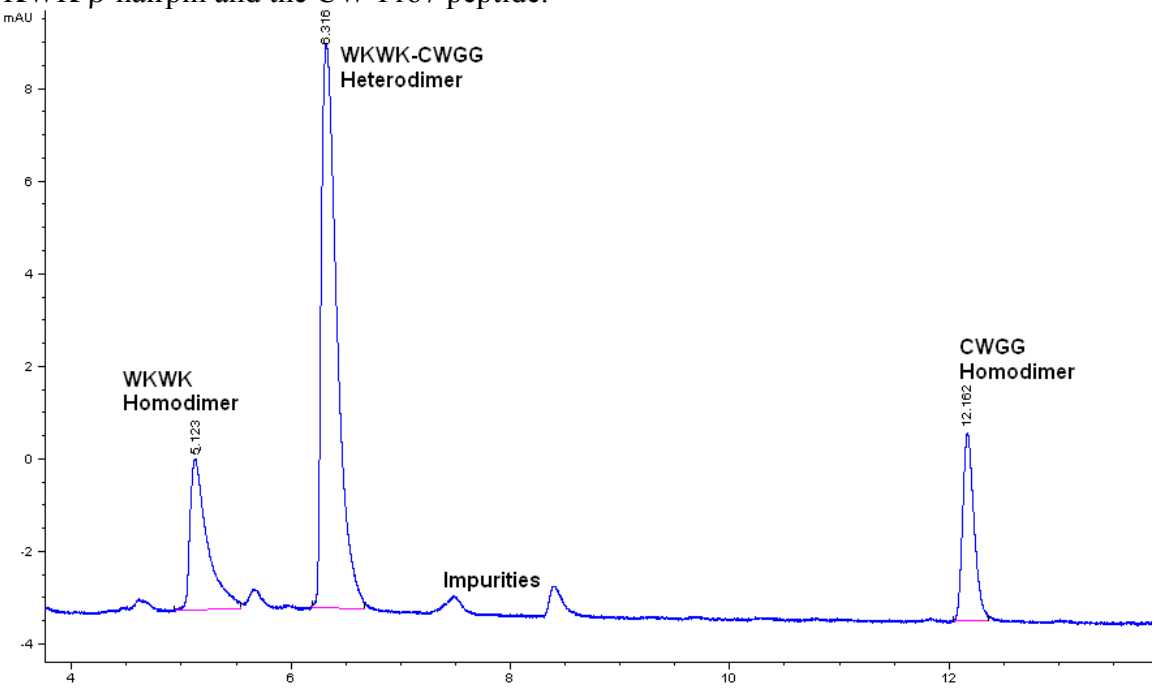

Figure 7.15 Sample chromatogram at 280 nm for the disulfide exchange experiment with the WKWK β-hairpin and the CWGG linker sequence.

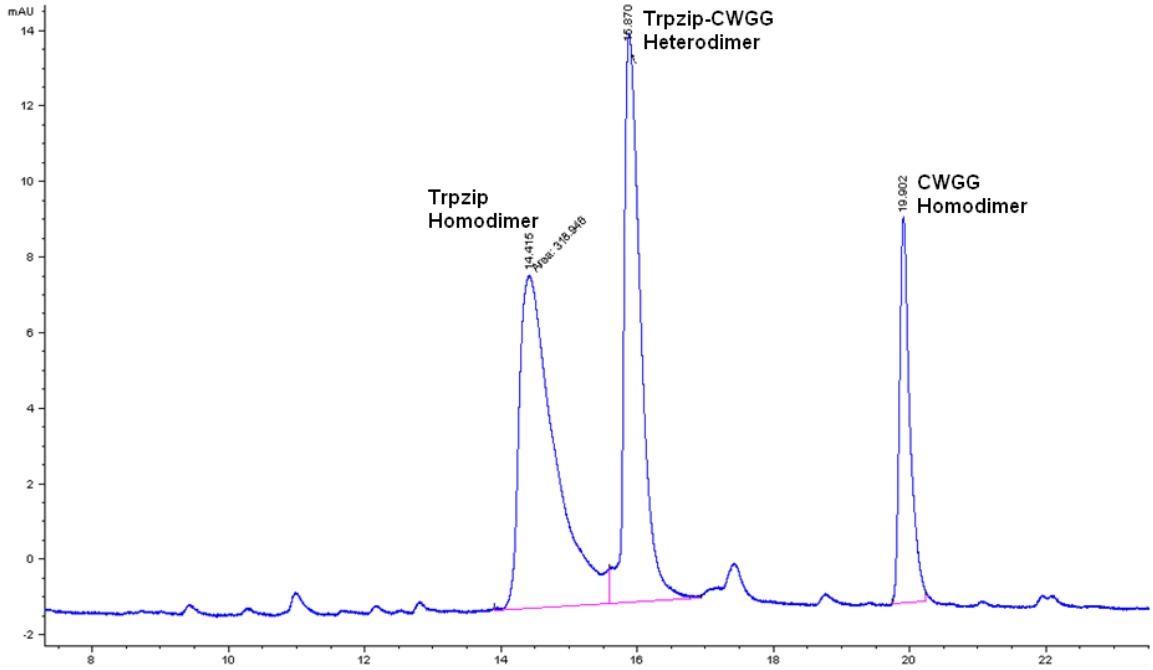

Figure 7.16 Sample chromatogram at 280 nm for the disulfide exchange experiment with the trpzip β-hairpin and the CWGG linker sequence.

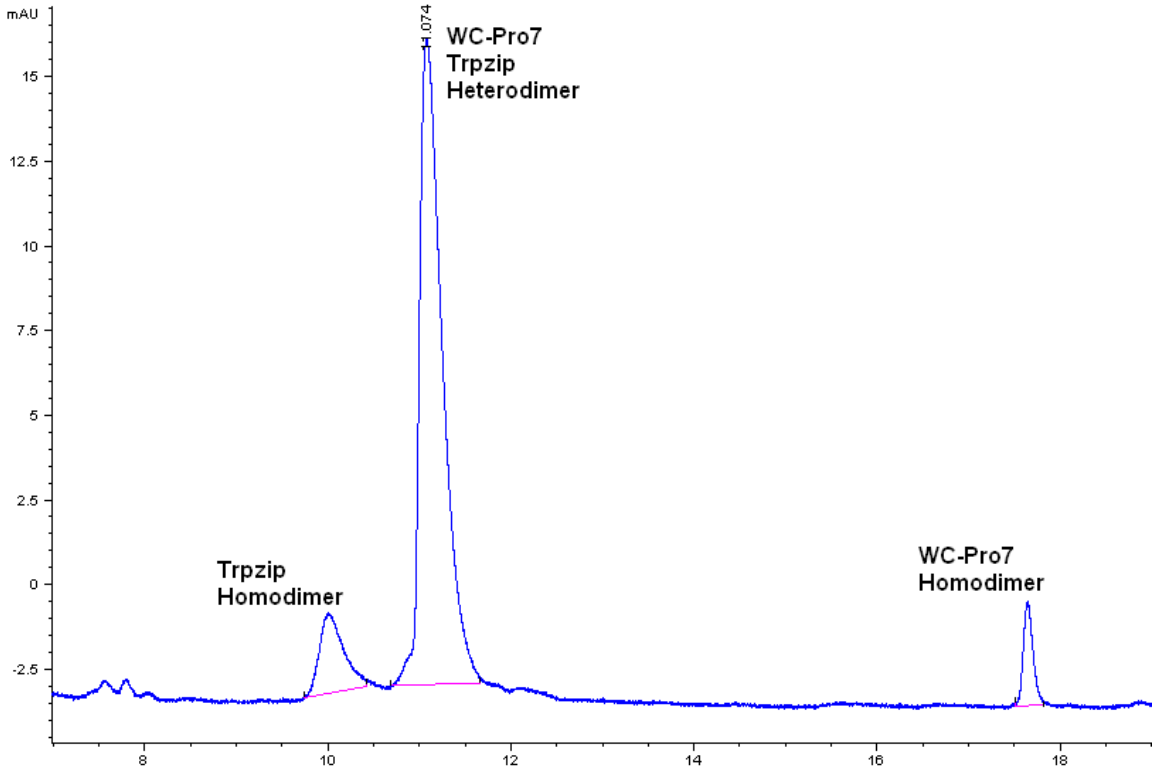

Figure 7.17 Sample chromatogram at 280 nm for the disulfide exchange experiment with the trpzip β-hairpin and the WC-Pro7 peptide.

v. TOCSY and NOESY NMR experiments

TOCSY and NOESY NMR experiments were performed by Jes Park (Waters laboratory) using either a Varian Inova 600 MHz or Bruker Ultrashield 600 MHz Plus spectrometer. 2D TOCSY data were acquired between 1-5 mM peptide concentration in 50 mM NaOAc and 0.5 mM DSS in deuterium oxide or 90% H_2O and 10% D_2O, adjusted in pD 4.0 with AcOD. TOCSY spectra were acquiered using 32 scans per increment and 128 increments in the indirect dimension. 2D NOESY data were acquired using 64 scans per increment and 256 scans in the indirect dimension. Solvent suppression was applied with the Varian or Bruker software. Peptide proton assignments of the TrpZip and TrpZip-Pro7 peptides were determined using standard methods.[19]

References

[1](a) Madison, V. *Biopolymers* **1977**, *16*, 2671-2692.

[2](a) Pal, D.; Chakrabarti, P. *J. Mol. Biol.* **1999**, *294*, 271-288. (b) Fischer, G. *Chem. Soc. Rev.* **2000**, *29*, 119-127. (c) Wedemeyer, W. J.; Welker, E.; Scheraga, H. A. *Biochemistry* **2002**, *41*, 14637-14644. (d) Meng, H. Y.; Thomas, K. M.; Lee, A. E.; Zondlo, N. J. *Biopolymers*, **2006**, *84*, 192-204. (e) Ball, L. J.; Kuhne, R.; Schneider-Mergener, J.; Oschkinat, H. *Angew. Chem., Int. Ed. Engl.* **2005**, *44*, 2852-2869. (f) Zarrinpar, A.; Bhattacharyya, R. P.; Lim, W. A. *Science's STKE* **2003**, *2003*, RE8.

[3](a) Yu, H. T.; Chen, J. K.; Feng, S. B.; Dalgarno, D. C.; Brauer, A. W.; Schreiber, S. L. *Cell* **1994**, *76*, 933-945. (b) Sparks, A. B.; Rider, J. E.; Hoffman, N. G.; Fowlkes, D. M.; Quilliam, L. A.; Kay, B. K. *Proc. Natl. Acad. Sci. U.S.A.* **1996**, *93*, 1540-1544. (c) Hoffman, N. G.; Sparks, A. B.; Carter, J. M.; Kay, B. K. *Molecular Diversity* **1996**, *2*, 5-12.

[4](a) Chen, H. I.; Sudol, M. *Proc. Natl. Acad. Sci. U.S.A.* **1995**, *92*, 7819-7823. (b) Sudol, M.; Chen, H. I.; Bougeret, C.; Einbond, A.; Bork, P. *Febs Lett.* **1995**, *369*, 67-71. (c) Macias, M. J.; Hyvonen, M.; Baraldi, E.; Schultz, J.; Sudol, M.; Saraste, M.; Oschkinat, H. *Nature* **1996**, *382*, 646-649.

[5](a) Ball, L. J.; Jarchau, T.; Oschkinat, H.; Walter, U. *Febs Lett.* **2002**, *513*, 45-52. (b) Tu, J. C.; Xiao, B.; Yuan, J. P.; Lanahan, A. A.; Leoffert, K.; Li, M.; Linden, D. J.; Worley, P. F. *Neuron* **1998**, *21*, 717-726. (c) Reinhard, M.; Jouvenal, K.; Tripier, D.; Walter, U. *Proc. Natl. Acad. Sci. U.S.A.* **1995**, *92*, 7956-7960. (d) Reinhard, M.; Rudiger, M.; Jockusch, B. M.; Walter, U. *FEBS Lett.* **1996**, *399*, 103-107. (e) Ball, L. J.; Kuhne, R.; Hoffmann, B.; Hafner, A.; Schmieder, P.; Volkmer-Engert, R.; Hof, M.; Wahl, M.; Schneider-Mergener, J.; Walter, U.; Oschkinat, H.; Jarchau, T. *EMBO J.* **2000**, *19*, 4903-4914. (f) Zettl, M.; Way, M. *Curr. Biol.* **2002**, *12*, 1617-1622.

[6](a) Nishizawa, K.; Freund, C.; Li, J.; Wagner, G.; Reinherz, E. L. *Proc. Natl. Acad. Sci. U.S.A.* **1998**, *95*, 14897-14902. (b) Freund, C.; Dotsch, V.; Nishizawa, K.; Reinherz, E. L.; Wagner, G. *Nat. Struct. Biol.* **1999**, *6*, 656-660. (c) Freund, C.; Kuhne, R.; Yang, H.; Park, S.; Reinherz, E. L.; Wagner, G. *EMBO J.* **2002**, *21*, 5985-5995.

[7](a) Pornillos, O.; Alam, S. L.; Davis, D. R.; Sundquist, W. I. *Nat. Struct. Biol.* **2002**, *9*, 812-817. (b) Pornillos, O.; Alam, S. L.; Rich, R. L.; Myszka, D. G.; Davis, D. R.; Sundquist, W. I. *EMBO J.* **2002**, *21*, 2397-2406.

[8](a) Holt, M. R.; Koffer, A. *Trends Cell Biol.* **2001**, *11*, 38-46. (b) Mahoney, N. M.; Janmey, P. A.; Almo, S. C. *Nat. Struct. Biol.* **1997**, *4*, 953-960. (c) Schutt, C. E.; Myslik, J. C.; Rozycki, M. D.; Goonesekere, N. C.; Lindberg, U. *Nature* **1993**, *365*, 810-816.

[9](a) Bhattacharyya, R.; Chakrabarti, P. *J. Mol. Biol.* **2003**, *331*, 925-940. (b) Nakagawa, Y.; Irie, K.; Yanagita, R. C.; Ohigashi, H.; Tsuda, K.-I. *J. Am. Chem. Soc.* **2005**, *127*, 5746-5747.

(c) Brandl, M.; Weiss, M. S.; Jabs, A.; Sühnel, J.; Hilgenfeld, R. *J. Mol. Biol.* **2001**, *307*, 357-377.

[10]Thomas, K. M. Naduthambi, D. Zondlo, N. J. *J. Am. Chem. Soc.* **2006**, *128*, 2216-2217.

[11](a) Cochran, A. G.; Skelton, N. J.; Starovasnik, M. A. *Proc. Natl. Acad. Sci. U.S.A.* **2001**, *98*, 5578-5583. (b) Cochran, A. G.; Tong, R. T.; Starovasnik, M. A.; Park, E. J.; McDowell, R. S.; Theaker, J. E.; Skelton, N. J. *J. Am. Chem. Soc.* **2001**, *123*, 625-632. (c) Russell, S. J.; Cochran, A. G. *J. Am. Chem. Soc.* **2001**, *122*, 12600-12601.

[12](a) Lumb, K. J.; Kim, P. S. *Biochemistry* **1995**, *34*, 8642-8648. (b) Oakley, M. G.; Kim, P. S. *Biochemistry* **1998**, *37*, 12603-12610. (c) Lai, J. R.; Fisk, J. D.; Weisblum, B.; Gellman, S. H. *J. Am. Chem. Soc.* **2004**, *126*, 10514-10515. (d) Hadley, E. B.; Witek, A. M.; Freire, F.; Peoples, A. J.; Gellman, S. H. *Angew. Chem. Int. Ed.* **2007**, *46*, 7056-7059. (e) Woll, M. G.; Gellman, S. H. *J. Am. Chem. Soc.* **2004**, *126*, 11172-4. (f) Hadley, E. B.; Gellman, S. H. *J. Am. Chem. Soc.* **2006**, *128*, 16444-16445. (g) Woll, M. G.; Hadley, E. B.; Mecozzi, S.; Gellman, S. H. *J. Am. Chem. Soc.* **2006**, *128*, 15932-15933.

[13](a) Stanger, H. E.; Gellman, S. H. *J. Am. Chem. Soc.* **1998**, *120*, 4236-4237. (b) Syud, F. A.; Espinosa, J. F.; Gellman, S. H. *J. Am. Chem. Soc.* **1999**, *121*, 11577-11578. (c) Espinosa, J. F.; Syud, F. A.; Gellman, S. H. *Protein Sci.* **2002**, *11*, 1492-1505.

[14](a) Butterfield, S. M.; Waters, M. L. *J. Am. Chem. Soc.* **2003**, *125*, 9580-9581. (b) Butterfield, S. M.; Cooper, W. J.; Waters, M. L. *J. Am. Chem. Soc.* **2005**, *127*, 24-25. (c) Butterfield, S. M.; Sweeney, M. M.; Waters, M. L. *J. Org. Chem.* **2005**, *70*, 1105-1114. (d) Cooper, W. J.; Waters, M. L. *Org. Lett.* **2005**, *7*, 3825-3828.

[15]Hughes, R. M., Ph.D. dissertation, University of North Carolina at Chapel Hill, 2007.

[16](a) Bovey, F. A.; Hood, F. P. *Biopolymers* **1967**, *5*, 325-326. (b) Chellgren, B. W.; Creamer, T. P. *Biochemistry* **2004**, *43*, 5864-5869. (c) Kuemin, M.; Schweizer, S.; Ochsenfeld, C.; Wennemers, H. *J. Am. Chem. Soc.* **2009**, *131*, 15474-15482. (d) Brahms, S.; Brahms, J. *J. Mol. Biol.* **1980**, *138*, 149-178.

[17]Grishina, I. B.; Woody, R. W. *Faraday Discuss.* **1994**, 245-262.

[18](a) Greenfield, N. J. *Nature Protocols* **2006**, *1*, 2876-2890. (b) Woody, R. W. *Methods Enzymol.* **1995**, *246*, 34-71.

[19]Wuthrich, K. (1986) NMR of Proteins and Nucleic Acids, Wiley-Interscience, New York.

BIBLIOGRAPHY

Adams, J. A., Kinetic and catalytic mechanisms of protein kinanses. *Chem. Rev.* **2001**, *101*, 2271-2290.

Alstrum-Acevedo, J. H.; Brennaman, M. K.; Meyer, T. J., Chemical approaches to artificial synthesis. 2. *Inorg. Chem.* **2005**, *44*, 6802-6827.

Ardo, S.; Meyer, G. J., Photodriven heterogeneous charge transfer with transition-metal compounds anchored to TiO_2 semiconductor surfaces. *Chem. Soc. Rev.* **2009**, *38*, 115-164.

Bae, E.; Choi, W., Effect of the anchoring group (carboxylate vs phosphonate) in Ru-complex-sensitized TiO_2 on hydrogen production under visible light. *J. Phys. Chem. B.* **2006**, *110*, 14792-14799.

Balducci, E.; Bellucci, L.; Petricci, E.; Taddei, M.; Tafi, A., Microwave-assisted intramolecular Huisgen cycloaddition of azido alkynes derived from a-amino acids. *J. Org. Chem.* **2009**, *74*, 1314-1321.

Ball, L. J.; Jarchau, T.; Oschkinat, H.; Walter, U., EVH1 domains: structure, function, and interactions. *Febs Lett.* **2002**, *513*, 45-52.

Ball, L. J.; Kuhne, R.; Hoffmann, B.; Hafner, A.; Schmieder, P.; Volkmer-Engert, R.; Hof, M.; Wahl, M.; Schneider-Mergener, J.; Walter, U.; Oschkinat, H.; Jarchau, T., Dual epitope recognition by the VASP EVH1 domain modulates polyproline ligand specificity and binding affinity. *EMBO J.* **2000**, *19*, 4903-14.

Ball, L. J.; Kuhne, R.; Schneider-Mergener, J.; Oschkinat, H., Recognition of proline-rich motifs by protein-protein-interaction domains. *Angew. Chem., Int. Ed.* **2005**, *44*, 2852-2869.

Bates, B. C.; Kundzewicz, Z. W.; Wu, S.; Palutikof, J. P. *Climate Change and Water. Technical Paper of the Intergovernmental Panel on Climate Change*, ed., IPCC Secretariat, Geneva, 210pp.

Bayly, C. I.; Cieplak, P.; Cornell, W. D.; Kollman, P. A., A well-behaved electrostatic potential based method using charge restraints for deriving atomic charges: The RESP model. *J. Phys. Chem.* **1993**, *97,* 10269–10280.

Bhattacharyya, R.; Chakrabarti, P., Stereospecific interactions of proline residues in protein structure and complexes. *J. Mol. Biol.* **2003**, *331*, 925-940.

Bovey, F. A.; Hood, F. P., Circular dichroism spectrum of poly-L-lysine. *Biopolymers* **1967**, *5*, 325-326.

Brahms, S.; Brahms, J., Determination of protein secondart structure in solution by vacuum ultraviolet circular dichroism. *J. Mol. Biol.* **1980**, *138*, 149-178.

Brandl, M.; Weiss, M. S.; Jabs, A.; Sühnel, J.; Hilgenfeld, R., C-h···π-interactions in proteins. *J. Mol. Biol.* **2001**, *307*, 357-377.

Brandt, P.; Norrby, T.; Akermark, B.; Norrby, P.-O., Molecular mechanics (MM3*) parameters for ruthenium(II)-polypyridyl complexes. *Inorg. Chem.* **1998**, *37*, 4120–4127.

Brandt, W. W.; Dwyer, F. P.; Gyarfas, E. D., Chelate complexes of 1,10-phenanroline and related compounds. *Chem. Rev.* **1954**, *54*, 959-1017.

Brandt, W. W.; Dwyer, F. P.; Gyarfas, E. D., Chelate complexes of 1,10-phenanroline and related compounds. *Chem. Rev.* **1954**, *54*, 959-1017.

Butterfield, S. M.; Cooper, W. J.; Waters, M. L., Minimalist protein design: a β-hairpin peptide that binds ssDNA. *J. Am. Chem. Soc.* **2005**, *127*, 24-25.

Butterfield, S. M.; Sweeney, M. M.; Waters, M. L., The recognition of nucleotides with model b-hairpin receptors: investigation of critical contacts and nucleotide selectivity. *J. Org. Chem.* **2005**, *70*, 1105-1114.

Butterfield, S. M.; Waters, M. L., A designed β-hairpin peptide for molecular recognition of ATP in water. *J. Am. Chem. Soc.* **2003**, *125*, 9580-9851.

Caramori, S.; Cristino, V.; Argazzi, R.; Meda, L.; Bignozzi, C. A., Photoelectrochemical behavior of sensitized TiO_2 photoanodes in an aqueous environment: application to hydrogen production. *Inorg. Chem.* **2010**, *49*, 3320-3328.

Caspar, J. V.; Meyer, T. J., Photochemistry of $Ru(bpy)_3^{2+}$. Solvent effects. *J. Am. Chem. Soc.* **1983**, *105*, 5583-5590.

Chan, T. R.; Hilgraf, R.; Sharpless, K. B.; Fokin, V. V., Polytriazoles as copper(I)-stabilizing ligands in catalysis. *Org. Lett.* **2004**, *6*, 2853-2855.

Chellgren, B. W.; Creamer, T. P., Short sequences of non-proline residues can adopt polyproline II helical conformations. *Biochemistry* **2004**, *43*, 5864-5869.

Chen, H. I.; Sudol, M., The WW domain of Yes-associated protein binds a proline-rich ligand that differs from the consensus established for the Src homology 3-binding modules. *Proc. Natl. Acad. Sci. U.S.A.* **1995**, *92*, 7819-7823.

Chen, Y.-H.; Yang, J. T.; Chau, K. H., Determination of the helix and β form of proteins in aqueous solution by circular dichroism. *Biochemistry* **1974**, *13*, 3350-3359.

Cherezov, V.; Clogston, J.; Papiz, M. Z.; Caffrey, M., Room to move: crystallizing membrane proteins in swollen lipidic mesophases. *J. Mol. Biol.* **2006**, *357*, 1605-1618.

Clark, W. D. K.; Sutin, N., Spectral sensitization of n-type TiO_2 electrodes by polypyridineruthenium(II) complexes. *J. Am. Chem. Soc.* **1977**, *66*, 4276-4282.

Cochran, A. G.; Skelton, N. J.; Starovasnik, M. A., Tryptophan zippers: stable, monomeric β-hairpins. *Proc. Natl. Acad. Sci. U.S.A.* **2001**, *98*, 5578-5583.

Cochran, A. G.; Tong, R. T.; Starovasnik, M. A.; Park, E. J.; McDowell, R. S.; Theaker, J. E.; Skelton, N. J., A minimal peptide scaffold for β-turn display: optimizing a strand position in disulfide-cyclized β-hairpins. *J. Am. Chem. Soc.* **2001**, *123*, 625-632.

Cooper, W. J.; Waters, M. L., Turn residues in β-hairpin peptides as points for covalent modification. *Org. Lett.* **2005**, *7*, 3825-3828.

Coury, J. E.; Anderson, J. R.; MsFail-Isom, L.; Williams, L. D.; Bottomley, L. A., Scanning force microscopy of small liagnd-nucleic acid complexes: tris(*o*-phenanthroline)ruthenium(II) as a test for a new assay. *J. Am. Chem. Soc.* **1997**, *119*, 3792-3796.

Creutz, C.; Chou, M.; Netzel, T. L.; Okumura, M.; Sutin, N., Lifetimes, spectra, and quenching of the excited states of polypyridine complexes of iron(II), ruthenium(II), and osmium(II). *J. Am. Chem. Soc.* **1980**, *102*, 1309-1319.

Crick, F. H. C., Is α-keratin a coiled coil? *Nature* **1952**, *170*, 882-883.

Damrauer, N. H.; Cerullo, G.; Yeh, A.; Boussie, T. R.; Shank, C. V.; McCusker, J. K., Femtosecond dynamics of excite-state evolution in $[Ru(bpy)_3]^{2+}$. *Science* **1997**, *275*, 54-57.

De Francesco, R.; Pastore, A.; Vecchio, G.; Cortese, R., Circular dichroism study on the conformational stability of the dimerization domain of transcription factor LFB1. *Biochemistry* **1991**, *30*, 143-147.

de Graaf, A. J.; Kooijman, M.; Hennink, W. E.; Mastrobattista, E., Nonnatural amino acids for site-specific protein conjugation. *Bioconjugate Chem.* **2009**, *20*, 1281-1295.

DeGrado, W. F.; Summa, C. M.; Pavone, V.; Nastri, F.; Lombardi, A., De novo design and structural characterization of proteins and metalloproteins. *Annu. Rev. Biochem.* **1999**, *68*, 779-819.

Demas, J. N.; Crosby, G. A., Quantum efficiencies on transition metal complexes. II. Charge-transfer luminescence. *J. Am. Chem. Soc.* **1971**, *93*, 2841-2847.

Desilvestro, J.; Grätzel, M.; Kavan, L.; Moser, J., Highly efficient sensitization if titanium dioxide. *J. Am. Chem. Soc.* **1985**, *107*, 2988-2990.

Dexter, D. L., A theory of sensitized luminescence in solids. *J. Chem. Phys.* **1953**, *21*, 836-850.

Donnelly, P. S.; Zanatta, S. D.; Zammit, S. C.; White, J. M. Williams, S. J., 'Click' cycloaddition catalyst: copper(I) and copper(II) tris(triazolylmethyl)amine complexes. *Chem. Commun.* **2008**, 2459-2461.

Dupray, L. M.; Devenney, M.; Striplin, D. R.; Meyer, T. J., An antenna polymer for visible energy transfer. *J. Am. Chem. Soc.* **1997**, *119*, 10243-10244.

Dupray, L. M.; Meyer, T. J., Synthesis and characterization of amide-derivatized, polypyridyl-based metallopolymers. *Inorg. Chem.* **1996**, *35*, 6299-6307.

Espinosa, J. F.; Syud, F. A.; Gellman, S. H., Analysis of the factors that stabilize a designed two-stranded antiparallel β-sheet. *Protein Sci.* **2002**, *11*, 1492-1505.

Fedorova, A.; Chaudhari, A.; Ogawa, M. Y., Photoinduced electron-transfer along α-helical and coiled-coil metalloproteins. *J. Am. Chem. Soc.* **2003**, *125*, 357-362.

Fedorova, A.; Ogawa, M. Y., Site-specific modification of de novo designed coiled-coil polypeptides with inorganic redox complexes. *Bioconjugate Chem.* **2002**, *13*, 150-154.

Ferreira, K. N.; Iverson, T. M.; Maghlaoui, K.; Barber, J.; Iwata, S., Architecture of the photosynthetic oxygen-evolving center. *Science*, **2004**, *303*, 1831-1838.

Fischer, G., Chemical aspects of peptide bond isomerisation. *Chem. Soc. Rev.* **2000**, *29*, 119-127.

Fleming, C. N.; Maxwell, K. A.; DeSimone, J. M.; Meyer, T. J.; Papanikolas, J. M., Ultrafast excited-state energy migration dynamics in an efficient light-harvesting antenna polymer based on Ru(II) and Os(II) polypyridyl complexes. *J. Am. Chem. Soc.* **2001**, *123*, 10336-10347.

Förster, T., Transfer mechanism of electronic excitation. *Discuss. Faraday Soc.* **1959**, *27*, 7-17.

Franke, R.; Doll, C.; Eichler, J., Peptide ligation through click chemistry for the generation of assembled and scaffolded peptides. *Tetrahedron Lett.* **2005**, *46*, 4479-4482.

Freund, C.; Dotsch, V.; Nishizawa, K.; Reinherz, E. L.; Wagner, G., The GYF domain is a novel structural fold that is involved in lymphoid signaling through proline-rich sequences. *Nat. Struct. Biol.* **1999**, *6*, 656-60.

Freund, C.; Kuhne, R.; Yang, H.; Park, S.; Reinherz, E. L.; Wagner, G., Dynamic interaction of CD2 with the GYF and the SH3 domain of compartmentalized effector molecules. *EMBO J.* **2002**, *21*, 5985-95.

Friesen, D. A.; Kajita, T.; Danielson, E.; Meyer, T. J., Preparation and photophysical properties of amide-linked, polypyridylruthenium-derivatized polystyrene. *Inorg. Chem.* **1998**, *37*, 2756-2762.

Furue, M.; Kinoshita, S.; Kushida, T., Intramolecular energy transfer in covalently linked ruthenium(II)/osmium(II) binuclear complex. $Ru(II)bpy_2Mebpy\text{-}CH_2CH(OH)CH_2\text{-}MebpyOs(II)bpy_2$. *Chem. Lett.* **1987**, 2355-2358.

Furue, M.; Yoshidzumi, T.; Kinoshita, S.; Kushida, T.; Nozakura, S.; Kamachi, M., Intramolecular energy transfer in covalently linked polypyridine ruthenium(II)/osmium(II) binuclear complexes. $Ru(II)(bpy)_2Mebpy\text{-}(CH_2)_n\text{-}MebpyOs(II)(bpy)_2$ (n=2,3,5, and 7). *Bull. Chem. Soc. Jpn.* **1991**, *64*, 1632-1640.

Galoppini, E., Linkers for anchoring sensitizers to semiconductor nanoparticles. *Coord. Chem. Rev.* **2004**, *248*, 1283-1297.

Geisser, B.; Ponce, A.; Alsfasser, R., pH-Dependent excited-state dynamics of $[Ru(bpy)_3]^{2+}$-modified amino acids: effects of an amide linkage and remote functional groups. *Inorg. Chem.* **1999**, *38*, 2030-2037.

Gertler, G.; Fleminger, G.; Rapaport, H., Characterizing the adsorption of peptides to TiO_2 in aqueous solutions by liquid chromatography. *Langmuir* **2010**, *26*, 6457-6463.

Gholamkhass, B.; Nazaki, K.; Ohno, T., Evaluation of electronic interaction matrix elements for photoinduced electron transfer processes within mixed-valence complexes. *J. Phys. Chem. B* **1997**, *101*, 9010-9021.

Gillaizeau-Gauthier, I.; Odobel, F.; Alebbi, M.; Argazzi, R.; Costa, E.; Bignozzi, C. A.; Qu, P.; Meyer, G. J., Phosphonate-based bipyridine dyes for stable photovoltaic devices. *Inorg. Chem.* **2001**, *40*, 6073-6079.

Goddard-Borger, E. D.; Stick, R. V., An efficient, inexpensive, and shelf-stable diazotransfer reagent: imidazole-1-sulfonyl azide hydrochloride. *Org. Lett.* **2007**, *9*, 3797-3800.

Goddard-Borger, E. D.; Stick, R. V. Additions and Corrections, An efficient, inexpensive, and shelf-stable diazotransfer reagent: imidazole-1-sulfonyl azide hydrochloride. *Org. Lett.* **2011**, *13*, 2514.

Gonzales, L., Jr.; Woolfson, D. N.; Alber, T., Buried polar residues and structural specificity in the GCN4 leucine zipper. *Nat. Struct. Biol.* **1996**, *3*, 1011-1018.

Greenfield, N. J., Using circular dichroism spectra to estimate protein secondary structure. *Nature Protocols* **2006**, *1*, 2876-2890.

Grishina, I. B.; Woody, R. W., Contributions of tryptophan side chains to the circular dichroism of globular proteins: exciton couplets and coupled oscillators. *Faraday Discuss.* **1994**, 245-262.

Gust, D.; Moore, T. A., Mimicking photosynthesis. *Science* **1989**, *244*, 35-41.

Gust, D.; Moore, T. A.; Moore, A. L. Mimicking photosynthetic solar energy transduction. *Acc. Chem. Res.* **2001**, *34*, 40-48.

Gust, D.; Moore, T. A.; Moore, A. L., Solar fuels via artificial photosynthesis. *Acc. Chem. Res.* **2009**, *42*, 1890-1898.

Hadley, E. B.; Gellman, S. H., An antiparallel α-helical coiled-coil model system for rapid assessment of side-chain recognition at the hydrophobic interface. *J. Am. Chem. Soc.* **2006**, *128*, 16444-16445.

Hadley, E. B.; Witek, A. M.; Freire, F.; Peoples, A. J.; Gellman, S. H. Thermodynamic analysis of β-sheet secondary structure by backbone thioester exchange. *Angew. Chem. Int. Ed.* **2007**, *46*, 7056-7059.

Harbury, P. B.; Zhang, T.; Kim, P. S.; Alber, T., A switch between two-, three-, and four-stranded coiled-coils in GCN4 leucine zipper mutants. *Science* **1993**, *262*, 1401-1407.

Hay, P. J.; Wadt, W. R., Ab initio effective core potentials for molecular calculations. Potentials for the transition metals Sc to Hg. *J. Chem. Phys.* **1985**, *82*, 270-283.

Hay, P. J.; Wadt, W. R., Ab initio effective core potentials for molecular calculations. Potentials for main group elements Na to Bi. *J. Chem. Phys.* **1985**, *82*, 284-298.

Hay, P. J.; Wadt, W. R., Ab initio effective core potentials for molecular calculations. Potentials for K to Au including the outermost core orbitals. *Chem. Phys.* **1985**, *82*, 299-310.

Hodges, R. S., De novo design of α-helical proteins: basic research to medical applications. *Biochem. Cell Biol.* **1996**, *74*, 133-154.

Hoffert, M. I.; Caldeira, K.; Jain, A. K.; Haites, E. F.; Harvey, L. D.; Potter, S. D. ; Schlesinger, M. E.; Schneider, S. H.; Watts, R. G.; Wigley, T. M.; Wuebbles, D. J., Energy implications of future stabilization of atmospheric CO_2 content. *Nature* **1998**, *395*, 881-884.

Lewis, N. S.; Nocera, D. G., Powering the planet: Chemical challenges in solar energy utilization. *Proc. Natl. Acad. Sci. U.S.A.* **2006**, *103*, 15729-15735.

Hoffman, N. G.; Sparks, A. B.; Carter, J. M.; Kay, B. K., Binding properties of SH3 peptide ligands identified from phage-displayed random peptide libraries. *Molecular Diversity* **1996**, *2*, 5-12.

Holt, M. R.; Koffer, A., Cell motility: proline-rich proteins promote protrusions. *Trends Cell Biol.* **2001**, *11*, 38-46.

Holtzer, A.; Holtzer, M. E., A statistical test of the proposition that intrahelix salt bridges constitute a significant stabilizing feature of the tropomyosin coiled-coil structure. *Macromolecules* **1987**, *20*, 671-675.

Homlin, R. E.; Tong, R. T.; Barton, J. K., Long-range triplet energy transfer between metallointercalators tethered to DNA: importance of intercalation, stacking, and distance. *J. Am. Chem. Soc.* **1998**, *120*, 9724-9725.

Hong, J.; Kharenko, O. A.; Ogawa, M. Y., Incorporating electron-transfer functionality into synthetic metalloproteins from the bottom-up. *Inorg. Chem.* **2006**, *45*, 9974-9984.

Hornak, V.; Abel, R.; Okur, A.; Strockbine, B.; Roitberg, A.; Simmerling, C., Comparison of multiple Amber force fields and development of improved protein backbone parameters. *Proteins* **2006**, *65*, 712– 725.

Hughes, R. M., Non-Covalent Interactions in Hairpin Peptides and Small Molecule Systems, Ph.D. dissertation. University of North Carolina at Chapel Hill, 2007.

Hurley, D. J.; Tor, Y., Donor/acceptor interactions in synthetically modified Ru^{II}-Os^{II} oligonucleotides. *J. Am. Chem. Soc.* **2002**, *124*, 13231-13241.

Hurley, D. J.; Tor, Y., Metal-containing oligonucleotides: Solid-phase synthesis and luminescence properties. *J. Am. Chem. Soc.* **1998**, *120*, 2194-2195.

Hurley, D. J.; Tor, Y., Ru(II) and Os(II) nucleosides and oligonucleotides: synthesis and properties. *J. Am. Chem. Soc.* **2002**, *124*, 3749-3762.

Isaad, A. L. C.; Barbetti, F.; Rovero, P.; D'Ursi, A. M.; Chelli, M.; Chorev, M.; Papini, A. M., N-alpha-Fmoc-protected omega-alkynyl-l-amino acids as building blocks for the synthesis of clickable peptides. *Eur. J. Org. Chem.* **2008**, *31*, 5308-5314.

Isidro-Llobet, A.; Alvarez, M.; Albericio, F., Amino acid-protecting groups. *Chem. Rev.* **2009**, *109*, 2455-2504.

Iqbal, A.; Arslan, S.; Okumus, B.; Wilson, T. J.; Giraud, G.; Norman, D. G.; Ha, T.; Lilley, D. M. J., Orientation dependence in fluorescent energy transfer between Cy3 and Cy5 terminally attached to double-stranded nucleic acids. *Proc. Natl. Acad. Sci. U.S.A.* **2008**, *105*, 11176-11181.

Johnson, S. R.; Westmoreland, T. D.; Caspar, J. V.; Barqawi, K. R.; Meyer, T. J., Influence of variations in the chromophoric ligand on the properties of metal-to-ligand charge-transfer excited states. *Inorg. Chem.* **1988**, *27*, 3195-3200.

Jones, Jr., W. E.; Baxter, S. M.; Strouse, G. F.; Meyer, T. J., Intrastrand electron and energy transfer between polypyridyl complexes on a soluble polymer. *J. Am. Chem. Soc.* **1993**, *115*, 7363-7373.

Jordan, P.; Fromme, P.; Witt, H. T.; Klukas, O.; Saenger, W.; Krauss, N., Three-dimensional structure of cyanobacterial photosystem I at 2.5 Å resolution. *Nature* **2001**, *411*, 909-917.

Juris, A.; Balzani, V.; Barigelletti, F.; Campagna, S.; Belser, P.; Von Zelewski, A., Ru(II) polypyridine complexes: photophysics, photochemistry, electrochemistry, and chemiluminescence. *Coord. Chem. Rev.* **1988**, *84*, 85-277.

Katoh, R.; Furube, A.; Yoshihara, T.; Hara, K.; Fujihashi, G.; Takano, S.; Murata, S.; Arakawa, H.; Tachiya, M., Efficiencies of electron injection from excited N3 dye into nanocrystalline semiconductor (ZrO_2, TiO_2, ZnO, Nb_2O_5, SnO_2, In_2O_3) films. *J. Phys. Chem. B.* **2004**, *108*, 4818-4822.

Khan, S. I.; Beilstein, A. E.; Grinstaff, M. W., Automated solid-phase synthesis of site-specifically labeled ruthenium-oligonucleotides. *Inorg. Chem.* **1999**, *38*, 418-419.

Khan, S. I.; Beilstein, Tierney, M. T.; Sykora, M.; Grinstaff, M. W., Solid-phase synthesis and photophysical properties of DNA labeled at the nucleobase with $Ru(bpy)_2(4\text{-m-}4'\text{-pa-bpy})^{2+}$. *Inorg. Chem.* **1999**, *38*, 5999-6002.

Khan, S. I.; Beilstein, A. E.; Grinstaff, M. W., Automated solid-phase synthesis of site-specifically labeled ruthenium-oligonucleotides. *Inorg. Chem.* **1999**, *38*, 418-419.

Khan, S. I.; Grinstaff, M. W., Palladium(0)-catalyzed modification of oligonucleotides during automated solid-phase synthesis. *J. Am. Chem. Soc.* **1999**, *121*, 4704-4705.

Kise, Jr., K. J.; Bowler, B. E., A ruthenium(II) tris(bipyridyl) amino acid: synthesis and direct incorporation into an α-helical peptide by solid-phase synthesis. *Inorg. Chem.* **2002**, *41*, 379-386.

Kise, Jr., K. J.; Bowler, B. E., Electron transfer through a prenucleated bimetallic alanine-based peptide helix. *Inorg. Chem.* **2003**, *42*, 3891-3897.

Kober, E. M.; Sullivan, B. P.; Meyer, T. J., Solvent dependence of metal-to-ligand charge-transfer transitions. Evidence for initial electron localization in MLCT excited states of 2,2'-bipyridine complexes of ruthenium(II) and osmium(II). *Inorg. Chem.* **1984**, *23*, 2098-2104.

Kohn, W. D.; Kay, C. M.; Hodges, R. S., Protein destabilization by electrostatic repulsions in the two-stranded α-helical coiled-coil/leucine zipper. *Protein Sci.* **1995**, *4*, 237-250.

Kohn, W. D.; Kay, C. M.; Hodges, R. S., Orientation, positional, additivity, and oligomerization-state effects of interhelical ion pairs in α-helical coiled-coils. *J. Mol. Biol.* **1998**, *283*, 993-1012.

König, P.; Richmond, T. J., The X-ray structure of the GCN4-bZIP bound to ATF/CREB sire DNA shows the complex depends on DNA flexibility. *J. Mol. Biol.* **1993**, *233*, 139-154.

Kornilova, A. Y.; Wishart, J. F.; Ogawa, M. Y., Effect of surface charge on the rates of intermolecular electron-transfer between de novo designed metalloproteins. *Biochemistry* **2001**, *40*, 12186-12192.

Kornilova, A. Y.; Wishart, J. F.; Xiao, W.; Lasey, R. C.; Fedorova, A.; Shin, Y.-K.; Ogawa, M. Y., Design and characterization of a synthetic electron-transfer protein. *J. Am. Chem. Soc.* **2000**, *122*, 7999-8006.

Kozlov, G. V.; Ogawa, M. Y., Electron transfer across a peptide-peptide interface within a designed metalloprotein. *J. Am. Chem. Soc.* **1997**, *119*, 8377-8378.

Kuemin, M.; Schweizer, S.; Ochsenfeld, C.; Wennemers, H., Effects of terminal functional groups on the stability of the polyproline II structure: a combined experimental and theoretical study. *J. Am. Chem. Soc.* **2009**, *131*, 15474-15482.

Lai, J. R.; Fisk, J. D.; Weisblum, B.; Gellman, S. H., Hydrophobic core repacking in a coiled-coil dimer via phage display: insights into plasticity and specificity at a protein-protein interface. *J. Am. Chem. Soc.* **2004**, *126*, 10514-10515.

Lee, C.; Yang, W.; Parr, R., Development of the Colle-Silvetti correlation-energy formula into functional of the electron density. *Phys. Rev. B* **1988**, *37*, 785–789.

Lewis, W. G.; Magallon, F. G.; Fokin, V. V.; Finn, M. G., Discovery and characterization of catalysts for azide-alkyne cycloaddition by fluorescence quenching. *J. Am. Chem. Soc.* **2004**, *126*, 9152-9153.

Lewis, N. S.; Nocera, D. G. *Proc. Natl. Acad. Sci. U.S.A.* **2006**, *103*, 15729-15735.

Litowski, J. R.; Hodges, R. S., Designing heterodimeric two-stranded α-helical coiled-coils. *J. Biol. Chem.* **2002**, *277*, 37272-37279.

Lumb, K. J.; Kim, P. S., A buried polar interaction imparts structural uniqueness in designed heterodimeric coiled coil. *Biochemistry* **1995**, *34*, 8642-8648.

Macias, M. J.; Hyvonen, M.; Baraldi, E.; Schultz, J.; Sudol, M.; Saraste, M.; Oschkinat, H., Structure of the WW domain of kinase-associated protein complexed with a proline-rich peptide. *Nature* **1996**, *382*, 646-649.

Madison, V., Flexibility if the pyrrolidine ring in proline peptides. *Biopolymers* **1977**, *16*, 2671-2692.

Mahmoud, Z. N.; Gunnoo, S. B.; Thomson, A. R.; Fletcher, J. M.; Woolfson, D. N., Bioorthogonal dual functionalization of self-assembling protein fibers. *Biomat.* **2011**, *32*, 3712-3720.

Mahoney, N. M.; Janmey, P. A.; Almo, S. C., structure of the profilin-poly-L-proline complex involved in morphogenesis and cytoskeletal regulation. *Nat. Struct. Biol.* **1997**, *4*, 953-960.

Mason, J. M.; Arndt, K. M., Coiled coil domains: stability, specificity, and biological implications. *Chem. Bio. Chem.* **2004**, *5*, 170-176.

McCafferty, D. G.; Bishop, B. M.; Wall, C. G.; Hughes, S. G.; Mecklenberg, S. L.; Meyer, T. J.; Erickson, B. W., Synthesis of redox derivatives of lysine and their use in solid-phase synthesis of a light-harvesting peptide. *Tetrahedron* **1995**, *51*, 1093-1106.

McCafferty, D. G.; Friesen, D. A.; Danielson, E.; Wall, C. G.; Saderholm, M. J.; Erickson, B. W.; Meyer, T. J., Photochemical energy conversion in a helical oligoproline assembly. *Proc. Natl. Acad. Sci. U.S.A.* **1996**, *93*, 8200-8204.

Meldal, M.; Tornøe, C. W., Cu-catalyzed azide-alkyne cycloaddition. *Chem. Rev.* **2008**, *108*, 2952-3015.

Meng, H. Y.; Thomas, K. M.; Lee, A. E.; Zondlo, N. J., Effects of *i* and *i*+3 residue identitiy on cis-trans isomerism of the aromatic$_{i+1}$-prolyl$_{i+2}$ amide bond: implications for type VI β-turn formation. *Biopolymers*, **2006**, *84*, 192-204.

Meyer, T. J., Chemical approaches to artificial photosynthesis. *Acc. Chem. Res.* **1989**, *22*, 163-170.

Nakagawa, Y.; Irie, K.; Yanagita, R. C.; Ohigashi, H.; Tsuda, K.-I. Iodolactam-V is involved in the CH/π interaction with Pro-11 of the PKCδ C1B domain: application for the structural optimization of the PKCδ ligand. *J. Am. Chem. Soc.* **2005**, *127*, 5746-5747.

Nishizawa, K.; Freund, C.; Li, J.; Wagner, G.; Reinherz, E. L., Identification of a proline-binding motif regulating CD2-triggered T lymphocyte activation. *Proc. Natl. Acad. Sci. U.S.A.* **1998**, *95*, 14897-902.

Nocera, D. G., Living healthy on a dying planet. *Chem. Soc. Rev.* **2009**, *38*, 13-15.

Oakley, M. G.; Kim, P. S., A buried polar interaction can direct the relative orientation of helices in a coiled coil. *Biochemistry* **1998**, *37*, 12603-12610.

O'Regan, B.; Grätzel, M., A low-cost, high-efficiency solar cell based on dye-sensitized colloidal TiO_2 films. *Nature* **1991**, *353*, 737-740.

O'Shea, E. K.; Klemm, J. D.; Kim, P. S.; Alber T., X-ray structure of the GCN4 leucine zipper, a two-stranded, parallel coiled coil. *Science* **1991**, *254*, 539-544.

O'Shea, E. K.; Lumb, K. J.; Kim, P. S., Peptide 'velcro': design of a heterodimeric coiled coil. *Curr. Biol.* **1993**, *3*, 658-667.

O'Shea, E. K.; Rutkowski, R.; Kim, P. S., Mechanism of specificity in the Fos-Jun oncoprotein heterodimer. *Cell* **1992**, *68*, 699-708.

Pace, C. N., Determination and analysis of urea and guanidine hydrochloride denaturation curves. *Methods Enzymol.* **1986**, *131*, 266-280.

Pal, D.; Chakrabarti, P., Cis peptide bonds in proteins: residues involved, their conformations, interactions, and locations. *J. Mol. Biol.* **1999**, *294*, 271-288.

Pandya, M. J.; Spooner, G. M.; Sunde, M.; Thorpe, J. R.; Rodger, A.; Woolfson, D. N., Sticky-end assembly of a designed peptide fiber provides insight into protein fibrillogenesis. *Biochemistry* **2000**, *39*, 8728-8734.

Park, H.; Bae, E.; Lee, J.-J.; Park, J.; Choi, W., effect of the anchoring group in Ru-bipyridyl sensitizers on the photoelectrochemical behavior of dye-sensitized TiO_2 electrodes: carboxylates versus phosphonate linkages. *J. Phys. Chem. B* **2006**, *110*, 8740-8749.

Pauling, L.; Corey, R. B.; Branson, H. R., The structure of proteins: two hydrogen-bonded helical arrangements of the polypeptide chain. *Proc. Nat. Acad. Sci., U.S.A.* **1951**, *37*, 205-211.

Peek, B. M.; Ross, G. T.; Edwards, S. W.; Meyer, G. J.; Meyer, T. J.; Erickson, B. W., Synthesis of redox derivatives of lysine and related peptides containing phenothiazine or tris(2,2'bipyridine)ruthenium(II). *Int. J. Peptide. Protein Res.* **1990**, *38*, 114-123.

Pinkse, M. W. H.; Uitto, P. M.; Hilhorst, M. J.; Ooms, B.; Heck, A. J. R., Selective isolation at the femtomole level of phosphopeptides from proteolytic digests using 2D-NanoLC-ESI-MS/MS and titanium oxide precolumns. *Anal. Chem.* **2004**, *76*, 3935-3943.

Pornillos, O.; Alam, S. L.; Davis, D. R.; Sundquist, W. I., Structure of the Tsg101 UEV domain in complex with the PTAP motif of the HIV-1 p6 protein. *Nat. Struct. Biol.* **2002**, *9*, 812-817.

Pornillos, O.; Alam, S. L.; Rich, R. L.; Myszka, D. G.; Davis, D. R.; Sundquist, W. I., Structure and functional interactions of the Tsg101 UEV domain. *EMBO J.* **2002**, *21*, 2397-2406.

Reinhard, M.; Jouvenal, K.; Tripier, D.; Walter, U., Identification, purification, and characterization of zyxin-related protein that binds the focal adhesion and microfilament protein VASP (vasodialator-stimulated phosphoprotein). *Proc. Natl. Acad. Sci. U.S.A.* **1995**, *92*, 7956-7960.

Reinhard, M.; Rudiger, M.; Jockusch, B. M.; Walter, U., VASP interaction with vinculin: a recurring theme of interaction with proline-rich motifs. *FEBS Lett.* **1996**, *399*, 103-7.

Rillema, D. P.; Jones, D. S.; Levy, H. A., Structure of tris(2,2'-bipyridyl)ruthenium(II) hexafluorophosphate, $[Ru(bipy)_3][PF_6]_2$; X-ray crystallographic determination. *J. Chem. Soc., Chem. Commun.* **1979**, 849-851.

Rodionov, V. O.; Fokin, V. V.; Finn, M. G., Mechanism of the ligand-free Cu^I-catalyzed azide-alkyne cycloaddition reaction. *Angew. Chem,. Int. Ed.* **2005**, *44*, 2210-2215.

Rostovtsev, V. V.; Green, L. G.; Fokin, V. V.; Sharpless, B. K., A stepwise Huisgen cycloaddition process: copper(I)-catalyzed regioselective "ligation" of azides and terminal alkynes. *Angew. Chem., Int. Ed.* **2002**, *41*, 2596-2599.

Russell, S. J.; Cochran, A. G., Designing stable β-hairpins: energetic contributions from cross-strand residues. *J. Am. Chem. Soc.* **2001**, *122*, 12600-12601.

Ryadnov, M. G.; Woolfson, D. N., Engineering the morphology of a self-assembling protein fibre. *Nat. Mater.* **2003**, *2*, 329-332.

Ryadnov, M. G.; Woolfson, D. N., Introducing branches into self-assembling peptide fiber. *Angew. Chem., Int. Ed. Engl.* **2003**, *42*, 3021-3023.

Ryadnov, M. G.; Woolfson, D. N., Fiber recruiting peptides: noncovalent decoration of an engineered protein scaffold. *J. Am. Chem. Soc.* **2004**, *126*, 7454-7455.

Sano, A.; Nakamura, H., Chemo-affinity of titania for the column-switching HPLC analysis of phosphopeptides. *Anal. Sci.* **2004**, *20*, 565-566.

Sano, A.; Nakamura, H., Titania as a chemo-affinity support for the column-switching HPLC analysis of phosphopeptides: application to the characterization of phosphorylation sites in proteins by combination with protease digestion and electrospray ionization mass spectrometry. *Anal. Sci.* **2004**, *20*, 861-864.

Satyanarayana, S.; Dabrowiak, J. C.; Chaires, J. B., Tris(phenanthroline)ruthenium(II) enantiomer interactions with DNA: Mode and specificity of binding. *Biochemistry* **1993**, *32*, 2573-2584.

Schmidt, S. R.; Schweikart, F.; Anderson, M. E., Current methods for phosphoprotein isolation and enrichment. *J. Chromatogr., B.* **2007**, *849*, 154-162.

Scholtz, J. M.; Qian, H.; York, E. J.; Stewart, J. M.; Baldwin, R. L., Parameters of helix-coil transition theory for alanine-based peptide of varying chain length in water. *Biopolymers* **1991**, *31*, 1463-1470.

Schutt, C. E.; Myslik, J. C.; Rozycki, M. D.; Goonesekere, N. C.; Lindberg, U., The structure of crystalline-β-actin. *Nature* **1993**, *365*, 810-816.

Serrano, J.; Horovitz, A.; Avron, B.; Bycroft, M.; Fersht, A. R., Estimating the contribution of engineered surface electrostatic interactions to protein stability by using double-mutant cycles. *Biochemistry* **1990**, *29*, 9343-9352.

Shaw, G. B.; Brown, C. L.; Papanikolas, J. M., Investigation of interligand electron transfer in polypyridyl complexes of osmium(II) using femtosecond polarization anisotropy methods: examination of $Os(bpy)_3^{2+}$ and $Os(bpy)_2(mab)^{2+}$. *J. Phys. Chem. A.* **2002**, *106*, 1483-1495.

Siegert, R.; Leroux, M. R.; Scheufler, C.; Hartl, F. U.; Moarefi, I., Structure of the molecular chaperone prefoldin: unique interaction of multiple coiled coil tentacles with unfolded proteins. *Cell* **2000**, *103*, 621-632.

Smith, A. M.; Banwell, E. F.; Edwards, W. R.; Padya, M. J.; Woolfson, D. N., Engineering increased stability into self-assembled protein fibers. *Adv. Funct. Mater.* **2006**, *16*, 1022-1030.

Song, W.; Brennaman, M. K.; Concepcion, J. J.; Jurss, J. W.; Hoertz, P. G.; Luo, H.; Chen, C.; Hanson, K.; Meyer, T. J., Interfacial electron transfer dynamics for $[Ru(bpy)_2((4,4'\text{-}PO_3H_2)_2bpy)]^{2+}$ sensitized TiO_2 in a dye-sensitized photoelectrosynthesis cell: factors influencing efficiency and dynamics. *J. Phys. Chem. C.* **2011**, *115*, 7081-7091.

Sparks, A. B.; Rider, J. E.; Hoffman, N. G.; Fowlkes, D. M.; Quilliam, L. A.; Kay, B. K., Distinct ligand preferences of Src homology 3 domains 3 domians from Src, Yes, Abl, cortactin, p53bp2, PLCγ, Crk, and Grb2. *Proc. Nat. Acad. Sci. U.S.A.* **1996**, *93*, 1540-1544.

Speiser, S., Photophysics and mechanisms of intramolecular electronic energy transfer in bichromophoric molecular systems: solution and supersonic jet studies. *Chem. Rev.* **1996**, *96*, 1953-1976.

Speiser, S.; Katriel, J., Intramolecular electronic energy transfer via exchange interaction in bichromophoric molecules. *Chem. Phys. Lett.* **1983**, *102*, 88-94.

Stanger, H. E.; Gellman, S. H., Rules for antiparallel β-sheet design: D-Pro-Gly is superior to L-Asn-Gly for β-hairpin nucleation. *J. Am. Chem. Soc.* **1998**, *120*, 4236-4237.

Stryer, L.; Haugland, R. P., Energy transfer: a spectroscopic ruler. *Proc. Natl. Acad. Sci. U.S.A.* **1967**, *58*, 719-726.

Su, J. Y.; Hodges, R. S.; Kay, C. M., Effect of chain length on the formation and stability of synthetic α-helical coiled coils. *Biochemistry* **1994**, *33*, 15501-15510.

Sudol, M.; Chen, H. I.; Bougeret, C.; Einbond, A.; Bork, P., Characterization of a novel protein-binding module – the WW domain. *Febs Lett.* **1995**, *369*, 67-71.

Syud, F. A.; Espinosa, J. F.; Gellman, S. H., NMR-Based quantification of β-sheet populations in aqueous solution through use of reference peptides for the folded and unfolded states. *J. Am. Chem. Soc.* **1999**, *121*, 11577-11578.

Telser, J.; Cruickshank, K. A.; Schanze, K. S.; Netzel, T. L., DNA oligomers and duplexes containing a covalently attached derivative of tris(2,2'bipyridine)ruthenium(II): synthesis and characterization by thermodynamic and optical spectroscopic measurements. *J. Am. Chem. Soc.* **1989**, *111*, 7221-7226.

Thomas, K. M. Naduthambi, D. Zondlo, N. J., Electronic control of amide cis-trans isomerization via the aromatic-prolyl interaction. *J. Am. Chem. Soc.* **2006**, *128*, 2216-2217.

Tierney, M. T.; Sykora, M.; Khan, S. I.; Grinstaff, M. W., Photoinduced electron transfer in an oligonucleotide duplex: observation of the electron-transfer intermediate. *J. Phys. Chem. B.* **2000**, *104*, 7574-7576.

Tornøe, C. W.; Christensen, C.; Meldal, M., Peptidotriazoles on solid phase: [1,2,3]-triazoles by regiospecific copper(I)-catalyzed 1,3-dipolar cycloadditions of temrinal alkynes to azides. *J. Org. Chem.* **2002**, *67*, 3057-3064.

Tu, J. C.; Xiao, B.; Yuan, J. P.; Lanahan, A. A.; Leoffert, K.; Li, M.; Linden, D. J.; Worley, P. F., Homer binds a novel proline-rich motif and links group 1 metabotropic glutamate receptors with IP3 receptors. *Neuron* **1998**, *21*, 717-726.

Vlachopoulos, N.; Liska, P.; Augustynski, J.; Grätzel, M., Very efficient visible light energy harvesting and conversion by spectral sensitization of high surface area polycrystalline titanium dioxide films. *J. Am. Chem. Soc.* **1988**, *110*, 1216-1220.

Wang, G.; Bergstrom, D. E., Controlled oxidation of dimethyl derivatives of pyridine, 2,2'-bipyridine, and 1,10-phenanthroline. *Synlett* **1992**, *5*, 422-424.

Wedemeyer, W. J.; Welker, E.; Scheraga, H. A., Proline *cis-trans* isomerization and protein folding. *Biochemistry* **2002**, *41*, 14637-14644.

Wendt, H.; Berger, C.; Baici, A.; Thomas, R. M. Bossard, H. R., Kinetics of folding of leucine zipper domains. *Biochemistry* **1995**, *34*, 4097-4107.

Woll, M. G.; Gellman, S. H., Nackbone thioester exchange: a new approach to evaluating higher order structural stability in polypeptides. *J. Am. Chem. Soc.* **2004**, *126*, 11172-4.

Woll, M. G.; Hadley, E. B.; Mecozzi, S.; Gellman, S. H., Stabilizing and destabilizing effects of phenylalanine→F_5-phenylalanine mutations on the folding of a small protein. *J. Am. Chem. Soc.* **2006**, *128*, 15932-15933.

Woody, R. W., Circular dichroism. *Methods in Enzymol.* **1995**, *246*, 34-71.

Woolfson, D. N., The design of coiled-coil structures and assemblies. *Adv. Protein Chem.* **2005**, *70*, 79-112.

Woolfson, D. N.; Alber, T., Predicting oligomerization states of coiled coils. *Protein Sci.* **1995**, *4*, 1596-1607.

Wuthrich, K. (1986) NMR of Proteins and Nucleic Acids, Wiley-Interscience, New York.

Yeh, A. T.; Shank, C. V.; McCusker, J. K., Ultrafast electron localization dynamics following photo-induced charge transfer. *Science* **2000**, *289*, 935-938.

Yu, H. T.; Chen, J. K.; Feng, S. B.; Dalgarno, D. C.; Brauer, A. W.; Schreiber, S. L., Structural basis for the binding of proline-rich peptides to SH3 domians. *Cell* **1994**, *76*, 933-945.

Zaloom, J.; Roberts, D. C., Preparation of azido derivatives from amino acids and peptides by diazo transfer. *J. Org. Chem.* **1981**, *46*, 5173-5176.

Zarrinpar, A.; Bhattacharyya, R. P.; Lim, W. A., The structure and function of proline recognition domains. *Science's STKE* **2003**, *2003*, RE8.

Zettl, M.; Way, M., The WH1 and EVH1 domains of WASP and Ena/VASP family members bind distinct sequence motifs. *Curr. Biol.* **2002**, *12*, 1617-22.

Zhou, N. E.; Kay, C. M.; Hodges, R. S., Synthetic model proteins. Positional effects of inetrchain hydrophobic interactions on stability of two-stranded α-helical coiled-coils. *J. Biol. Chem.* **1992**, *267*, 2664-2670.

Zhou, N. E.; Kay, C. M.; Hodges, R. S., Synthetic model proteins: the relative contribution of leucine residues at the nonequivalent positions of the 3-4 hydrophobic repeat to the stability of the two-stranded α-helical coiled-coil. *Biochemistry* **1992**, *31*, 5739-5746.

Zhou, N. E.; Kay, C. M.; Hodges, R. S., The role of interhelical ionic interactions in controlling protein folding and stability: de novo designed synthetic two-stranded α-helical coiled-coils. *J. Mol. Biol.* **1994**, *237*, 500-512.

Zhou, N. E.; Zhu, B. Y.; Kay, C. M.; Hodges, R. S., The two-stranded a-helical coiled-coil is an ideal model for studying protein stability and subunit interactions. *Biopolymers* **1992**, *32*, 419-426.